Earth-Science Reviews 220 (2021) 103706

Contents lists available at ScienceDirect

Earth-Science Reviews

journal homepage: www.elsevier.com/locate/earscirev

Mediterranean tephrostratigraphy and peri-Tyrrhenian explosive activity revaluated in light of the 430-365 ka record from Fucino Basin (central Italy)

Lorenzo Monaco [a], Danilo M. Palladino [a], Mario Gaeta [a], Fabrizio Marra [b], Gianluca Sottili [a], Niklas Leicher [c], Giorgio Mannella [d], Sébastien Nomade [e], Alison Pereira [f], Eleonora Regattieri [g], Bernd Wagner [c], Giovanni Zanchetta [d,b,l], Paul G. Albert [h], Ilenia Arienzo [i], Massimo D'Antonio [j], Paola Petrosino [j], Christina J. Manning [k], Biagio Giaccio [l,b,*]

[a] Dipartimento di Scienze della Terra, Sapienza-Università di Roma, Rome, Italy
[b] Istituto Nazionale di Geofisica e Vulcanologia, Rome, Italy
[c] Institute of Geology and Mineralogy, University of Cologne, Cologne, Germany
[d] Dipartimento di Scienze della Terra, University of Pisa, Pisa, Italy
[e] Laboratoire de Sciences du Climat et de l'Environnement, UMR 8212, CEA-UVSQ, IPSL and Université de Paris-Saclay, Gif-sur-Yvette, France
[f] Université Paris-Saclay, CNRS, UMR 8148 GEOPS, Orsay 91405, France
[g] Istituto di Geoscieze e Georisorse, IGG-CNR, Pisa, Italy
[h] Department of Geography, Swansea University, Swansea, UK
[i] Istituto Nazionale di Geofisica e Vulcanologia, Osservatorio Vesuviano, Naples, Italy
[j] Dipartimento di Scienze della Terra, dell'Ambiente e delle Risorse, Università degli Studi di Napoli Federico II, Naples, Italy
[k] Department of Earth Sciences, Royal Holloway, University of London, Egham, Surrey, UK
[l] Istituto di Geologia Ambientale e Geoingegneria, IGAG-CNR, Rome, Italy

ARTICLE INFO

Keywords:
Peri-Tyrrhenian explosive volcanism
Mediterranean tephrochronology
Marine Isotope Stage 11

ABSTRACT

Accurately reconstructing the scale and timing of dynamic processes, such as Middle-Late Pleistocene explosive volcanism and rapid climatic changes, requires rigorous and independent chronological constraints. In this framework, the study of distal volcanic ash layers, or tephra, transported and deposited over wide regions during explosive volcanic eruptions, is increasingly being recognised as a fundamental chronostratigraphic tool for addressing these challenging issues. Here we present a high-resolution distal tephra record preserved in the lacustrine sedimentary succession of the Fucino Basin, central Italy. The investigated record spans the 430-365 ka time interval, covering the entirety of Marine Isotope Stage 11 (MIS 11), and provides important insights into peri-Tyrrhenian potassic explosive volcanism from sources located in central Italy against a backdrop of Mediterranean palaeoclimate records. The succession of ash fall events of this time interval is reconstructed through a detailed lithostratigraphic, geochemical and $^{40}Ar/^{39}Ar$ geochronological characterization of the deposits preserved as discrete layers in the Fucino F4-F5 sediment core. This work is complemented by similarly detailed characterization of selected proximal pyroclastic units from the peri-Tyrrhenian potassic volcanoes. Geochemical fingerprinting of the tephra deposits by means of their major, minor and trace elements and Sr isotope composition indicates that all the thirty-two investigated ash layers derived from the peri-Tyrrhenian potassic volcanoes. The stratigraphically continuous succession of the Fucino tephra layers allowed the development of a fully independent, $^{40}Ar/^{39}Ar$ age-constrained, Bayesian age-depth model for the investigated time interval. The age-model allows us to establish modelled ages for the tephra layers within the succession that are not directly dated. The resulting dated tephra record clearly reveals a highly time resolved and previously unparalelled chronicle of explosive activity from the Vulsini, Vico, Sabatini, Colli Albani and Roccamonfina volcanic complexes. Our study provides a benchmark and valuable geochemical and geochronological dataset to be used as a reference for any future development and application of the tephrostratigraphic methods across the central Mediterranean area both during the investigated 430-365 ka time interval, and deeper in time. This contribution

* Corresponding author.
E-mail address: biagio.giaccio@cnr.it (B. Giaccio).

https://doi.org/10.1016/j.earscirev.2021.103706
Received 19 March 2021; Received in revised form 27 May 2021; Accepted 3 June 2021
Available online 6 June 2021

underlines the importance of integrating proximal and distal sedimentary records to more accurately establish long-term and comprehensive volcanic eruption records.

1. Introduction

Reconstructing the history of explosive volcanism, including the dynamics, timing, and recurrence intervals of eruptions, is a fundamental requirement for understanding the temporal evolution of the volcanic systems and for assessing the related hazards (e.g., Gehrels et al., 2006). The required stratigraphic, chronological and volcanological data are commonly acquired in near-vent (proximal) volcanic areas, where the geological record provides key data for evaluating eruptive and emplacement dynamics, as well as the evolution of the volcanic edifices. Furthermore, the presence of coarse-grained K-rich crystals in proximal deposits from volcanoes fed by highly potassic evolved magmas enables direct and precise radiometric dating using the $^{40}Ar/^{39}Ar$ technique. However, due to the intense volcano-tectonic and sedimentary processes occurring in near-source volcanic regions, many proximal deposits are often buried, inaccessible, or partially eroded. In contrast, intermediate and distal archives, usually located downwind with respect to volcanic sources, can offer a more continuous record of volcanic ash layers (or "tephra") derived from sustained columns and co-ignimbrite ash clouds, thus enabling the reconstruction of the eruptive history and dynamics of individual volcanic systems and regions (e.g., Paterne et al., 1986, 1988; Newnham et al., 1999; de Fontaine et al., 2007; Dugmore et al., 2013; Giaccio et al., 2014; Leicher et al., 2016, 2019; Albert et al., 2018, 2019; Larsen et al., 2020; Wulf et al., 2020).

The relevance of tephrostratigraphy extends beyond volcanological applications, as these instantaneously deposited layers are also outstanding chronological, stratigraphic and correlation tools for addressing numerous issues in Quaternary sciences (e.g., Lowe, 2011). Through diagnostic geochemical, stratigraphic, and chronological features, the volcanic ash, widely dispersed during explosive eruptions and deposited on regional to global scale (Ponomareva et al., 2015), can be recognized and correlated to eruptive events or distal tephra of known ages. This provides an effective and reliable way through which sedimentary archives with co-located tephra can be accurately and precisely dated and correlated over wide regions. Indeed, when combined with high-precision and accurate radiometric $^{40}Ar/^{39}Ar$ dating and detailed multiproxy series, long and continuous distal tephra successions become the cornerstones for reconstructing both the paleoclimatic change and the history of explosive volcanism (e.g., Thorarinsons, 1981a, 1981b; Paterne et al., 1986, 1988; Dugmore, 1989; Narcisi and Vezzoli, 1999; Wastergärd, 2002; Wulf et al., 2004, 2008, 2012; Lane et al., 2013; Giaccio et al., 2015a; Kousis et al., 2018; Leicher et al., 2019; Mannella et al., 2019; Regattieri et al., 2019).

Tephrostratigraphy is most successfully applied when long and continuous sedimentary successions containing well-preserved tephra layers are in a suitable range of distances from sources of recurrent explosive activity. These requirements are fulfilled in the Mediterranean area, particularly in central-southern Italy. Indeed, the recurrent and continuous explosive activity of the peri-Tyrrhenian volcanism, fed by potassic to ultrapotassic magmas (e.g., Peccerillo, 2017), as well as the presence of numerous Quaternary tectonic basins hosting thick sedimentary successions, constitute a unique combination which has allowed the retrieval of extremely rich tephra repositories and, consequently, eruption event stratigraphies. An increasing number of studies on marine (Keller et al., 1978; Paterne et al., 2008; Bourne et al., 2010, 2015; Tamburrino et al., 2012; Insinga et al., 2014; Morabito et al., 2014; Matthews et al., 2015; Petrosino et al., 2015, 2016; D'Antonio et al., 2016), lacustrine (Wulf et al., 2004, 2008; Petrosino et al., 2014a; Giaccio et al., 2015a; Di Roberto et al., 2018; Leicher et al., 2019; Regattieri et al., 2019) and sub-aerial (Giaccio et al., 2012a; Gatta et al., 2016; Donato et al., 2016; Zanchetta et al., 2018; Bini et al., 2020) sedimentary environments of the Mediterranean region have documented this potential. However, despite these recent advances, the tephrostratigraphic framework of the central Mediterranean area is still fragmentary and unexplored, especially for the Middle Pleistocene (~780-130 ka).

Among the lacustrine successions hosted in the Pliocene-Quaternary inter-mountain tectonic basins of the central-southern Apennines (Italy), Fucino's is the most continuous and temporally resolved, with ~900 m of seemingly uninterrupted sedimentary infill, documenting the sediment accumulation since the Lower Pleistocene up to historical times (Cavinato et al., 2002; Giaccio et al., 2015b) and a rich tephra record (Giaccio et al., 2017, 2019; Di Roberto et al., 2018; Mannella et al., 2019; Del Carlo et al., 2020). Three factors make the Fucino Basin unique for reconstructing the eruptive history of the Italian peri-Tyrrhenian potassic to ultra-potassic volcanic activity and improving the central Mediterranean Middle Pleistocene tephrostratigraphic framework: (i) its relatively short distance from the peri-Tyrrhenian volcanoes of central Italy (~70 to ~150 km, Fig. 1a); (ii) its downwind location with respect to these volcanoes, i.e., along the preferential ash dispersal axes (Fig. 1b); (iii) the occurrence of tephra with K-rich minerals, which facilitates the laser fusion single crystals $^{40}Ar/^{39}Ar$ dating approach.

Recently, Giaccio et al. (2019) reported the presence of ~130 volcanic ash layers in a composite ~98 m-long sediment core (F4-F5) from Fucino Basin spanning the last 430 kyr (Fig. 2) confirming the great potential of this succession to become one of the cornerstones in the tephrostratigraphic network of the entire Mediterranean region. However, so far less than a quarter of these ~130 tephra layers have been stratigraphically, geochemically, and chronologically characterized (Giaccio et al., 2017, 2019). In this paper, we present detailed lithostratigraphic, geochemical and chronological data for the lowermost 28 tephra layers from the F4-F5 core, along with proximal deposits from 5 selected volcanic units of the peri-Tyrrhenian volcanoes, all constrained within the Marine Isotope Stage (MIS) 11 period (i.e., ~430-365 ka). The MIS 11 period is particularly important both in terms of volcanological and tephrochronological investigations. Indeed, it marks the onset of activity at Vico volcano (e.g., Perini et al., 2004; Pereira et al., 2020), thus adding a further volcanic source to the already rich central Mediterranean Middle Pleistocene tephrostratigraphic framework (Fig. 3). Furthermore, currently only very few tephrostratigraphic records spanning the MIS 11 period in the Mediterranean region have been investigated (Leicher et al., 2019; Vakhrameeva et al., 2018, 2021; Fig. 1a). The results of this study are discussed in the general context of the Middle Pleistocene Mediterranean tephrostratigraphy and that of the central Italy peri-Tyrrhenian explosive volcanism, providing a major contribution towards an improved framework of the regional to extra-regional tephrochronology and of the explosive volcanism history. They also provide the basis for developing a robust and independent age-model for the multi-proxy paleoclimate information of the Fucino succession during MIS 11, a key period in the Late Quaternary climatic history, whose analogies with the Holocene have long been debated (e.g., McManus et al., 2003; Tzedakis, 2010).

2. Geological and volcanological setting

2.1. The Fucino Basin

The Fucino Basin (42° 00' 00" N; 013° 30' 00" E) is one of the largest inter-Apennine tectonic basins that developed during the extensional phase related to the geodynamic evolution of the Tyrrhenian Basin and central-southern Apennine chain (e.g., Doglioni et al., 1996).

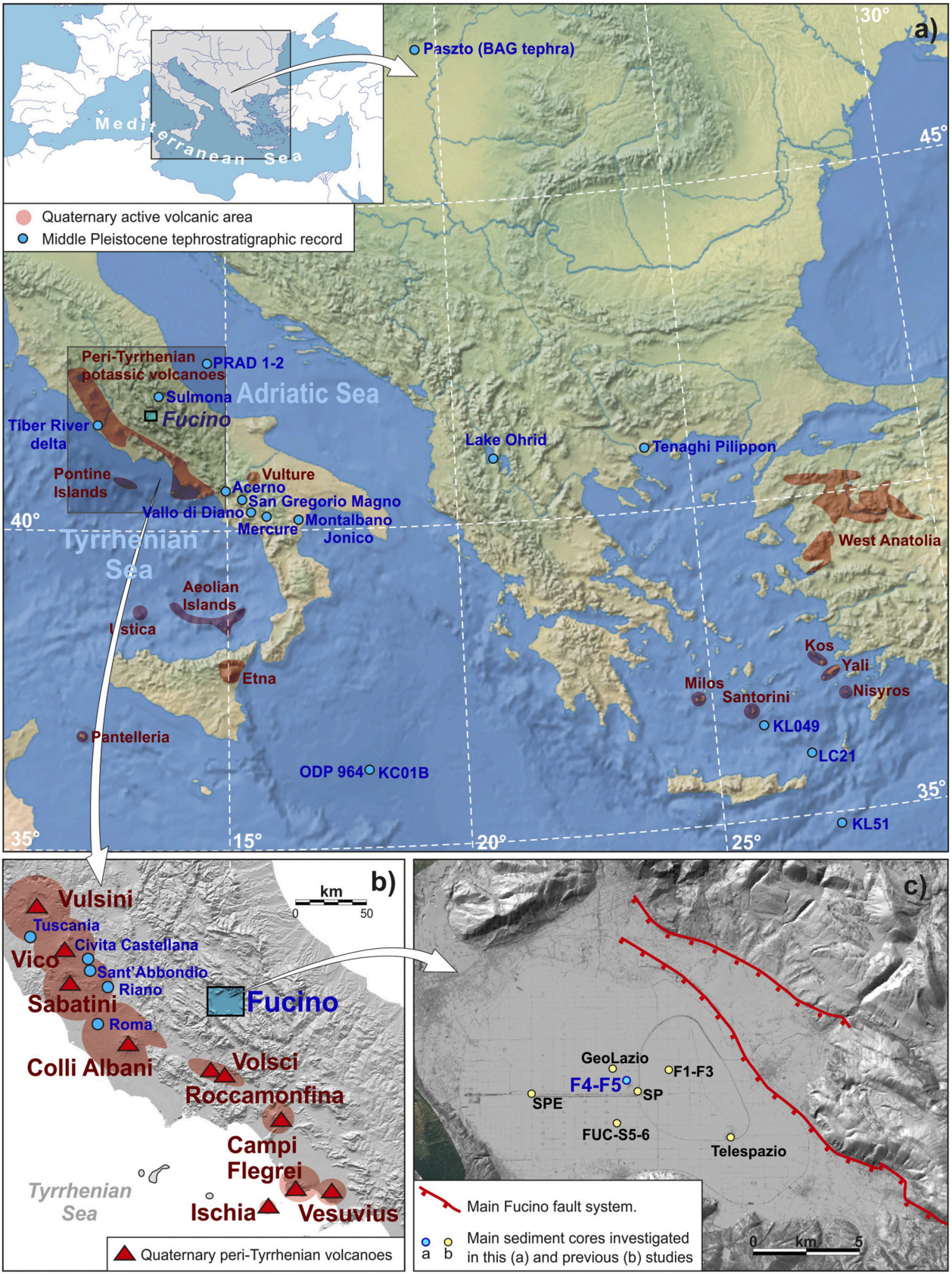

Fig. 1. Reference maps. a) The Fucino Basin and the peri-Tyrrhenian potassic volcanoes in the context of the Mediterranean Quaternary volcanism and the Middle Pleistocene tephrostratigraphic records (blue dots) cited in the text. b) Magnification of the area highlighted in a) showing in detail the location of Fucino Basin relative to the peri-Tyrrhenian potassic volcanic systems of central-southern Italy. c) DEM map of Fucino Basin highlighting the location of the F4-F5 core, along with other cores from this lacustrine basin.

Extensional tectonics, mainly acting along E-W, NE-SW and NW-SE oriented high-angle faults, caused the stretching of the mountain chain (e.g., D'Agostino et al., 2001). The opening and evolution of these intermountain basins started from the Late Pliocene-Lower Pleistocene period (Galadini and Galli, 2000; Boncio et al., 2004; Giaccio et al., 2012a; Amato et al., 2014). The Plio-Quaternary tectonic and sedimentary evolution of the Fucino Basin was driven by the *Fucino Fault System* (FFS, Galadini and Galli, 2000; Fig. 1c), which depicts a semi-graben architecture with a thickness of the Plio-Quaternary sedimentary infilling increasing up to ~900 m from west to east toward the depocenter (Cavinato et al., 2002; Patacca et al., 2008).

The Fucino Basin, unlike other intra-Apennine basins, has likely undergone continuous sedimentation (~0,45 mm/yr on average in the central-eastern sector of the basin; Giaccio et al., 2017, 2019; Mannella et al., 2019) since the Plio-Pleistocene and to recent historical times, i.e., potentially covering the last ~2.0 Myr (Giaccio et al., 2015b). Indeed, the basin hosted a lake, *Lacus Fucinus*, which was first partially reclaimed during Emperors Claudius and Adrian reigns (1st-2nd century CE), and then completely drained by the Torlonia family at the end of the 19th century.

2.2. The peri-Tyrrhenian potassic volcanic systems

The Quaternary peri-Tyrrhenian volcanic systems of central-southern Italy (hereafter peri-Tyrrhenian potassic volcanoes) belong to the *Roman Comagmatic Region* of Washington (1906), which comprises the volcanic centers and areas fed by potassic and ultrapotassic magmas extending from southern Tuscany, through Latium and Campania, i.e., from north-west to south-east (Fig. 1a and 1b): Vulsini, Vico, Sabatini and Colli Albani (grouped in the *Roman Province s.s.* by Peccerillo, 2017), Volsci and Roccamonfina (*Ernici-Roccamonfina Province*; Peccerillo, 2017) and the active volcanoes of the so-called *Campanian Volcanic Zone* (Rolandi et al., 2003) or *Campanian Province* (Peccerillo, 2017), including Campi Flegrei, Ischia, Procida and Somma-Vesuvius, also known as the *Neapolitan* volcanoes. Volcanism in the region started at the beginning of the Middle Pleistocene, but the volcanic centers have been active during different time intervals (Fig. 3). Direct evidence, i.e., near-vent deposits, of the oldest activity is documented within the Volsci

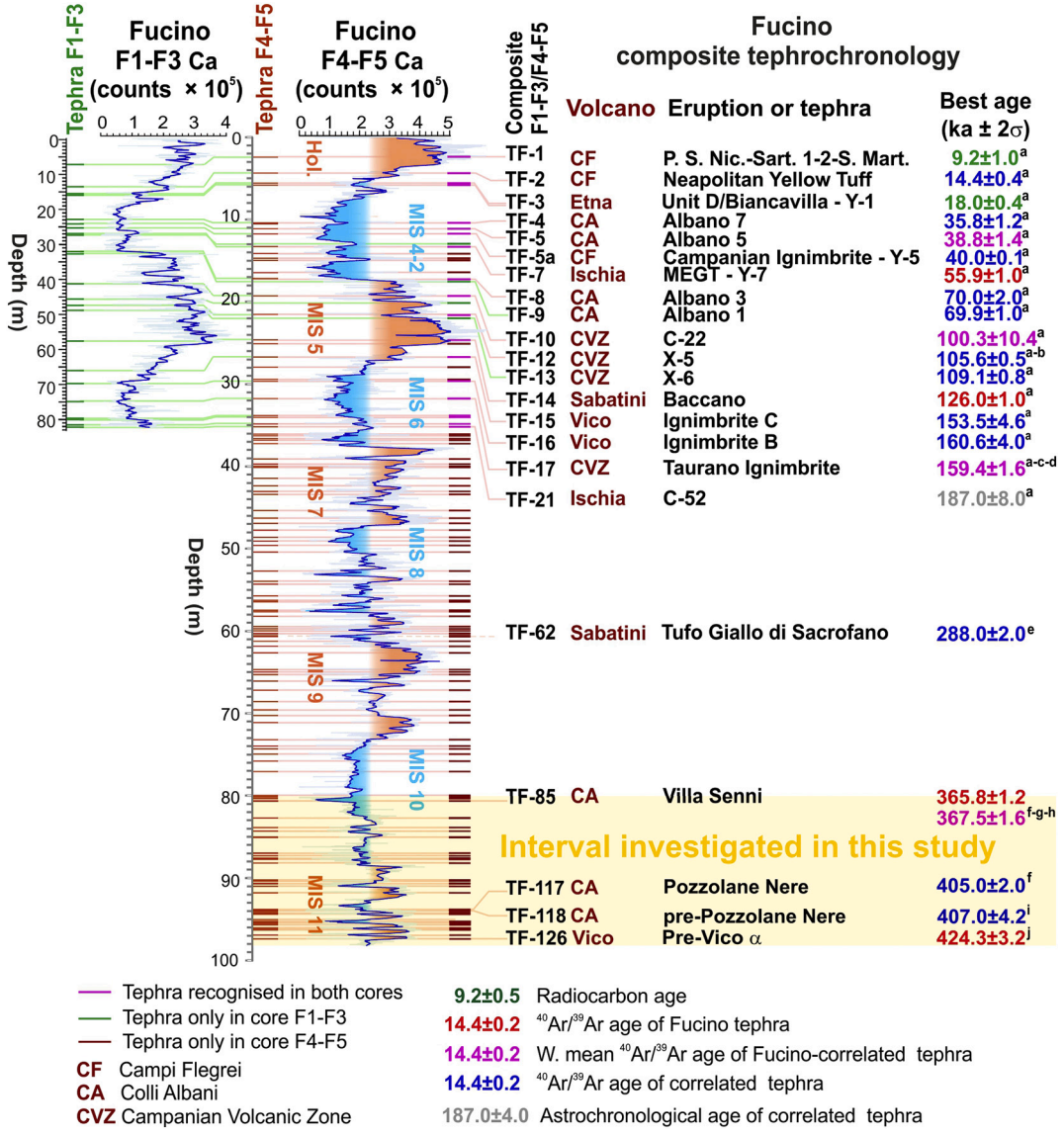

Fig. 2. Stratigraphic interval of the F4-F5 Fucino Basin sediment core investigated in this study (modified after Giaccio et al., 2019). $^{40}Ar/^{39}Ar$ ages are recalculated relatively to an age of 1.1891 Ma for the Alder Creek sanidine monitor standard (Niespolo et al., 2017), with the uncertainty expressed at 2σ. $^{40}Ar/^{39}Ar$ ages data source: [a] Mannella et al. (2019 and references therein); [b] Petrosino et al. (2016) [c] Amato et al. (2018); [d] De Vivo et al. (2001); [e] Sottili et al. (2010); [f] Marra et al. (2009); [g] Marra et al. (2019); [h] Giaccio et al. (2012a, 2012b); [i] Pereira et al. (2018); [j] Giaccio et al. (2019).

Volcanic Field (Cardello et al., 2020; Marra et al., 2021), which covers the 760-230 ka interval (Boari et al., 2009; Centamore et al., 2010; Marra et al., 2021). Possible evidence of similarly old activity at Sabatini is provided by distal tephra layers found in the Tiber River delta, dated between 750 and 810 ka (Marra et al., 2014). During the ~600-415 ka interval, the Vulsini, Sabatini, Colli Albani, Volsci and Roccamonfina volcanic districts were all simultaneously active (e.g., Sottili et al., 2004; Rouchon et al., 2008; Boari et al., 2009; Palladino et al., 2010; Soligo and Tuccimei, 2010). Around ~415 ka, volcanic activity also started at Vico volcano (Pereira et al., 2020). Finally, the onset of volcanic activity at Neapolitan volcanoes occurred around ~300 ka (Rolandi et al., 2003), although there is growing evidence from distal settings of significantly older activity in this region, extending as far back as at least 560 ka or perhaps more (e.g., Giaccio et al., 2014; Petrosino et al., 2015; Wagner et al., 2019).

In summary, all the Latium (i.e., Vulsini, Vico, Sabatini, Colli Albani and Volsci) and Roccamonfina volcanoes were active during the interval investigated in this study (i.e., 430-365 ka); consequently, there is quite a degree of complexity when trying to establish the volcanic source of distal ash layers deposited during this interval (Fig. 3).

3. Materials and methods

3.1. Investigated tephra from F4-F5 cores and Roman volcanic province

A summary of the here investigated tephra from Fucino and the Roman volcanic area in this study, and those available in the literature, is reported in Table 1.

Two cores were recovered at the F4-F5 drill site in the central area of the basin (Fig. 1c) and combined to a composite profile 98 meters long. Drilling site selection strategy and recovery procedure are reported in Giaccio et al. (2019). The F4-F5 composite record contains at least 130 tephra (Giaccio et al., 2019; Fig. 2). Based on correlations with tephra layers from the nearby F1-F3 record covering the last 190 kyr (Fig. 2; Giaccio et al., 2017), the geochemical fingerprinting of 11 relevant tephra markers, one direct $^{40}Ar/^{39}Ar$ age determination, and the recognition of a climatic proxy variability linked to glacial-interglacial cyclicity, the sediment succession from F4-F5 was ascribed to the last 430 kyr (Fig. 2; Giaccio et al., 2019). In this paper, we focus on the lowermost ~17-meter-thick interval (between ~80 and ~98 m composite depth) of the F4-F5 core, spanning a ~60 kyr time interval. The interval includes the lowermost tephra layer labelled TF-126, which is directly dated by $^{40}Ar/^{39}Ar$ method at 424.3 ± 3.2 ka (Giaccio et al., 2019), and up to TF-85, correlated to the Villa Senni eruption (i.e., Tufo Lionato) from the Colli Albani volcano (Giaccio et al., 2019), which is dated at 367.6 ± 1.6 ka (Marra et al., 2009; Giaccio et al., 2012b; Fig. 2). This interval contains 32 ash layers, 28 out of which are investigated and presented in this study, while 4 (i.e., TF-85, TF-117, TF-118 and TF-126) were already studied and reported in Giaccio et al. (2019; Table 1).

In order to improve the reference geochemical dataset required for establishing reliable tephra correlations of the Fucino tephra, we re-examined the key pyroclastic succession at Tuscania-San Pietro (southern Vulsini; Cioni et al., 1987; Palladino et al., 1994, 2010; 42° 24' 43.32" N, 011° 52' 45.13" E; Fig. 1b; Fig. 4) and performed new analyses on four pumice fall units (TSP#). Of these, TSP-1 is correlated to the Vico α Plinian fall marker (Cioni et al., 1987), while TSP-2 and TSP-3 are referred to the Plinian activity of the Vulsini Fields (although with undefined source locations). TSP-3 in particular is tentatively correlated to the Pumice Fall 0 (PF-0) of Turbeville (1992, 1993) dated at 399.8 ± 18.0 ka (Turbeville, 1992; age recalculated according to the Alder Creek sanidine at 1.1891 Ma). We stress that this attribution is just putative until it can be corroborated by stratigraphic and geochemical characterization of proximal PF-0 products collected at the type locality. Finally, the Plinian fall horizon TSP-4 is attributed to Vico Plinian

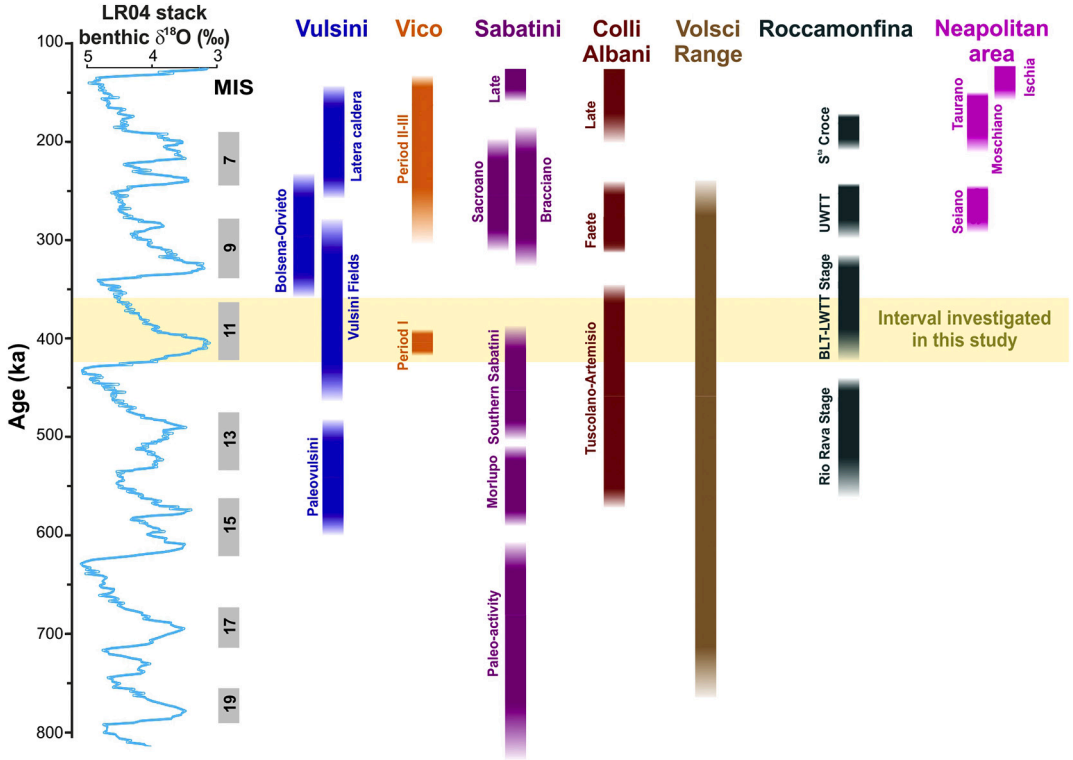

Fig. 3. Temporal distribution of the Middle Pleistocene volcanic activity from the peri-Tyrrhenian potassic volcanic systems, plotted against the LR04 benthic stack record (Lisiecki and Raymo, 2005) Data source: Vulsini volcanic district: Palladino et al. (2010), Marra et al. (2020a); Vico: Perini et al. (2004), Pereira et al. (2020); Monti Sabatini volcanic district: Sottili et al. (2010), Marra et al. (2014, 2020b); Colli Albani: Marra et al. (2009); Volsci Volcanic Field: Boari et al. (2009), Centamore et al. (2010), Marra et al. (2021); Roccamonfina: Giannetti (1996a, 1996b), Giannetti and De Casa (2000), Rouchon et al. (2008), Scaillet et al. (2008); Neapolitan area: De Vivo et al. (2001), Rolandi et al. (2003), Belkin et al. (2016), Sbrana et al. (2018).

Table 1
Data acquired in this study and available from literature for each investigated Fucino tephra or proximal volcanic unit.

Tephra	Site/Section	Type of analysis			
		Glass-WDS (EMPA)	Trace elements (LA-ICP-MS)	Sr isotopes (TIMS)	$^{40}Ar/^{39}Ar$
TF-85	F4-F5	Yes[a]	No	Yes[b]	Yes[b]
TF-88	F4-F5	Yes[b]	No	No	No
TF-89	F4-F5	Yes[b]	No	No	No
TF-90	F4-F5	Yes[b]	No	No	No
TF-93	F4-F5	Yes[b]	No	No	No
TF-94	F4-F5	Yes[b]	No	No	No
TF-96	F4-F5	Yes[b]	No	No	No
TF-97	F4-F5	Yes[b]	No	No	No
TF-98	F4-F5	Yes[b]	No	No	No
TF-99	F4-F5	Yes[b]	No	No	No
TF-100	F4-F5	Yes[b]	No	No	No
TF-102	F4-F5	Yes[b]	No	No	No
TF-103	F4-F5	Yes[b]	No	No	No
TF-104	F4-F5	Yes[b]	No	No	No
TF-106	F4-F5	Yes[b]	No	No	No
TF-107	F4-F5	Yes[b]	Yes[b]	Yes[b]	No
TF-108	F4-F5	Yes[b]	No	No	No
TF-109	F4-F5	Yes[b]	No	No	No
TF-110	F4-F5	Yes[b]	No	No	No
TF-111	F4-F5	Yes[b]	Yes[b]	Yes[b]	No
TF-114	F4-F5	Yes[b]	No	No	No
TF-115	F4-F5	Yes[b]	No	No	No
TF-116	F4-F5	Yes[b]	Yes[b]	No	No
TF-117	F4-F5	Yes[a]	No	No	Yes[b]
TF-118	F4-F5	Yesa	No	No	No
TF-120	F4-F5	Yes[b]	No	No	No
TF-121	F4-F5	Yes[b]	No	No	No
TF-122	F4-F5	Yes[b]	No	No	No
TF-123	F4-F5	Yes[b]	No	No	No
TF-124	F4-F5	Yes[b]	No	No	No
TF-125	F4-F5	Yes[b]	Yes[b]	No	No
TF-126	F4-F5	Yes[a]	Yes[b]	Yes[b]	Yes[a]
Casale delle Piane	Tuscania	Yes[b]	No	No	No
Castel Broco	Tuscania	Yes[a]	Yes[b]	Yes[b]	No
Vico α (TSP-1)	Tuscania	Yes[b]	No	No	No
TSP-2	Tuscania	Yes[b]	No	No	No
TSP-3	Tuscania	Yes[b]	No	Yes[b]	No
TSP-4	Tuscania	Yes[b]	No	No	No
Riano R-1	Riano	Yes[b]	Yes[b]	Yes[b]	Yes[c]
Pozzolane Nere	Rome	Yes[d]	No	Yes[f]	Yes[b]
Vico β	Vignanello	Yes[e]	Yes[b]	No	Yes[e]
Vico α type locality	Viterbo	Yes[e]	Yes[b]	No	Yes[e]

[a]Giaccio et al. (2019); [b] This study; [c] Marra et al. (2018); [d] Marra et al. (2009); [e] Pereira et al. (2020); [f] Gaeta et al. (2006).

activity, although with an uncertain correlation. The TSP succession also includes the Casale delle Piane and Castel Broco major pyroclastic flow deposits (investigated also in the present study, see below) and is topped by the Tuscania lavas (Palladino et al., 1994, 2010), which are broadly coeval with the Quarticciolo lavas (356 ± 15 ka; Funiciello et al., 2012) outcropping in other nearby localities.

To supplement the major element datasets for Vico volcano presented in Pereira et al. (2020), we provide trace element glass analyses of selected proximal Vico α and β samples collected from Viterbo (Vico α; Lower fall [VT-Base Vico α] and Upper fall [VT-1A, VT-1B and VT-1C]) and Vignanello (Vico β; [VIG-3]) sections.

With the same aim, we also analysed the Riano R-1 tephra (Fig. 4), found within a lacustrine (diatomite) succession outcropping along the Flaminia road (42° 05' 24.06" N, 012° 31' 57.43" E), north of Rome (Fig. 1b), and dated at 404.7 ± 5.0 ka by Marra et al. (2018). The Riano R-1 tephra is a 10-cm-thick, coarse to fine blackish ash layer, likely representing a relatively distal occurrence of a major fall deposit, of uncertain, Sabatini or external (i.e., from another Latium volcano), source area. The Riano diatomite succession contains three additional tephra layers (R-2, R-3, and R-4; Fig. 4). However, while R-2 is a 10-cm-thick layer of dense scoria lapilli, likely derived from a minor local (i.e., Sabatini) Strombolian eruption, the ash layers R-3 and R-4 did not yield fresh glass suitable for geochemical analyses.

Finally, in order to acquire a new $^{40}Ar/^{39}Ar$ age for the Colli Albani Pozzolane Nere caldera-forming eruption, we sampled an exposure in Rome City (41° 50' 44.74" N, 012° 28' 40.56" E). Indeed, since we could not establish which of the two different monitor standards was used for determining the previous set of $^{40}Ar/^{39}Ar$ ages for this deposit (Karner and Renne, 1998), the existing age of 407 ± 2 ka can not be recalculated with respect to the current monitor standard improved ages, and thus

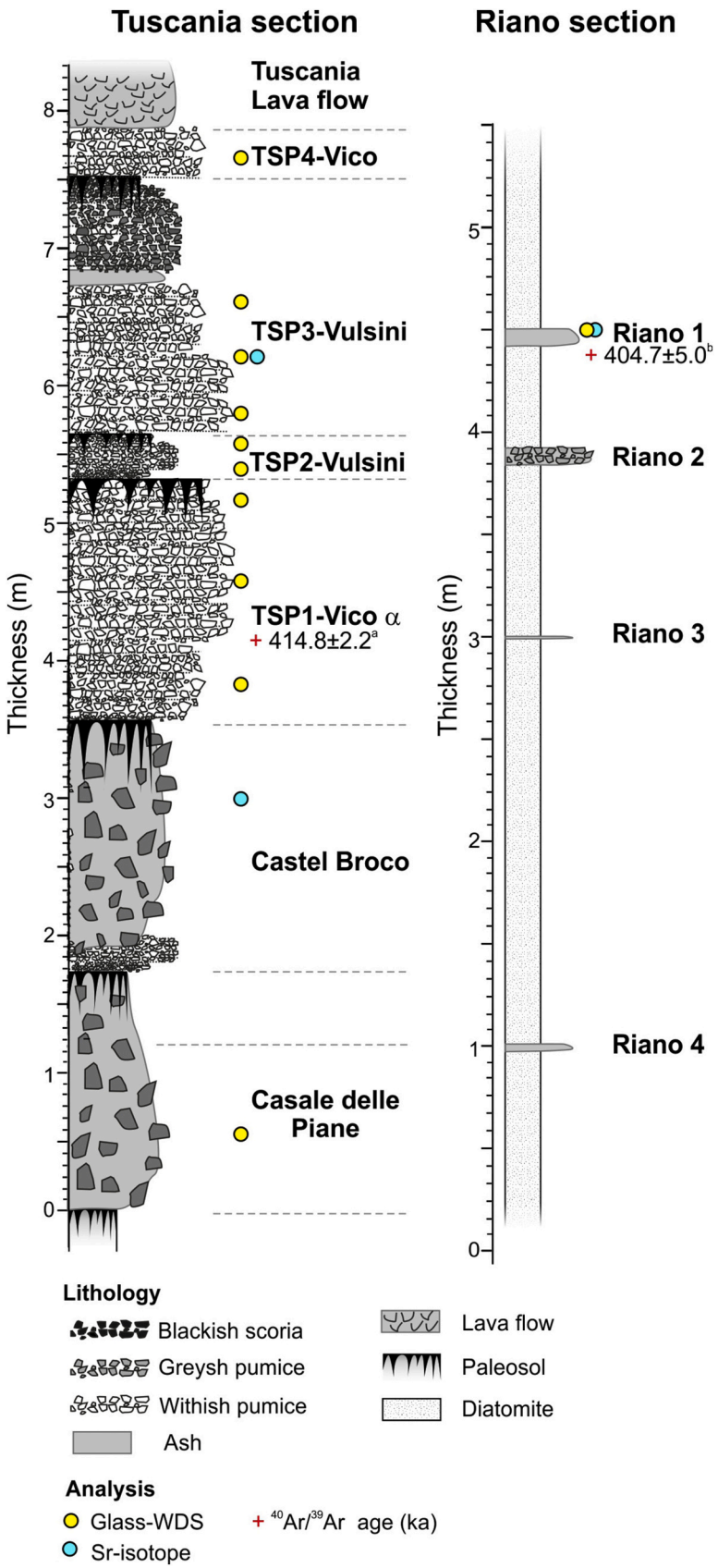

Fig. 4. Reference stratigraphic successions outcropping at Tuscania-San Pietro (southern Vulsini) and Riano (eastern Sabatini) (see Fig. 1b for locations). The stratigraphic position of the samples used for geochemical analyses in this study are also shown. $^{40}Ar/^{39}Ar$ dating: [a] Pereira et al. (2020); [b] Marra et al. (2018).

does not allow direct comparisons.

3.2. EPMA-WDS

Major and minor element compositions were determined on micro-pumice fragments and/or glass shards of the 28 tephra layers from the F4-F5 record (Table 1), which were labelled following the same criterions adopted in previous studies of the F1-F3 and F4-F5 cores (Giaccio et al., 2017, 2019), and for the above described five proximal samples (Table 1). To have a good statistical expression of the tephra composition and their geochemical variability, we aimed at analysing at least 10-15 shards/micro-pumices from each tephra. However, in some cases (i.e., TF-96, TF-100, TF-103, TF-104, TF-123 and TF-124), the dense microlithic texture of the juvenile clasts or the incipient alteration of the glass prevented us from acquiring such a satisfactory number of analyses. Neverthless, also in those cases, the relative homogeneity and/or geochemical consistency of the analysed glasses indicate a satisfactory reliability and representativity of the compositional data for tephrochronological purposes. A synthesis of all acquired data for each of the 28 tephra and 5 proximal pyroclastic units can be found in Table 1, along with information on previously investigated tephra from F4-F5 core and proximal volcanics.

Polishing and carbon coating of the epoxy slides were performed for electronprobe microanalyser wavelength dispersive spectroscopy (EPMA-WDS) analysis at the *Istituto di Geologia Ambientale e Geoingegneria* of the Italian National Research Council (IGAG-CNR, Rome). Major and minor elements quantitative analyses were performed with a CAMECA SX-50 EPMA equipped with five-wavelength dispersive spectrometers (WDS), operating at 15 kV accelerating voltage, 15 nA beam current, 10 μm defocused beam diameter - to limit Na mobilization and loss - and 20 s element counting time for all elements. Wollastonite (Si and Ca), corundum (Al), periclase (Mg), magnetite (Fe), rutile (Ti), orthoclase (K), jadeite (Na), phlogopite (F), potassium chloride (Cl), barite (S), F-apatite (P) and metals (Mn) were used as calibration standards. The Kakanui augite and Rhyolite RLS132 glasses from the United States Geological Survey were measured prior to each analytical run to evaluate the accuracy of the electron-microprobe analysis. Obtained mean values are shown in Supplementary Dataset-4 (SD-4), along with the % difference between each oxide with respect to the recommended values. The mean values show ~0.5% difference for SiO_2, ranging in concentrations from 50 wt% to 77 wt%, <0.2% for oxides in the 15-16 wt% concentration range, 3.3-1.8% for oxide concentrations between 5 and 12 wt%, 4.2-0.1% for oxides in the 2-5 wt% range, up to 5.7% for the oxides ranging from 0.2 wt% to 2 wt% and up to 39% for minor elements (i.e., oxides with concentrations <0.2 wt%).

In order to test the quality and reproducibility of our data, we also performed a series of analyses on the MPI-DING glass standards of Jochum et al. (2006) and a rhyolitic Lipari obsidian (i.e., ID3506; Kuehn et al., 2011). The results show <1.1% difference for SiO_2, ranging between 46 wt% and 77 wt% range, 2.8-0.2% for oxides ranging from 15 wt% to 27 wt%, 4.0-1.0% for oxides in the 5-13 wt% range, 5.2-0.6% for oxides ranging from 2 wt% to 5 wt%, 8.1-1.5 for oxides in the 0.2-2 wt% range and up to 62% for minor elements (SD-4).

Data reduction was carried out using the PAP correction, while data processing was performed in Microsoft Excel. We adopted 93 wt% as a threshold for the measured total: analyses with total values lower than 93 wt% were discarded. All compositional data are shown as oxide weight percentages (wt%) in the Total Alkali vs Silica (TAS; Le Maitre et al., 2002) classification diagram - as well as bi-plots diagrams - with total iron (FeOt) expressed as FeO and normalized to 100% on a volatile-free basis (i.e., excluding Cl, SO_3 and F volatiles) for correlation purposes. Collected data are all reported in Supplementary Dataset-1 (SD-1), along with secondary standards and MPI-DING measured values.

3.3. LA-ICP-MS

Trace element analyses were conducted on volcanic glasses from five Fucino tephra units, i.e., TF-107, TF-111, TF-116, TF-125, and TF-126, and four proximal-medial pyroclastic deposits, i.e., the Castel Broco unit, from the above described Tuscania-San Pietro section at Vulsini (Fig. 4), Vico α and β, and the Riano R-1 Tephra (unknown source) (Table 1). These samples have been selected (i) to test if compositions of the trace elements and/or the ratios of incompatible trace elements allow distinguishing tephra layers with similar major element composition (e.g., TF-107, TF-111, TF-126, Castel Broco, Riano R-1), and (ii) to obtain the complete geochemical composition of the products from the two major eruptions of Vico Period I (i.e., Vico α and Vico β), likely dispersed over wide areas of the central Mediterranean and thus representing potential tephra markers for this region. The analysis was performed using an Agilent 8900 triple quadrupole ICP-MS (ICP-QQQ) coupled to a Resonetics 193nm ArF excimer laser-ablation at the Department of Earth Sciences, Royal Holloway, University of London. Full analytical procedures used for volcanic glass analysis are reported in Tomlinson et al. (2010). Spot sizes of 25 and 34 μm were used depending on the sample vesicularity and/or size of glass surfaces available for analysis. The repetition rate was 5 Hz, with a count time of 40 s on the sample, and 40 seconds on the gas blank to allow the subtraction of the background signal. Typically, blocks of eight or nine glass shards and one MPI-DING reference glass were bracketed by the NIST612 glass adopted as the calibration standard. The internal standard applied was ^{29}Si (determined by EPMA-WDS analysis). In addition, MPI-DING reference glasses were used to monitor analytical accuracy (Jochum et al., 2006). LA-ICP-MS data reduction was performed in Microsoft Excel, as outlined in Tomlinson et al. (2010). Accuracies of LA-ICP-MS analyses of the MPI-DING , ATHO-G and StHs6/80-G reference glasses, were typically $\leq$ 5% for most elements measured. These measurements are provided in Supplementary Dataset-2 (SD-2), along with those of selected proximal eruption units and the full Fucino dataset.

3.4. Isotopic composition of strontium

Strontium (Sr) isotope compositions were determined on glass shards/pumices and mineral phases (i.e., feldspar, leucite, and pyroxene) from six selected samples, as summarised in Table 1. The rationale underlying the selection of these samples is similar to that for LA-ICP-MS analysis, i.e., obtaining a further geochemical characterization of the tephra from some major eruptions of the peri-Tyrrhenian volcanoes during MIS 11 period, in order to have, if any, an additional fingerprinting tool for strengthening their recognition/discrimination in distal settings. The variable fractions were handpicked under a binocular microscope. When possible, the cleanest crystals were selected, avoiding the presence of glass rinds attached. Before chemical dissolution, glass shards and pumices were acid leached three to five times to reduce alteration effects. Leaching was carried out each time by placing the beakers containing samples and high-purity 6 N HCl on a hot plate for 10 min. Feldspar and pyroxene separates coated by a thin film of glass were leached with high-purity 7% HF for 10 min in an ultrasonic bath. After leaching, samples were rinsed with Milli Q® H_2O and dissolved with high-purity HF–HNO_3–HCl mixtures. Sr was separated from the matrix through conventional ion-exchange procedures at the clean chemistry laboratory of the *Istituto Nazionale di Geofisica e Vulcanologia, Osservatorio Vesuviano*. Sr blank was on the order of 0.3 ng during chemistry processing.

Sr isotopic compositions were determined by thermal ionization mass spectrometry (TIMS) at DiSTAR (Naples, Italy), using a Thermo Scientific Triton Plus mass spectrometer equipped with one fixed and eight adjustable Faraday cups. $2\sigma_{mean}$, i.e., the standard error with N = 150, was better than ± 0.000008 for all Sr measurements. Measured $^{87}Sr/^{86}Sr$ ratios were normalized for within-run isotopic fractionation to $^{88}Sr/^{86}Sr$ = 8.37521. During the period of isotopic data collection,

replicate analyses of NIST–SRM 987 ($SrCO_3$) international reference standard were carried out to check for external reproducibility at 2σ level (where σ is the standard deviation of the standard results, according to Goldstein et al., 2003). No correction has been applied to the measured $^{87}Sr/^{86}Sr$ values, since the mean measured value of $^{87}Sr/^{86}Sr$ for NIST–SRM 987 standard was 0.710248 ± 0.000006 (2σ, N = 17), which is indistinguishable from the recommended value of $^{87}Sr/^{86}Sr$ = 0.710248 (Thirlwall, 1991).

3.5. $^{40}Ar/^{39}Ar$ geochronology

In order to improve the chronology of the investigated interval of the F4-F5 record, three new $^{40}Ar/^{39}Ar$ datings were performed on TF-85 and TF-117 samples, correlated to the Villa Senni and Pozzolane Nere eruptions, respectively (Giaccio et al., 2019), and on a sample of the proximal Pozzolane Nere (PN) unit collected from the above-mentioned outcrop in Rome City (Table 1). Samples were sieved and cleaned in distilled water, while undesirable magnetic crystals were removed by magnetic separation. Approximately thirty crystals were selected from each sample and loaded into an aluminium disk in three individual pits. All crystals from the individual samples were irradiated for 120 min in the Cd-lined, in-core CLICIT facility of the Oregon State University TRIGA reactor (IRR CO002). Interference corrections were based on the nucleogenic production ratios given in Renne et al. (2015). After irradiation, samples were transferred into a copper sample holder and loaded individually into a differential vacuum Cleartan© window. All measurements were performed in the LSCE $^{40}Ar/^{39}Ar$ facility (France). Detailed analytical procedures can be found in Nomade et al. (2010). Single crystals were fused individually using a 25 Watts Synrad CO_2 laser at about 10 to 15 % of the nominal power. Extracted gas was then purified for 10 min by two hot GP 10 and two GP 50 getters (ZrAl). Argon isotopes (^{40}Ar, ^{39}Ar, ^{38}Ar, ^{37}Ar and ^{36}Ar) were successively measured using a VG 5400 mass spectrometer equipped with an electron multiplier (Balzer SEV 217 SEN) coupled with an ion counter. Each argon isotope measurement consisted of 20 cycles of peak-hopping. Neutron fluence J for each sample was calculated-using co-irradiated Alder Creek sanidine standard (ACs at 1.1891 Ma; Niespolo et al., 2017) and the K total decay constant of Renne et al. (2011). This calibration produces ages independent of the astronomical tuning. J-values are the followings: TF-85 (Villa Senni) = 0.00053020 ± 0.00000053, TF-117 (Pozzolane Nere) = 0.00052950 ± 0.00000053 and PN = 0.00053260 ± 0.00000059. Mass discriminations were monitored by analysis of air pipette throughout the analytical period, and relative to a $^{40}Ar/^{36}Ar$ ratio of 298.56 (Lee et al., 2006). Procedural blank measurements were achieved after every two or three unknown samples. For 10 min times of isolation typical backgrounds are about 2.5-4.0 x 10^{-17} and 5.0 to 7.0 x 10^{-19} moles for ^{40}Ar and ^{36}Ar, respectively.

3.6. Age-depth modelling

The age model and corresponding 95%-confidence interval were both obtained using the Bacon software (Blaauw and Christen, 2011) written in the open-source statistical environment R (R Core Team, 2017).

To accommodate large differences in the sedimentation rate occurring during the investigated interval, we split the record into three sedimentary zones, A to C. Zone boundaries are defined through a preliminary evaluation of changes in sedimentary facies and on the availability of the dated points. The definition of sedimentary facies is based on the analysis of the composite profile derived by stacking consecutive core images acquired by the ITRAX core scanner (Giaccio et al., 2019). For each interval, the mean sedimentation rate is estimated by dividing the thickness of the interval for the time span elapsed between the deposition of the youngest and oldest dated tephra layers bracketing the interval, or at least, a large part of it. In the case of multiple dated layers in close stratigraphic position, we choose those featuring the most accurate dating. Sedimentary intervals and estimated mean sedimentation rates are as follows:

- Zone A: 80.520 – 91.810 m, 33.33 cm/kyr
- Zone B: 91.810 – 95.950 m, 30.30 cm/kyr
- Zone C: 95.950 – 98.100 m, 4.76 cm/kyr

These zones do not represent homogeneous sedimentary facies; however, they represent the most accurate approximation of long term (>4 kyr) changes in mean sedimentation rate that can be made based on currently available tephrochronological information.

4. Results

4.1. Depositional and sedimentological features of the Fucino tephra succession

Tephra horizons in the Fucino lacustrine succession occur as discrete layers of ash with variable thickness (Table 2) and grain-size, well separated from each other by fine lake sediments (marl) (Fig. 5). Despite a slight bioturbation and/or mechanic disturbance related to the drilling operation (Fig. 5), each tephra layer shows distinctive lithological (i.e., grain-size, shape, colour, vesicularity pattern and textural features of the juvenile clasts, type, and assemblage of the crystal and lithic components) and geochemical (glass-WDS major element composition) features. These circumstances are verified also in the case of closely clustered tephra layers, i.e., each layer forming the cluster presents its own distinctive lithological and geochemical characteristics with respect to the adjacent ones. In some cases, tephra layers are also characterised by a sharp lower boundary and by an upsection lithological zonation (e.g., TF-126; Fig. 5). These features indicate that tephra layers are undoubtedly primary fallout deposits and that post-depositional processes are negligible and did not affect the integrity of the tephra succession.

4.2. Tephra lithology and glass composition

4.2.1. Data summary

The thickness and main lithological features of the 32 Fucino tephra and proximal volcanic units are summarized in Tables 2 and 3, respectively. Full glass compositions are provided in Supplementary Dataset-1 (SD-1), while their classification according to the total alkali vs silica (TAS) diagram (Le Maitre et al., 2002) is shown in Fig. 6. Description of the geochemistry (i.e., major, minor and trace elements and Sr-isotopes) of the volcanic glasses is given in the following sections.

4.2.2. Major and minor elements

In the TAS diagram, the analysed tephra layers can be conveniently divided into three compositional groups (CGs; see also Table 2 for a classification summary). CG-1 (green area in Fig. 6) comprisestwo tephra layers (i.e., TF-100 and TF-108), plus the previously investigated TF- 85, TF-117 and TF-118 layers (Giaccio et al., 2019), all displaying a K-foiditic composition. CG-2 (light-orange area) includes twenty-one F4-F5 tephra, plus two proximal units (TSP-2 and TSP-3), and the Riano R-1 tephra, which are classified as potassic phonotephrites, tephriphonolites, phonolites, latites and trachytes, each being often variable in composition and covering two or more fields of the TAS diagram (Fig. 6). Finally, CG-3 (blue area) includes six F4-F5 tephra (i.e., TF-99, TF-109, TF-114, TF-115, TF-116 and TF-125), and two proximal units (TSP-1/Vico α and TSP-4), which are phonolites-trachytes-rhyolites, trachytes-rhyolites, and rhyolites. Although partially overlapping with CG-2 (Fig. 6), CG-3 tephra layers are clearly distinguishable owing to their distinctive rhyolitic components.

4.2.3. Trace elements

The full trace element glass dataset of the tephra samples can be

Table 2
Main lithological, mineralogical, and geochemical features of the 365-430 ka F4-F5 Fucino tephra.

Tephra	Thickness (cm)	Composite depth (m)	Core section and depth (cm)	CG	Lithology			Rock type
					Juvenile clasts	Minerals	Lithic content	
TF-85*	14.00	80.520	F5-49 74-88	*ND*	Black-brown scoria	Lc>bmca>cpx	Poor	K-f
TF-88	1.25/ 2.00	83.770	F4-51 131-133/ F5-51 65-66	CG-2	White pumice and grey-brown scoria	Kfs>cpx>bmca	Poor	ph-tr
TF-89	2.00	84.168	F5-51 107-109	CG-2	Grey scoria	Kfs>cpx>bmca	Poor	ph
TF-90	2.00	84.388	F5-51 130-131	CG-2	Black-grey scoria	Kfs>cpx>bmca	Rich	tr
TF-93	0.90	86.140	F4-53 51.3-52.2/ F5-52 149-150	CG-2	White pumice	Kfs>cpx	No	tph-ph
TF-94	0.75	86.853	F4-53 53.6-54.6	CG-2	White pumice	Kfs	No	ph-tr
TF-96	1.20	87.166	F4-53 85-86.2	CG-2	White pumice and grey scoria	Kfs>cpx	Poor	ph
TF-97	2.50	87.470	F4-53 110-112	CG-2	Grey scoria	Kfs>bmca	Poor	lat
TF-98	1.00	87.575	F4-53 119-120	CG-2	Grey scoria and whitish pumice	Kfs>bmca	Poor	lat-tph-ph-tr
TF-99	1.00	87.677	F4-53 128-129	CG-3	Highly vesicular white pumice and brown scoria	Kfs>bmca	Poor	K-tr-rhy
TF-100	6.75	88.045	F5-54 0-4.5	CG-1	Dense black scoria	Lc	Poor	K-f
TF-102	2.00	90.230	F4-55 58-60/ F5-54 125-126	CG-2	Poorly vesicular black scoria	Kfs>Lc>bmca	Poor	t-pht
TF-103	3.00	90.485	F4-55 83-86/ F5-54 133-134.2	CG-2	Poorly vesicular black scoria	Kfs>Lc>bmca	Poor	pht-tph
TF-104	2.00	90.560	F4-55 92-93/ F5-54 142-144	CG-2	Poorly vesicular grey scoria	Kfs>Lc>bmca	Poor	pht-tph
TF-106	1.40	90.860	F4-55 123-124.4	CG-2	Poorly vesicular grey scoria	Kfs>Lc>bmca	Rich	trb-pht-tph-sho
TF-107	2.00	91.620	F4-56 29-31/ F5-55 57.2-59	CG-2	Moderately vesicular whitish pumice and poorly vesicular greyish scoria	Kfs>bmca>cpx	Rich	ph-tr
TF-108	3.00	93.650	F5-56 110-113	CG-1	Dense, leucite-bearing black scoria	Lc	No	K-f
TF-109	3.00	93.690	F5-56 114-117	CG-3	Highly vesicular white pumice and greyish scoria	Kfs>bmca	Poor	K-ph-tr-rhy
TF-110	2.00	93.810	F5-56 126-128	CG-2	Highly vesicular white pumice and greyish scoria	Kfs>bmca	Poor	ph-tr
TF-111	3.00	93.885	F4-57 47-50	CG-2	Highly vesicular white pumice	Kfs>bmca	Very poor	ph-tr
TF-114	2.00	94.166	F4-57 77-79	CG-3	Highly vesicular white pumice and greyish scoria	Kfs>bmca>cpx	Poor	K-tr-rhy
TF-115	2.00	94.211	F4-57 81-83	CG-3	Highly vesicular white pumice	Kfs>bmca>cpx	Poor	K-tr-rhy
TF-116	2.00	94.251	F4-57 85-87	CG-3	Highly vesicular white pumice	Kfs>bmca>cpx	Poor	K-ph-tr-rhy
TF-117*	9.00	95.130	F4-57 151-152/ F5-57 0-7	*ND*	Poorly vesicular leucite-bearing black scoria	Lc>cpx	Poor	K-f
TF-118*	5.50	95.290	F5-57 16-23	*ND*	Poorly vesicular leucite-bearing black scoria	Lc	Poor	K-f
TF-120	2.00	95.540	F5-57 45-47	CG-2	Highly vesicular white pumice	Kfs>bmca	Very poor	ph-tr
TF-121	8.00	95.910	F5-57 77-85	CG-2	Poorly vesicular greyish-brownish scoria	bmca>Kfs>Lc	Poor	tph-ph-tr
TF-122	1.00	95.930	F5-57 85-86	CG-2	Dense, leucite-bearing brown scoria	Kfs>bmca>Lc	Poor	tph-ph-lat-tr
TF-123	5.50	96.005	F5-57 87-94	CG-2	Poorly vesicular black scoria	Lc>cpx>Kfs> bmca	Very rich	pht-tph
TF-124	0.75	96.155	F5-57 107-110	CG-2	Poorly vesicular black scoria and whitish pumice	Lc>cpx>bmca	Rich	sho
TF-125	3.50	96.775	F5-58 16-19.5	CG-3	Highly vesicular white pumice	Kfs>bmca>cpx>op	Poor	K-ph-tr-rhy
TF-126*	2.00	97.250	F5-58 64-66	*ND*	Highly vesicular white (base) and honey (top) pumice	Kfs>bmca>cpx>op	Poor	ph-tr

* =EPMA data in Giaccio et al. (2019); *ND*=Not determined in this study. Rock type abbreviations: K- = potassium- (suffix); f = foidite; ph = phonolite; tr = trachyte; tph = tephriphonolite; lat = latite; rhy = rhyolite. Mineral abbreviations: Kfs = K-feldspar; bmca = black mica; cpx = clinopyroxene; Lc = leucite; op = opaques. CG = compositional group (see Fig. 6).

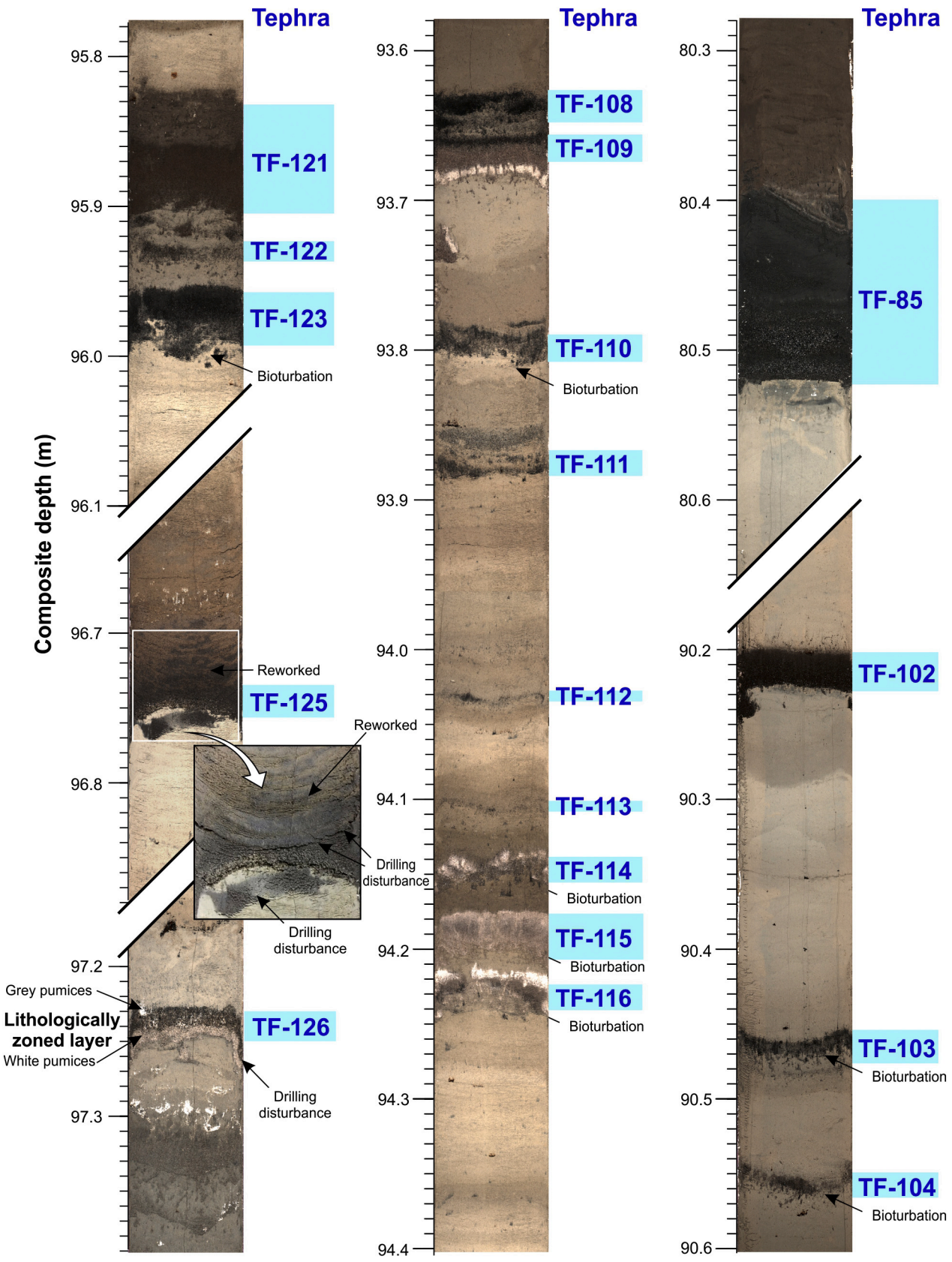

Fig. 5. Representative, selected intervals of Fucino core sections, showing the general sedimentological and lithological features of the investigated tephra.

Table 3
Geochemical and mineralogical data summary of the investigated proximal units.

Outcrop/ Location	Coordinates	Unit	Volcanic source	Lithology		Rock type
				Juvenile clasts	Minerals	
Tuscania-San Pietro	42° 24' 43.32" N – 11° 52' 45.13" E	Casale delle Piane	Vulsini	Highly vesicular dark grey, Kfs+bmca-bearing scoria	Kfs>bmca	Ph
		Vico α	Vico	Highly vesicular white, Kfs+bmca-bearing pumice and grey scoria	Kfs>bmca>cpx	K-tr-rhy
		TSP-2	Vulsini	Moderately vesicular grey Kfs-bearing pumice	Kfs>cpx	Ph
		TSP-3 (PF-0?)	Vulsini	Highly vesicular white, Kfs+bmca-bearing pumice	Kfs>bmca>cpx	Ph
		TSP-4	Vico	Reddish (thermally altered) Kfs-bearing pumice	Kfs>cpx	K-tr-rhy
Riano	42° 05' 24.06" N – 12° 31' 57.43" E	Riano R-1	*ND (Sabatini?)*	Blackish ash	Kfs>cpx>lc	Ph-tph-lat
Rome	41° 50' 44.74" N – 12° 28' 40.56" E	Pozzolane Nere	Colli Albani	Lc-bearing black scoria	Lc>cpx>bmca	K-f

ND=undetermined. Rock type abbreviations: K- = potassium- (suffix); f = foidite; ph = phonolite; tr = trachyte; tph = tephriphonolite; lat = latite; rhy = rhyolite. Mineral abbreviations: Kfs = K-feldspar; bmca = black mica; cpx = clinopyroxene; lc = leucite.

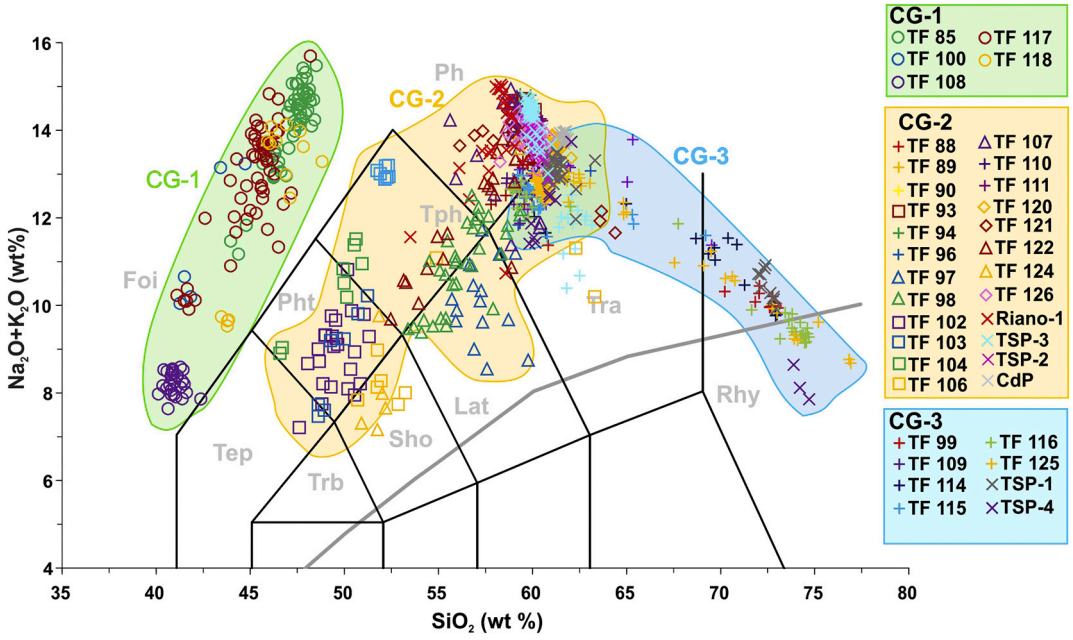

Fig. 6. *Total alkali vs silica* (TAS) classification diagram (Le Maitre et al., 2002). The thirty-two F4-F5 MIS11 tephra and the proximal pyroclastic units plot in three compositional groups (CG-1, CG-2 and CG-3). Data source: glass-WDS of TF-85, TF-117, TF-118 and TF-126: Giaccio et al. (2019); glass-WDS compositions of all others Fucino tephra and proximal pyroclastic units: this study. Foi=foidite; Pht=phonotephrite; Tph=Tephriphonolite; Ph=phonolite; Rhy=rhyolite; Tra=Trachyte; Lat=latite; Sho=Shoshonite; Trb=trachybasalt; Tep=tephrite; CdP=Casale delle Piane unit (Tuscania-San Pietro section).

found in Supplementary Dataset-2 (SD-2).

Phonolite tephra layers TF-107 and TF-111 (CG2) display relatively heterogeneous, yet largely overlapping trace element concentrations. For instance, Th contents range from 67-91 ppm and 66-95 ppm, respectively (Fig. 7a). Despite the variability in absolute incompatible trace element concentrations, ratios of High Field Strength Element (HFSE) to Th in both TF-107 (Nb/Th = 0.39 ± 0.02; Ta/Th = 0.021 ± 0.001; Zr/Th = 5.5 ± 0.5 [2 s.d.]) and TF-111 (Nb/Th = 0.39 ± 0.03; Ta/Th = 0.021 ± 0.001; Zr/Th = 5.6 ± 0.3 [2 s.d.]) remain constant, and indistinguishable from one another, possibly implying a common volcanic source.

TF-116 belongs to CG3 and comprises phonolitic-trachytic to rhyolitic glasses. However, our trace element analyses derive from glass shards relating to the phonolite-trachyte end-member only. These TF-116 glasses are heterogeneous in terms of their trace element contents (e.g., 82-139 ppm Th; 31-55 ppm Nb; 469-718 ppm Zr) and are more enriched in incompatible trace elements than the overlying phonolitic tephra layers (TF-107 and TF-111) (Fig. 7a). Ratios of HFSE to Th in these glasses remain constant, including Nb/Th ratio (0.41 ± 0.04 [2 s.d.]), Ta/Th (0.020 ± 0.001 [2 s.d.]) and Zr/Th (5.3 ± 0.4 [2 s.d.]) which all remain largely consistent with the overlying tephra (TF-107 and TF-111) (Fig. 7b).

TF-125 also belongs to CG3, ranging from phonolitic-trachytic (mainly trachytic) to rhyolitic glasses, and this major element variability is captured by a large degree of trace element heterogeneity (e.g., 57-184 ppm Th; 1462-151 ppm Sr; 522-879 ppm Rb). Incompatible trace element concentrations observed in the phonolite-trachyte end-member glasses are consistent with TF-107 and TF-111 glasses. The TF-125 phonolite-trachyte glasses are more enriched in Sr, Ba and Eu relative to the rhyolitic end-member glasses, illustrating their compatibility during K-feldspar fractionation. Ratios of HFSE to Th in TF-125 glasses also differ between the phonolitic-trachytic (Nb/Th = 0.39 ± 0.2; Zr/Th = 5.5 ± 0.3; Hf/Th = 0.13 ± 0.005 [2 s.d.]) and rhyolitic (Nb/Th = 0.30 ± 0.3; Zr/Th = 2.7 ± 0.7; Hf/Th = 0.07 ± 0.01 [2 s.d.]) end-members. Moreover, HFSE to Th ratios in the rhyolitic glasses show more variability than those of the phonolite-trachyte glasses, particularly in terms of Zr/Th, where Zr becomes depleted, probably driven by zircon fractionation (Fig. 11a).

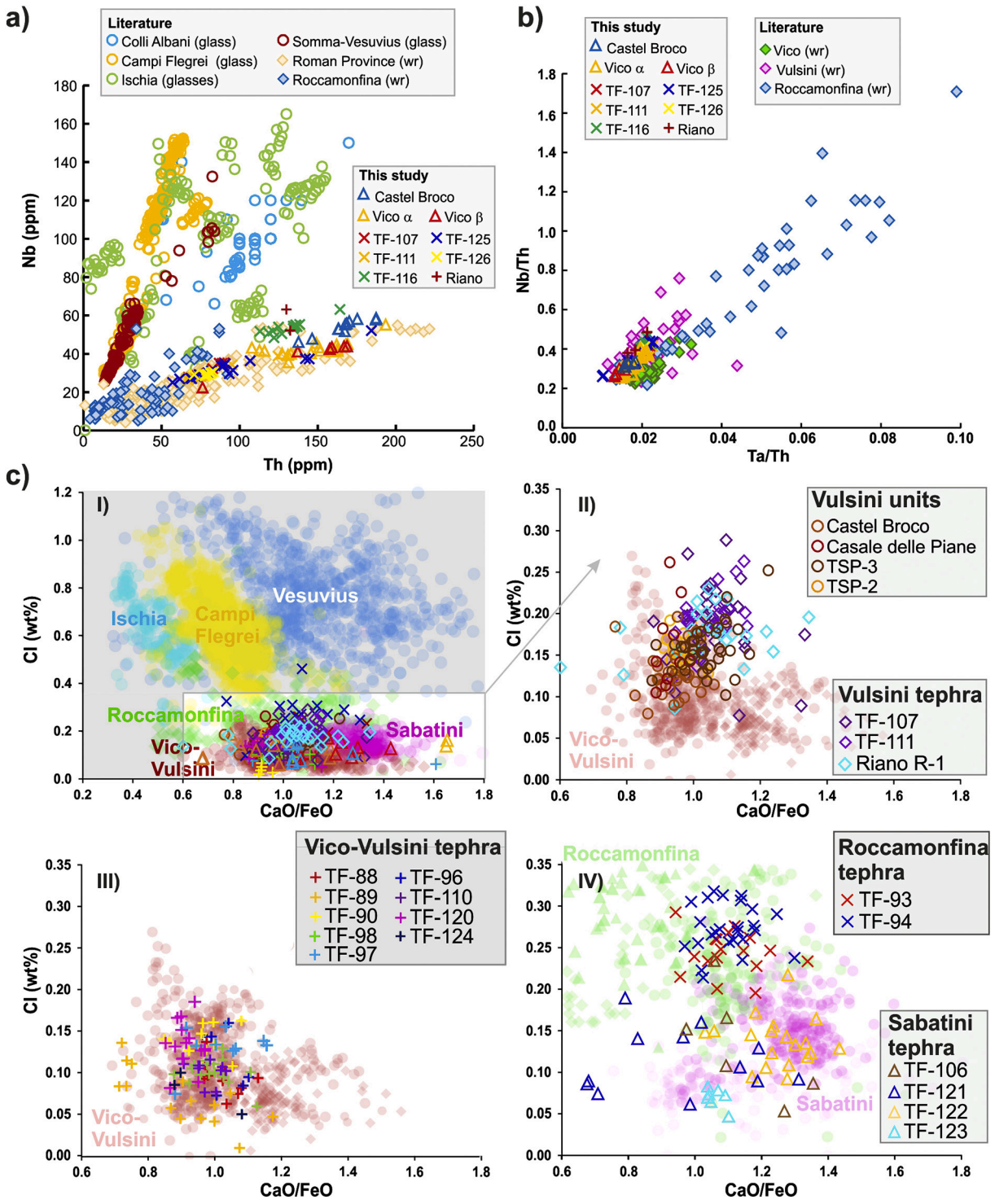

Fig. 7. Discrimination diagrams for F4-F5 tephra. a) Th vs Nb bi-plot of the investigated tephra compared with literature data for the glasses of Neapolitan (i.e., Campi Flegrei, Somma-Vesuvius and Ischia) and Colli Albani volcanoes, which are characterized by a higher Nb/Th ratio than Roman/northern Latium (Vulsini, Sabatini, Vico) and Roccamonfina volcanoes; the compositions of the four tephra are compatible with either a Latium or Roccamonfina origin. b) Ta/Th vs Nb/Th discrimination diagram for Roccamonfina and Latium Volcanoes; the four tephra here investigated are characterized by ratios compatible with either a Vulsini or Vico origin. Data source: TF-107, TF-111, TF-116 and TF-126: this study; literature data of whole rock (wr) compositions of products from Latium volcanoes and Roccamonfina: Lustrino et al. (2011) and references therein; glass composition of products from Colli Albani: Cross et al., 2014; Ischia: Tomlinson et al., 2014; Campi Flegrei: Smith et al., 2011, Tomlinson et al., 2012; Somma-Vesuvius: Tomlinson et al., 2015. c) CaO/FeO vs Cl discriminating diagram of the volcanic sources of the Italian potassic trachyte-phonolite and tephriphonolite tephra (modified after Giaccio et al., 2017) for the F4-F5 and Riano R-1 tephra here shown in the Vulsini group for comparison. The compositions of the Vico and Vulsini pyroclastic units collected at Tuscania-San Pietro section, are also shown.

TF-126, previously reported in Giaccio et al. (2019), has a phonolite-trachyte composition and plots in CG-2. Incompatible trace element concentrations reveal a relatively homogeneous composition (e.g., 79 ± 7 ppm Th; 29 ± 1 ppm Nb; 393 ± 29 ppm Zr [2 s.d.]), and as such the ratios of HFSE to Th show very limited variability, consistent with the homogeneous major element composition of the tephra (e.g., Nb/Th = 0.37 ± 0.01; Ta/Th = 0.020 ± 0.001; Zr/Th = 4.9 ± 0.5 [2 s.d.]).

Concerning the proximal pyroclastic deposits, the Castel Broco phonolitic glasses show a slight heterogeneity and are anriched in certain incompatible trace elements (e.g., 138-188 ppm Th [Fig. 7a]; 627-750 ppm ppm Zr; 30-42 ppm Y). Ratios of HFSE to Th remain constant within these glasses (Nb/Th = 0.32 ± 0.02; Zr/Th = 4.1 ± 0.5 [2.d.]).

Vico α trace element glass compositions are extremely heterogeneous (75-194 ppm Th; 1303-87 ppm Sr; 248-955 ppm Rb), consistent with their major element variability ranging from phonolite-trachytes to rhyolites (Pereira et al., 2020). The less evolved phonolite-trachyte glasses are more enriched in Sr, Ba and Eu relative to the rhyoltic end-member glasses, where these elements clearly behave compatibly during K-feldspar fractionation. Ratios of HFSE to Th in these glasses also differ between the phonolitic-trachytic (Nb/Th ~ 0.38; Zr/Th ~ 5.6) and rhyolitic (Nb/Th ~ 0.29; Zr/Th = 1.9-5.6) end-members.

Vico β analyses focused on the predominantly rhyolitic sub-unit (VIG-3; Pereira et al., 2020); these rhyolitic glasses are relatively heterogeneous in the case of some incompatible elements (e.g., 137-169 ppm Th; 948-995 ppm Rb). Sr, Ba and Eu contents are more depleted in the rhyolitic glasses of Vico β than in Vico α.

Only two successful analyses were obtained from the phonolitic Riano R-1 tephra, but the compositions are internally consistent for most incompatible elements, with the noticeable exception being the variable Nb content leading to a Nb/Th ratio of 0.39-0.48. Levels of incompatible trace element enrichement in the R-1 glasses (of unknown source area) appear more akin to those of Vulsini (e.g., Castel Broco), rather than Vico (Fig. 7b). Unfortunately, available trace element data for Sabatini are scant and cannot be considered here for comparison.

Ratios of HFSE to Th are seemingly useful when evaluating the origin of the five tephra layers characterised here in the context of peri-Tyrrhenian potassic volcanism, particularly given the limited trace element glass data available for some regional volcanic sources, and thus a reliance on whole-rock datasets, which are not always directly comparable to volcanic glass data (e.g., Tomlinson et al., 2012). The Nb/Th ratios of the five Fucino layers analysed (TF-107, TF-111, TF-116, TF-125 and TF-126) clearly preclude an origin from the Neapolitan volcanic zone (e.g., Campi Flegrei, Ischia, Vesuvius), where Nb values are far higher at overlapping Th content, and Nb/Th ratios are typically > 1.5 (glass datasets; Fig. 7a).

TF-107, TF-111, TF-116, TF-125 and TF-126 all have incompatible trace element concentrations and ratios of HFSE to Th compatible with the published analyses of the Latium and Roccamonfina volcanics (Fig. 7a). However, Roccamonfina appears an unlikely source of the five Fucino tephra layers owing to its typically higher Ta/Th ratios (Fig. 7b). In the investigated timespan, Colli Albani exclusively erupted K-foidites (CG-1) and can easily be discounted as the possible volcanic source of these Fucino layers, thus leaving the remaining Latium (Vulsini, Sabatini and Vico) volcanoes as the most obvious candidates. Indeed, ratios of HFSE to Th observed in TF-107, TF-111, TF-116, TF-125 and TF-126 are broadly consistent with those from published whole-rock (e.g., Lustrino et al., 2011 and references therein) and our preliminary glass (reported above) data from Vulsini and Vico (although similarities to Sabatini products cannot be excluded owing to a paucity of data).

4.2.4. Strontium (Sr) Isotopes

Results for each analysed sample, along with associated uncertainty (2σ), are presented in Table 4, while a comparison with literature values for proximal Vulsini, Vico, Sabatini and Colli Albani products, erupted in the 430-350 ka time interval, is shown in Fig. 8. In literature there are very few Sr-isotopic data (i.e., just one from Perini et al., 2004) for the Vico activity in the investigated 430-365 ka time interval, thus making it challenging to identify eruptive units from this volcano based on Sr-isotope signature. This knowledge gap should be filled in the future to better constrain the attribution of several TF tephra layers.

$^{87}Sr/^{86}Sr$ values were measured on either pyroxene or feldspar minerals on each sample, except for TSP-3, for which a matrix (pumice) measurement was obtained as well. For sample TF-85 a mineral fraction enriched in leucite crystals was analysed. The lowest value (0.709507) was measured on pumice fragments from the TF-111. Pyroxenes and feldspar from TF-111 are featured by $^{87}Sr/^{86}Sr$ ratio of 0.710149 and 0.710671, respectively. The highest value (0.71120) was mesured on feldspars of TSP-3. Therefore, all the measured ratios suggest a Roman province origin for the investigated tephra (Fig. 8). Minerals from TF-85=Villa Senni have a $^{87}Sr/^{86}Sr$ ratio of 0.71043, which agrees with literature data (Gaeta et al., 2016). Measured values of proximal units from Vulsini (i.e., TSP-3 and Castel Broco) range up to 0.71125 (TSP-3 fsp), thus slightly extending the literature range for Vulsini (Fig. 8). The Riano R-1 tephra value of 0.71081 is broadly compatible with either a Sabatini or Vulsini source (rather than Vico). Finally, TF-126 has $^{87}Sr/^{86}Sr$ ratio of 0.71111 that would support the attribution of this tephra to a Vulsini eruption, as already suggested by Giaccio et al. (2019).

Overall, the measured $^{87}Sr/^{86}Sr$ values do not provide conclusive evidence to be used as correlation tool for the Latium volcanoes, except for perhaps Vico: indeed, the amount of literature data on proximal samples is still too limited to allow solid attributions to a specific volcano. Nevertheless, the Latium volcanics, as previously known and confirmed by our data, show similar $^{87}Sr/^{86}Sr$ ranges, which are different from the products of other Italian volcanoes (e.g., Peccerillo, 2017). Thus, $^{87}Sr/^{86}Sr$ ratio can support an ascription of a tephra of unknown origin to the Latium volcanism, narrowing down the list of possible sources.

Table 4
$^{87}Sr/^{86}Sr$ ratio values of the selected four Fucino tephra and three proximal units.

Tephra/ sample	Setting	Volcano	Glass composition	Analysed material	$^{87}Sr/^{86}Sr$	2σ
TF-85	Distal	Colli Albani	K-foidite	lc	0.710430	±0.000007
TF-107	Distal	Unknown	Phonolite	fsp	0.710851	±0.000006
TF-111	Distal	Vulsini-Vico	Phonolite	pum	0.709507	±0.000006
				fsp	0.710671	±0.000006
				cpx	0.710149	±0.000007
TF-126	Distal	Vulsini	Phonolite	fsp	0.711105	±0.000007
Castel Broco	Proximal	Vulsini	Phonolite	cpx	0.710960	±0.000006
				fsp	0.710965	±0.000006
TSP-3	Proximal	Vulsini	Phonolite	pum	0.711199	±0.000007
				fsp	0.711245	±0.000006
Riano R-1	mid-proximal	Vulsini	Phonolite	K-fsp	0.710810	±0.000007

Abbreviations: K-fsp=K-feldspar; fsp=feldspar; cpx=clinopyroxene; pum=pumice.

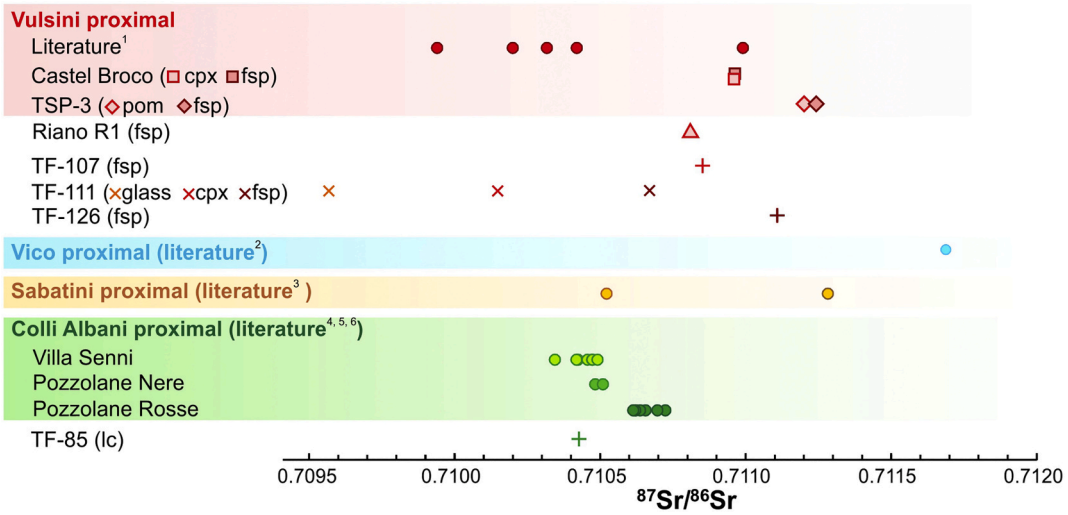

Fig. 8. $^{87}Sr/^{86}Sr$ ratio values of selected tephra layers and literature proximal references for the 430-350 ka time interval. Abbreviations: cpx=clinopyroxene; fs=feldspar; pom=pumice. Data source: TF-85, TF-107, TF-111, TF-126, Castel Broco, TSP-3, Riano R-1: this study; literature data: [1] Peccerillo (2017); [2] Perini et al. (2004); [3] Sottili et al. (2019); [4] Gaeta et al. (2006, 2016); [5] Giaccio et al. (2013a).

4.3. $^{40}Ar/^{39}Ar$ age of TF-85, TF-117 and Pozzolane Nere

The results for each dated deposit are presented as probability diagrams in Fig. 9. Reported uncertainties are analytical at a 95.5% of confidence limit (J-value included), as well as fully propagated ones. Detailed analytical data are available in Supplementary Dataset-3 (SD-3).

TF-85 (Villa Senni): A total of eleven leucite single crystals were dated. All crystals yielded an undistinguishable age, allowing us to calculate a meaningful weighted mean age of 365.8 ± 1.4/1.8 ka (MSWD =0.7, P=0.7).

TF-117 (Pozzolane Nere): Nine leucite crystals were individually dated. All crystals yielded an undistinguishable age, allowing the straightforward calculation of a weighted mean age of 407.7 ± 4.0/4.4 ka (MSWD =0.04, P=1.0).

Pozzolane Nere (Rome proximal setting): Twelve leucite crystals were dated. They all share a similar age within uncertainties, allowing us to calculate a statistically meaningful weighted mean age of 408.5 ± 1.2/2.0 ka (MSWD =0.8, P=0.6). In Fig. 9 we also combined the 21 single leucite ages obtained on the Pozzolane Nere from both the

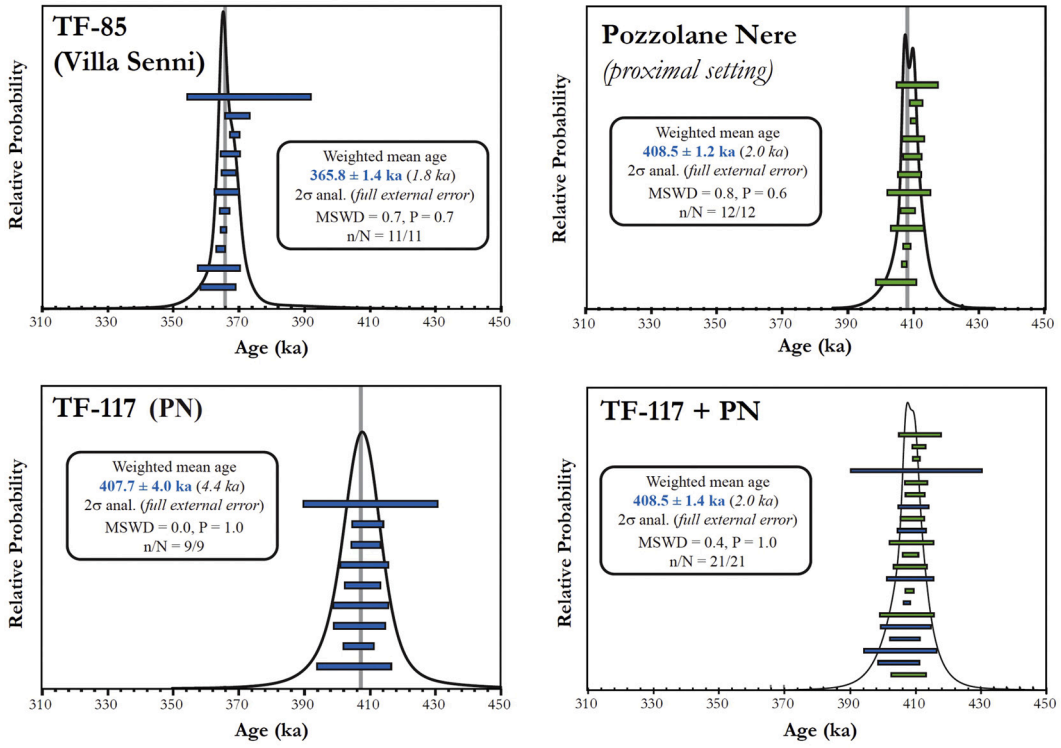

Fig. 9. $^{40}Ar/^{39}Ar$ on single grain results (leucite crystals), presented as probability diagrams, for TF-85 (Villa Senni), TF-117 (Pozzolane Nere) and Pozzolane Nere (Rome proximal setting). A combined weighted mean age of TF-117/Pozzolane Nere is then proposed. Ages are calibrated according to Renne et al. (2011) total ^{40}K decay constant and from the optimization calibrated age of 1.1891 Ma for the flux standard ACs-2 (Niespolo et al., 2017). Individual crystal error bars are at 1σ of uncertainties.

proximal deposits (PN) and distal equivalent (TF-117), allowing us to propose a new, more precise weighted mean age of 408.5 ± 1.4/2.0 ka (MSWD =0.4, P=1.0) for the Pozzolane Nere regional marker.

5. Discussion

5.1. Volcanic sources of tephra layers from core F4-F5

5.1.1. K-foidites (CG-1)

The K-foidite compositions of the two tephra layers from CG-1 (Fig. 6) are distinctive within the context of Quaternary Italian volcanism, being limited to a few eruptive sources (e.g., Peccerillo, 2017). Among these, the Colli Albani volcanic district has produced and dispersed several K-foiditic tephra (e.g., Marra et al., 2009) from moderate to major eruptions that have been traced in both medial and distal settings (e.g., Giaccio et al., 2013a, 2014; Petrosino et al., 2014b; Leicher et al., 2016). Consequently, Colli Albani should be regarded as the most likely source of TF-100 and TF-108.

5.1.2. Potassic phonotephrites, tephriphonolites, phonolites, trachytes, trachyte-phonolites and latites (CG2)

The glass geochemical compositions of tephra from CG-2 (i.e., potassic phonotephrites, tephriphonolites, phonolites, trachytes, trachyte-phonolites and latites) are quite common and shared by almost all peri-Tyrrhenian potassic volcanoes of central-southern Italy (e.g., Peccerillo, 2017). However, considering the time interval investigated here (430-365 ka), we can confidently exclude the Neapolitan volcanoes (i.e., Ischia, Procida, Campi Flegrei and Somma-Vesuvius) as possible sources of any of the twenty-one CG-2 tephra layers, since the so-far oldest known eruption from these volcanoes is significantly younger (i.e., the ~289.6 ± 1.9 ka Seiano Ignimbrite; De Vivo et al., 2001; Rolandi et al., 2003; Belkin et al., 2016; Fig. 3). Nevertheless, a geochemical fingerprinting approach remains essential, as there is always the possibility that Neapolitan volcanism may be extended deeper in time with future investigations, particularly since some distal archives seem to suggest an older activity in the region (e.g., Giaccio et al., 2014; Petrosino et al., 2015).

To discriminate the source of this large group of tephra, we employed the CaO/FeO vs Cl classification diagram (Giaccio et al., 2017), which defines quite distinct fields for the individual sources of the Latium and Neapolitan pyroclastic rocks with a SiO_2 content ranging from 52 wt% to 67 wt% (Fig. 7c-I). This confirms the lack of products from the Neapolitan volcanoes and points to the Latium or Roccamonfina volcanoes as the only plausible sources of 17 out of 21 - i.e., those with 52 < SiO_2 wt% < 67 - CG-2 Fucino tephra (Fig. 7c-I). Furthermore, the trace element compositions of all the phonolite and trachyte glass shards from the CG-2 (and CG-3) tephra layers also clearly precludes the Neapolitan volcanoes as possible eruptive sources (Fig. 7a-b).

Vulsini – In the CaO/FeO vs Cl diagram, TF-107 and TF-111 plot at the boundary between Vulsini-Vico (northern Latium) and Roccamonfina fields (Figs. 7c-II and 7c-IV), making the attribuition to one of these sources not straightforward. However, a slight difference in Cl content between Vulsini-Vico and Roccamonfina tephra, clustering between 0.05 wt% up to 0.20 wt% and 0.25-0.33 wt%, respectively (cfr. Fig. 7c-II with 7c-IV), makes the distinction between the two volcanic sources still tenable. More importantly, in this diagram, TF-107 and TF-111 overlap the composition of the Vulsini proximal pyroclastic units analysed in the present study (especially TSP-3 Pumice fall from Tuscania-San Pietro section; Fig. 7c-II), suggesting that Vulsini is the most probable source of these tephra layers. More detailed, individual tephra correlations are discussed below (see section *5.2.3.3.*) and fully support this volcanic source attribution. Finally, despite the paucity of the proximal reference dataset, $^{87}Sr/^{86}Sr$ ratios also support a Vulsini origin for these two tephra layers (Fig. 8), while the trace elements confirm an origin from northern Latium (Vulsini or Vico) volcanoes (Fig. 7b).

The Riano R-1 tephra (404.7 ± 5.0 ka; Marra et al., 2018), for which a clear stratigraphic/compositional correlation is still lacking, also matches the compositions of the Vulsini units analysed in this study. It is therefore compatible with a possible distal origin from Vulsini, rather than from the nearest Sabatini source.

Vulsini-Vico – Cl contents and CaO/FeO ratios of TF-88, TF-89, TF-90, TF-96, TF-97, TF-98, TF-110, TF-120 and TF-124 are consistent with either Vico or Vulsini compositions, and thus do not allow a further discrimination between these two potential sources (Fig. 7c-III). However, a possible distinction is based on further oxides composition, as discussed in section 5.2.3.4.

Sabatini – According to the CaO/FeO vs Cl diagram, TF-106 and TF-122 can be related to the Sabatini Volcanic District based on the high (i.e., >1.15) CaO/FeO ratio (Fig. 7c-IV). TF-106, along with TF-102, TF-103 and TF-104, forms a well-defined cluster of tephra that share a similar phonotephritic composition (Fig. 6; SD-1) and lithology (Table 2). Therefore, though the CaO/FeO vs Cl discrimination diagram cannot be applied to TF-102, TF-103 and TF-104 owing to their SiO_2 content lower than 52 wt%, (Giaccio et al., 2017), they can be reliaby regarded as part of a cluster of eruptions from Sabatini. Although showing a more scattered composition in the CaO/FeO vs Cl diagram (Fig. 7c-IV), TF-121 can be attributed to the Sabatini as well, because of its close geochemical similarity with the directly underlying TF-122 layer (Fig. 5). Finally, TF-123 can be also likely attributed to the Sabatini, because of its homogenous composition in the CaO/FeO vs Cl diagram that matches a second well-defined compositional cluster of the Sabatini rock types (Fig. 7c-IV).

Roccamonfina – TF-93 and TF-94 can be confidently attributed to the Roccamonfina volcano, based on their relatively high Cl content (i.e., >0.25 wt%), and thus their clear position in the Roccamonfina field of the CaO/FeO vs Cl diagram (Fig. 7c-IV), which is quite distinctive with respect to the Latium volcanoes (Fig. 7c-IV).

5.1.3. K-rhyolites (CG-3)

The six tephra layers forming CG-3 (TF-99, 109, 114, 115, 116, 125; Fig. 6) show K-rich rhyolitic and trachy-rhyolitic compositions, which are quite unusual within the context of the peri-Tyrrhenian Quaternary Italian volcanism, and peculiar to Vico Volcano (e.g., Perini et al., 1997, 2000, 2003, 2004; Perini and Conticelli, 2002; Pereira et al., 2020), hence the most probable source of the Fucino CG-3 tephra layers.

In summary, based on distinctive chemical compositions, stratigraphic clues and lithological features and affinities, we propose an attribution of the Fucino tephra layers to the peri-Tyrrhenian potassic volcanoes, as summarized in Table 5.

5.2. Individual tephra correlation

5.2.1. Tephra from Colli Albani (CG-1).

TF-100 and TF-108 - These two K-foiditic tephra layers (CG-1), ascribed to the Colli Albani activity, occur between TF-85 and TF-117 (Fig. 2), which were attributed to the Villa Senni (365.8 ± 1.4 ka) and Pozzolane Nere (408.5 ± 1.4 ka) eruptions, respectively (Giaccio et al., 2019). The $^{87}Sr/^{86}Sr$ composition determined in this study for TF-85 further supports its attribution to the Villa Senni eruption. Indeed, $^{87}Sr/^{86}Sr$ ratios of the Colli Albani products show a strong time-

Table 5
Volcanic sources of the investigated Fucino tephra, inferred from glass chemical composition and lithological features.

Volcano	Fucino tephra
Vulsini	TF-107, TF-111
Vico	TF-99, TF-109, TF-114, TF-115, TF-116, TF-125
Vulsini or Vico	TF-88, TF-89, TF-90, TF-96, TF-97, TF-98, TF-110, TF-120, TF-124
Sabatini	TF-102, TF-103, TF-104, TF-106, TF-121, TF-122, TF-123
Colli Albani	TF-100, TF-108
Roccamonfina	TF-93, TF-94

dependent variability (Gaeta et al., 2006, 2016; Giaccio et al., 2013a) and the $^{87}Sr/^{86}Sr$ value obtained for TF-85 precisely matches that of Villa Senni (Fig. 8).

Considering the available chronological constraints and its relative proximity to the TF-117/Pozzolane Nere, TF-108 can be attributed to the post-caldera phase of the Pozzolane Nere eruptive cycle (*sensu* Gaeta et al., 2016), which is equivalent to the Centogocce fall succession of Giordano et al. (2006). In proximal settings, the Centogocce deposits consist of a series of scoria-lapilli fall beds and lava flows overlying the Pozzolane Nere deposits, emplaced in the 403.4 ± 5 ka - 396.4 ± 5 ka time interval (recalculated ages from Marra et al., 2009 and Gaeta et al., 2016). Unfortunately, no glass composition is available for this scoria fall succession and, therefore, we used the composition of TF-117/Pozzolane Nere for comparison (Fig. 10a). Furthermore, Pereira et al. (2020) have recently reported the occurrence, within the San Paolo Formation aggradational succession, of a tephra layer (SPF4), with a polymodal rhyolite, K-foidite and phonotephrite composition, interpreted as a reworked volcaniclastic layer containing both Vico and Colli Albani eruption products. Pereira et al. (2020) reported an age of 403.5 ± 4.2 ka for SPF4, which is consistent with the time interval (403.4 ± 5 ka - 396.4 ± 5 ka) covered by the Centogocce fall succession, despite a geochemical mismatch of TF-108 with SPF4 (Fig. 10a), which can be expected for multiple explosive and effusive eruptions occurred during a relatively long interval. Based on glass composition and stratigraphic position relatively to the TF-117/Pozzolane Nere, we attribute TF-108 to the Centogocce activity. The stratigraphic position of TF-100, between the TF-117/Pozzolane Nere and the TF-85/Villa Senni (Fig. 2), suggests an age substantially younger than the Centogocce equivalent TF-108. In spite of this, for its composition, which partially overlaps the wide composition field of the Pozzolane Nere (Fig. 10a), TF-100 could still be considered as part of the final stage of the Pozzolane Nere eruptive cycle.

5.2.2. Tephra from Vico (CG-3).

TF-125 – This tephra occurs in the lowermost portion of the F4-F5 record, ~50 cm upsection from TF-126 that was directly dated at 424.3 ± 3.2 ka (Giaccio et al., 2019). TF-125 is characterized by a heterogeneous phonolite-trachyte to rhyolite composition, with a silica content ranging from 59 to 77 wt% and an alkali content from 14 to 8 wt %. Recently, Pereira et al. (2020) published new glass geochemical compositions for the early-emplaced volcanics of Vico activity (Vico Period I; Perini et al., 2004), including Vico α and Vico β Plinian fall markers (Cioni et al., 1987), both with a dominant rhyolitic composition, along with the characterization of three minor events (i.e., Vico β_{top}, Vico γ and Vico δ; Cioni et al., 1987). In addition, Pereira et al. (2020) acquired very precise $^{40}Ar/^{39}Ar$ ages for Vico α (414.8 ± 2.2 ka), Vico β (406.5 ± 2.4 ka), Vico β_{top} (406.4 ± 2.0 ka) and Vico δ (399.7 ± 3.0 ka).

Using this updated geochemical dataset for the Vico Period I products, we found that TF-125 major element composition matches that of Vico α of Pereira et al. (2020) and of Tuscania-San Pietro TSP-1 (this study; Fig. 10b), and this correlation is further strengthened by the similarities in the trace element glass compositions obtained here for Vico α and TF-125 (Fig. 11a). Considering this geochemical affinity and its stratigraphic position between TF-126 (424.3 ± 3.2 ka) and TF-117/Pozzolane Nere (408.5 ± 1.4 ka), consistent with an age of 414.8 ± 2.2 ka, we can confidently correlate TF-125 to the Vico α Plinian eruption.

TF-116 and TF-115 – TF-116 is located less than 1 m upsection from TF-117, the latter dated at 407.7 ± 4.0 ka and correlated to the Pozzolane Nere eruption (Giaccio et al., 2019), which has been dated here more precisely at 408.5 ± 1.4 ka (Fig. 9). Like TF-125, this tephra is characterized by a heterogeneous trachytic-rhyolitic composition, with a dominant SiO_2-rich (>75 wt%) rhyolitic component, and a minor scattered phonolitic-trachytic one (58-68 wt% SiO_2), which is a distinctive, common feature of the Vico Period I units (Pereira et al., 2020). Trace element analyses (Fig. 7a-b) also support a Latium origin for this tephra. Specifically, the glass rhyolitic composition of TF-116 matches that of Vico β (Fig. 10c) that, along with its position on top of TF-117/Pozzolane Nere, allows us to correlate TF-116 to Vico β eruption (406.5 ± 2.4 ka; Pereira et al., 2020). Noteworthy, TF-116 contains a significant trachyte-phonolite component that is poorly represented or documented in proximal settings (Fig. 10c).

TF-115 tephra is found 2 cm above TF-116 and is characterized by a heterogeneous composition, consisting of a main phonolitic-trachytic component (SiO_2 59-66 wt%) and a minor SiO_2-rich (~69 wt%) rhyolitic one. These geochemical features allow unambiguous correlation to Vico β_{top} (Fig. 10c), consistent with the superposition of the tephra just on top of TF-116/Vico β. Furthermore, consistent with its strict stratigraphic proximity to TF-116/Vico β, the proximal Vico β_{top} has a $^{40}Ar/^{39}Ar$ age of 406.5 ± 2.4 ka that is indistinguishable from that of Vico β (Pereira et al., 2020). Noteworthy, Pereira et al. (2020) also pointed out that the combined glass composition of Vico β and Vico β_{top} is to some extent similar to that of Vico α, so that, in the absence of strong chronological and/or tephrostratigraphic constraints, the geochemical composition of the two units could be potentially confused. However, in the F4-F5 record, the TF-115 and TF-116 couplet occurs on top of the 408.5 ± 1.2 ka Pozzolane Nere tephra, well upsection from the Vico α correlative (TF-125). Furthemore, when dealing with sedimentary archives less constrained chronostratigraphically than Fucino, trace element analysis of the Vico eruption products may offer useful means to discriminate the distal equivalents of Vico α and Vico β. In fact, the phonolite-trachyte end-member glasses of TF-116/Vico β extend to greater levels of incompatible trace element enrichment with respect to TF-125/Vico α (Fig. 11a-left), whilst the analysis of proximal and distal Vico rhyolitic products reveals greater depletions in Sr associated with the Vico β tephra (Fig, 11a-right), likely induced by major K-feldspar fractionation. In conclusion, the general stratigraphic, chronological, and geochemical features of TF-116 and TF-115 consistently support their unambiguous attribution to Vico β and Vico β_{top}, respectively.

TF-114 - This tephra is separated from the underlying TF-115 by 2-cm-thick lacustrine sediments. It is characterized by a heterogeneous trachyte-rhyolite composition, with a silica content ranging from 60 to 73 wt% and an alkali content from 9 to 13 wt%, with a peculiar alkali vs silica pattern: indeed, first the alkali content increases with increasing SiO_2 from 60 to 65 wt%, then the alkali content decreases with increasing SiO_2 from 65 to 73 wt%. This peculiar pattern is also observed for Vico γ (Fig. 10d; Pereira et al., 2020). Since $^{40}Ar/^{39}Ar$ datings for Vico γ are not available, its age should be constrained by the bracketing Vico β_{top} (406.5 ± 2.4 ka) and Vico δ (399.7 ± 3.0 ka) units. More specifically, the stratigraphic position of TF-114/Vico γ closer to TF-115/Vico β_{top}, would indicate an age closer to 406.5 ± 2.4 ka.

TF-99 and TF-109 - TF-99 has a predominantly homogeneous rhyolitic composition (70-73 wt% of SiO_2) with a single trachytic shard (60 wt% SiO_2), while TF-109 is characterized by a heterogeneous trachytic composition (59-65 wt% SiO_2) with a minor rhyolitic component (one shard with ~69 wt% SiO_2; Fig. 12a). As stated in section 5.1.3, the occurrence of a rhyolitic component in these tephra makes their attribution to the Vico volcano quite straightforward, because it is the only known Middle Pleistocene peri-Tyrrhenian volcanic source that produced K-rich rhyolitic tephra. Indeed, in the TAS diagram, both tephra plot within the compositional field of the Vico α and Vico β Plinian eruptions (Fig. 12a).

Considering the stratigraphic position of TF-99 and TF-109 within the F4-F5 record, the most plausible candidate for at least one of these tephra layers would be Vico δ, dated at 399.7 ± 3.0 ka (Pereira et al., 2020). However, neither TF-99 nor TF-109 match Vico δ in composition (Fig. 12a). Although in the TAS diagram TF-109 would seem compatible with Vico δ, suitable bi-plot diagrams show significant differences on several oxides (e.g., CaO content; Fig. 12a). On the other hand, the geochemical composition of TF-109 is consistent with the TSP-4 unit of the Tuscania-San Pietro succession (Fig. 12a). Thus, TF-109/TSP-4 and TF-99 can be only generically attributed to the Vico Period I, their proximal equivalents at Vico being not yet identified.

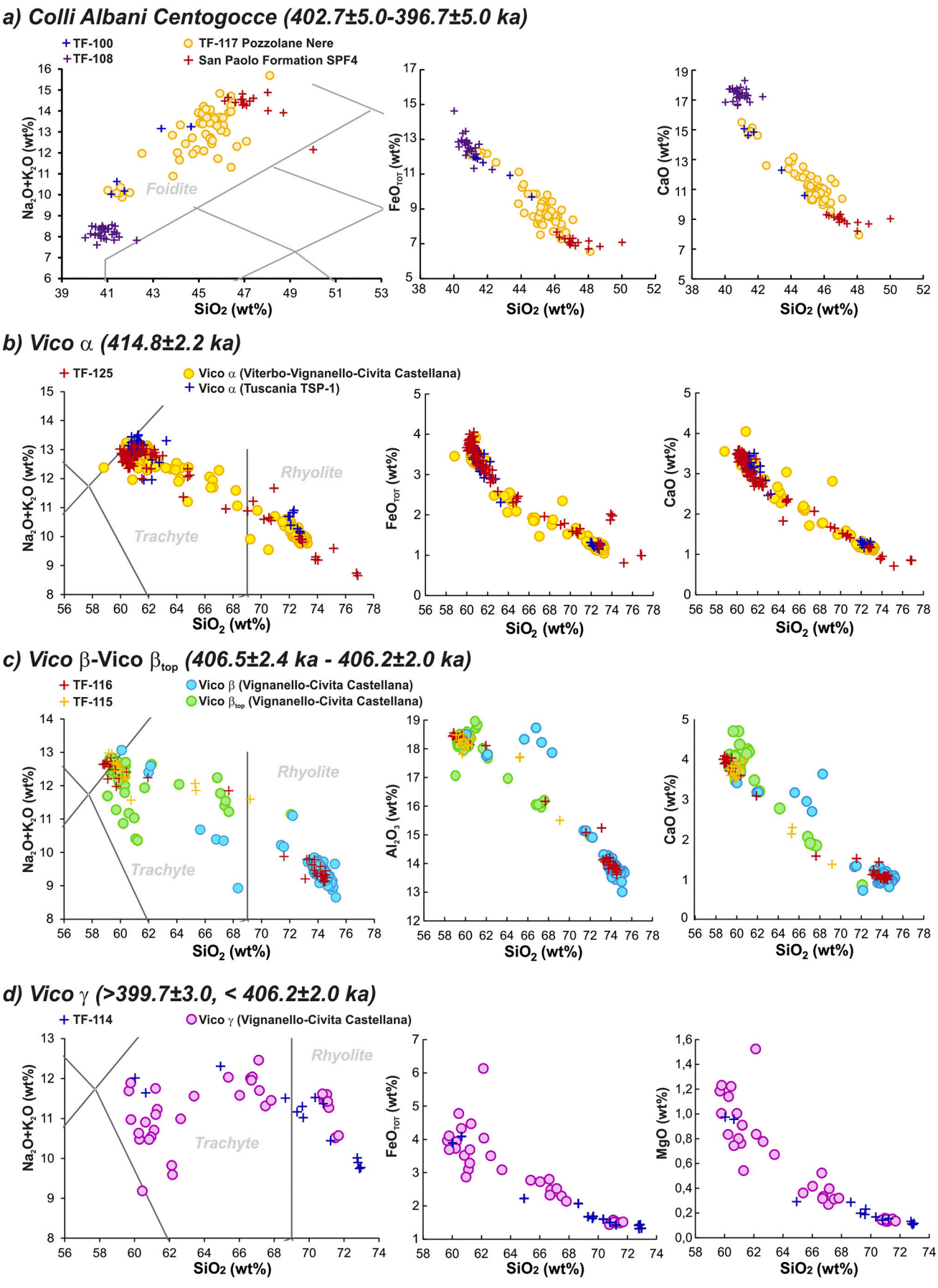

(caption on next page)

Fig. 10. Total alkali versus silica (TAS) classification diagram after Le Maitre et al. (2002) and representative bi-plots for TF-100, TF-108, TF-114, TF-115, TF-116 and TF-125 from the F4-F5 tephra record, compared with SPF4 tephra layer from the San Paolo aggradational succession, Pozzolane Nere (TF-117), proximal Vico α, Vico β, Vico β_{top} and Vico γ units from Vico volcano. Data source: WDS glass composition of TF-100, TF-108, TF-114, TF-115, TF-116, TF-125 and Vico α (TSP-1): this study; WDS glass composition of TF-117/Pozzolane Nere: Giaccio et al. (2017); WDS glass composition and $^{40}Ar/^{39}Ar$ age of tephra SPF4, Vico α, Vico β, Vico β_{top} and Vico γ, sampled at Viterbo (VT), Civita Castellana (CC) and Vignanello (VIG): Pereira et al. (2020). $^{40}Ar/^{39}Ar$ ages are recalculated relative to an age of 1.1891 Ma for the Alder Creek sanidine monitor standard (Niespolo et al., 2017), with the uncertainty expressed at 2σ.

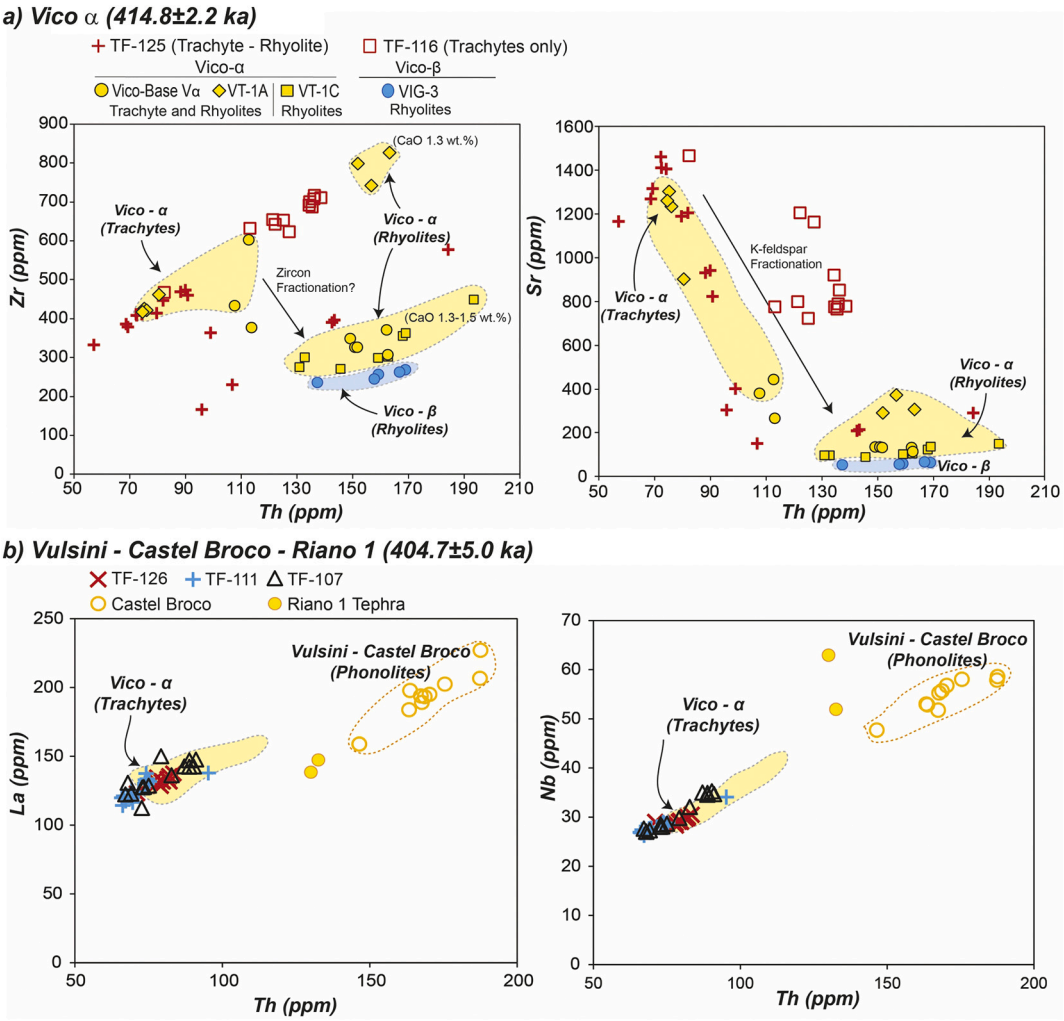

Fig. 11. Trace element glass compositions of the Fucino tephra compared to proximal glass data from the Vico and Vulsini volcanoes. a) TF-125 and TF-116 compared to the glass compositions of Vico α and Vico β eruption products. Note that in the case of TF-116, only the phonolite-trachyte end-member glasses were analysed, while in proximal settings trace elements were determined only for Vico β rhyolite glasses. b) TF-126, TF-111 and TF-107 compared to the Vulsini eruptive products, and specifically the Castel Broco fall deposit. The compositions of the Riano R-1 tephra of unknown origin are also shown.

5.2.3. *Tephra of Compositional Group-2 (CG-2)*

5.2.3.1. Sabatini tephra. TF-102, TF-103, TF-104, TF-106, TF-121, TF-122 and 123 - The geochemical composition of the TF-102/106 and TF-121/122 clusters are quite heterogeneous, with a SiO_2 content ranging from 46 wt% to 55 wt% and from 52 wt% to 64 wt%, respectively (Fig. 12c and 12b, respectively). TF-123 shows instead a homogenous high-alkali tephriphonolitic composition (Fig. 6).

The TF-102/106 cluster occurs just on top of TF-108, thus constraining its position close to the Centogocce succession time interval (403.4 ± 5 ka - 396.4 ± 5 ka). TF-121/122 and TF-123 occur instead between TF-125 (Vico α, 414.8 ± 2.2 ka; Pereira et al., 2020) and TF-118 (Fontana Ranuccio, 407.0 ± 4.2 ka; Pereira et al., 2018), or the more precisely dated TF-117/PN (408.5 ± 1.2 ka), constraining their ages in the narrow time interval between ~415 ka and ~408 ka. Hence, both the TF-102/106 and TF-121/122 clusters and TF-123 can be attributed to the Southern Sabatini activity (Fig. 3; Sottili et al., 2004, 2010), which was characterized by the emplacement of widespread sub-Plinian to Plinian fall deposits in the ~500-380 ka time interval (Marra et al., 2014; Sottili et al., 2019).

Though no relevant activity is documented in the ~414-402 ka timespan of TF-121/122 and TF-102/106 clusters, recent investigations point to the occurrence of a previously unrecognized Sabatini unit chronologically and geochemically consistent with TF-121/122 (Pereira et al., 2020). Specifically, at Civita Castellana (Fig. 1b), Pereira et al. (2020) described a ~1 m-thick pumice fall unit (CC-2), phonolitic in composition and tentatively ascribed to Sabatini activity, sandwiched between Vico α (CC-1; 414.8 ± 2.2 ka) and Vico β (CC-3; 406.5 ± 2.4 ka), i.e., a similar stratigraphic position of TF-121/122 within the F4-F5 succession. This unit was also found at Sant'Abbondio section (Fig. 1b) immediately on top of Vico α (Pereira et al., 2020). Although more variable in terms of geochemical composition, both TF-121 and

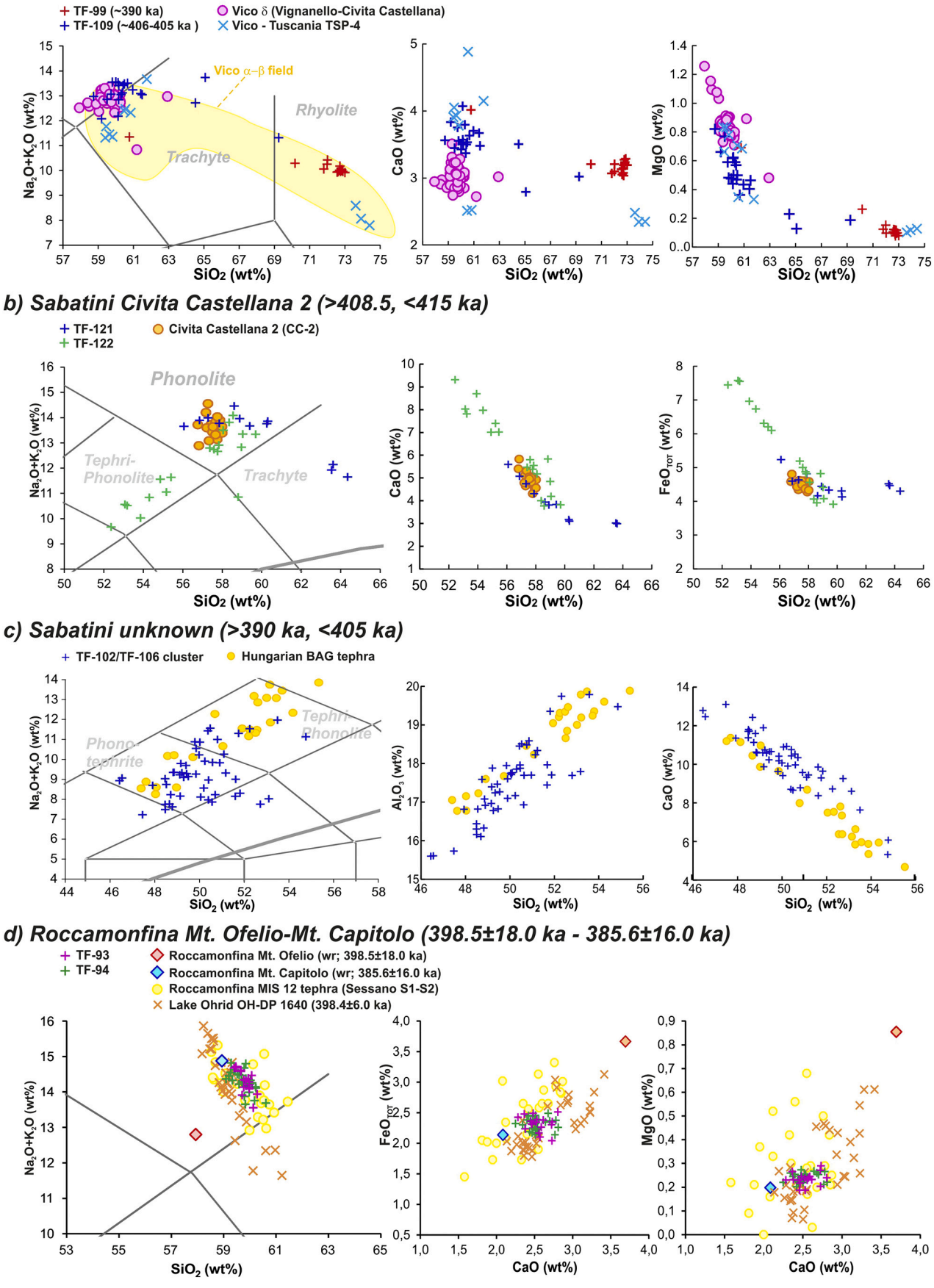

(caption on next page)

Fig. 12. TAS diagram after Le Maitre et al. (2002) and representative bi-plots for the tephra TF-93, TF-94, TF-99, TF-102, TF-103, TF-104, TF-106, TF-109, TF-121 and TF-122 from the F4-F5 record, compared with proximal Vico δ units from Vico volcano, TSP-4 from Tuscania-San Pietro succession, CC-2 from Civita Castellana succession, the distal Bag tephra from the MIS 10 Hungarian loess, tephra OH-DP-1640 from Lake Ohrid and Sessano-1 and 2 (S1-S2) tephra from Sessano basin. For comparison, in panel a), the compositional field of the major Vico α and Vico β Plinian eruptions is also shown. Data source: WDS glass composition of TF-93, TF-94, TF-99, TF-102, TF-103, TF-104, TF-106, TF-109, TF-121, TF-122, TF-123, and TSP-4: this study; WDS glass composition and $^{40}Ar/^{39}Ar$ age of Vico δ and CC-2, sampled at Vignanello (VIG) and Civita Castellana (CC), respectively: Pereira et al., 2020; WDS glass composition and modelled age of tephra OH-DP-1640: Leicher et al. (2019); WDS glass composition and of Bag tephra: Pouclet et al. (1999); post-Rio Rava – pre-Brown Leucitic Tuff whole-rock compositions: Rouchon et al. (2008); S1 and S2 SEM-EDS glass composition: Russo Ermolli et al. (2010). $^{40}Ar/^{39}Ar$ ages are recalculated relative to an age of 1.1891 Ma for the Alder Creek sanidine monitor standard (Niespolo et al., 2017), with the uncertainty expressed at 2σ.

TF-122 are compatible with CC-2 phonolitic glass composition (Fig. 12b). Between the two layers, the thickest one, TF-121, seems to show a higher degree of geochemical similarity, and thus is a good candidate for correlation with CC-2 pumice fall, while the thinnest one, TF-122, could represent a minor eruption slightly preceding CC-2 fall.

In contrast, TF-123, whilst sharing a broadly similar chronostratigraphic position to the overlying TF-121/122 deposits, shows no geochemical similarity to the CC-2 pumice fall and thus must be considered the product of a slightly older, undefined Sabatini eruption.

Similarly, the TF-102/106 cluster lacks a chronological and stratigraphical correlative in the currently determined Sabatini proximal eruption record. This cluster would be instead chronologically consistent with the activity of the Volsci volcanic field and, specifically, with Pofi scoria cone and Arnara scoria cone, dated at 393.0 ± 3.5 ka and 394.5 ± 6.1 ka (Marra et al., 2021), respectively, likely equivalent to the Cava Pompi scoria fall (392.7 ± 3.0 ka) and Isoletta I scoria fall (401.7 ± 3.0 ka) (Pereira et al., 2018). However, the lack of geochemical glass compositional data currently prevents any possible comparison and correlation with TF-102/106.

In contrast, in the ultra-distal setting, the TF-102/106 cluster would be geochemically and chronologically compatible with the so-called Bag Tephra (Fig. 12c), interbedded in Quaternary loess deposits of Hungary and Slovakia (Pouclet et al., 1999; Hum, 2005; Sági et al., 2008). In fact, the Bag Tephra has a phonotephritic-tephriphonolitic glass composition (Pouclet et al., 1999) very similar to that of the TF-102/106 cluster (Fig. 12c). The Bag tephra is commonly found below the so-called Basaharc Lower paleosol of the MIS 9 period (Horváth and Bradák, 2014), thus consistent with the age of TF-102/106. The previous tentative correlation to the Villa Senni eruption (Pouclet et al., 1999) is ruled out by glass geochemistry. More recent petrographic investigations (Sági et al., 2008) point out that the Bag tephra likely represents multiple tephra layers. Therefore, the tephra cluster TF-102/106 would be a good candidate for a correlation with such an important marker of the Hungarian loess. However, at present we can only propose a tentative correlation with either an unknown Sabatini eruption cluster or the Pofi and Arnara centers of the Volsci volcanic field.

5.2.3.2. Roccamonfina tephra. TF-93 and TF-94 – Both tephra layers are characterized by an almost homogeneous phonolitic composition, with a SiO_2 content of ~59-61 wt% and alkali content ranging between ~13.5 and ~14.5 wt%. Considering their position within the F4-F5 succession, between TF-85 (Villa Senni, 365.8 ± 1.2 ka) and TF-115 (Vico β_{top}, 406.4 ± 2.0 ka), the two tephra can be associated with the post-Rio Rava/pre-Brown Leucitic Tuff stage (355-440 ka; Rouchon et al., 2008) of Roccamonfina Volcano, and, more specifically, to the activity of the Monte Ofelio-Monte Capitolo centers, dated to 398.5 ± 18.0 ka and 385.6 ± 16.0 ka (recalculated ages from Rouchon et al., 2008). Although no glass composition is available for these Roccamonfina units, sample RMF6 of Monte Capitolo (398.5 ± 18.0 ka; Rouchon et al., 2008) has a whole rock phonolitic composition, which is consistent with that of the two Fucino tephra (Fig. 12d). The attribution of the two tephra to Roccamonfina is further supported by the analogous composition of two slightly older (i.e., MIS 12) Roccamonfina tephra layers (S1-S2) from the Sessano basin, southern Italy, located immediately east of this volcano (Russo Ermolli et al., 2010). Furthermore, the OH-DP-1640 tephra from Lake Ohrid (modelled age of 398.4 ± 6.0 ka; Leicher et al., 2019), ascribed to Roccamonfina, could be tentatively correlated with TF-93/94 (Fig. 12d), based on a similar age and geochemical composition (besides minor differences). Therefore, TF-93 and TF-94 can be attributed to the Monte Ofelio-Monte Capitolo centers and, based on the good geochemical matching, more likely to the latter. Future higher precision $^{40}Ar/^{39}Ar$ dating of these volcanic units in proximal setting will be of great interest to strengthen the chronology and attribution proposed here.

5.2.3.3. Vulsini tephra. TF-107, TF-111 and TF-126 – In addition to TF-107 and TF-111, likely attributed to the Vulsini activity based on the Cl vs CaO/FeO diagram (Fig. 7c) as discussed above, here we also re-evaluate the TF-126 layer, in light of the new aquired trace element data. Previously, TF-126 was tentatively correlated to the Castel Broco eruption deposit of Vulsini volcano, as well as geochemically matched to the pumice fall pre-Vico α, found immediately below Vico α in the proximal area of Vico Volcano (Pereira et al., 2020).

TF-107 and TF-111 are stratigraphically constrained between the ~365 ka TF-85/Villa Senni tephra and the ~406 ka TF-115/Vico β_{top}. Within the Vulsini volcanic history (e.g., Palladino et al., 2010), the Pumice Fall 0 (PF-0) eruption (399.8 ± 18.0 ka; Turbeville, 1992), here tentatively indentified with TSP-3 of the Tuscania-San Pietro section, is the only known explosive event geochronologically consistent with both TF-107 and TF-111. Of the two potential distal equivalents of PF-0/TSP-3, TF-111 shows a better geochemical match with TSP-3 (Fig. 13a). Moreover, TSP-3 occurs below TSP-4 that has been here correlated to TF-109 (Fig. 12a), which supports a possible correlation of TF-111 with PF-0/TSP-3, in spite of $^{87}Sr/^{86}Sr$ ratios (Fig. 7).

Regarding the trace element compositions, we notice that both TF-111 and TF-126 share similar levels of incompatible trace element enrichment to the trachytic components of the Vico α deposits, while they strongly differ from Castel Broco (Fig. 11b). This feature, on one hand, would preclude the correlation of TF-126 with Castel Broco and, on the other hand, would also raise doubts over the attribution of TF-111 and TF-126 layers to Vulsini, suggesting instead an origin from Vico. We note, however, that trace element data for Vulsini pyroclastic deposits are currently limited to only one sample from the co-eruptive basal fallout of Castel Broco (Fig. 11b), thus, they may not be fully representative of either the entire compositional spectrum of the Castel Broco eruption products, or even more so, the whole Vulsini eruptive successions. Therefore, to take a conservative approach, while retaining a preferential attribution of TF-111 and TF-126 to the Vulsini district, we cannot fully exclude a Vico source for TF-111/TSP-3 and TF-126/pre-Vico α. Indeed, the unambiguous solution of this issue requires a statistically representative trace element dataset for both Vulsini and Vico products, which is not available yet.

TF-107 shares a similar lithology and major element geochemistry with Riano R-1 tephra (Fig. 13a), here tentatively attributed to the activity of the Vulsini volcanic district (Fig. 7c-II) and dated at 404.7 ± 5.0 ka (Marra et al., 2018). While a correlation is further supported by very similar $^{87}Sr/^{86}Sr$ values (Fig. 8; Table 4), preliminary trace element glass analyses reveal some inconsistency (Fig. 11b).

5.2.3.4. Vulsini vs. Vico tephra. TF-88, TF-89, TF-90, TF-96, TF-97, TF-98, TF-110, TF-120, TF-124 – These nine tephra layers are characterized by Cl contents and CaO/FeO ratios consistent with both Vico and Vulsini

a) Vulsini Pumice Fall 0(?) (~405-406 ka) - Riano 1 (404.7±5.0 ka)

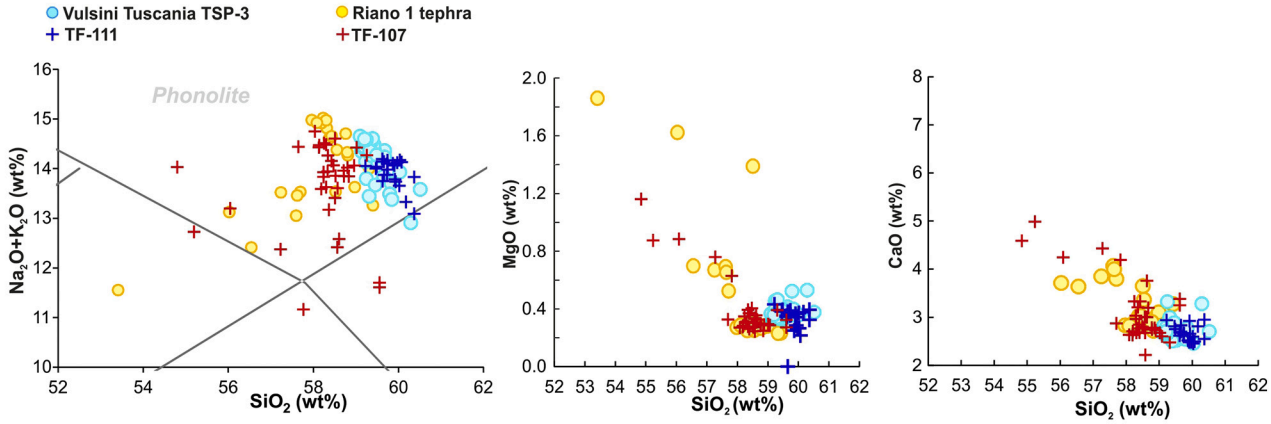

b) Vico Sant'Angelo-Sant'Abbondio (390.4±4.0 ka)

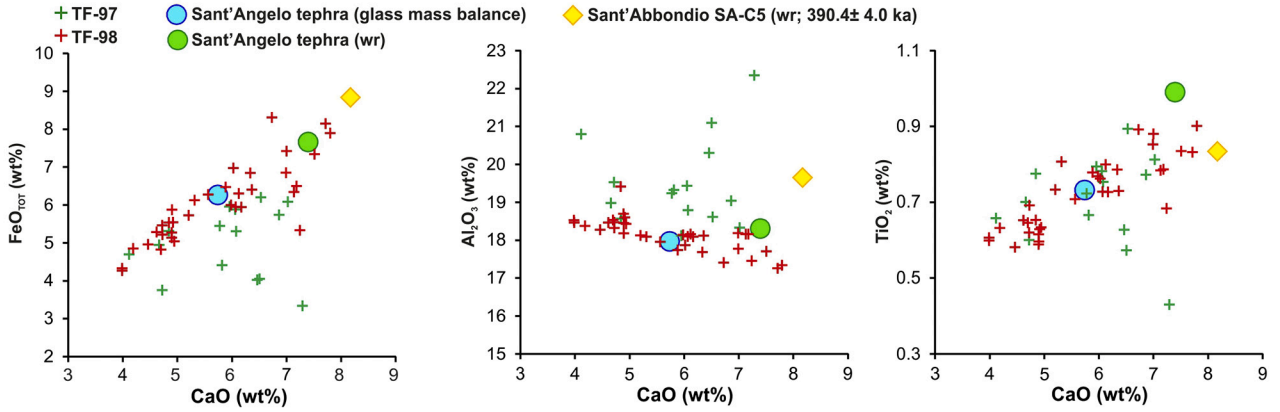

c) Vico (~415-408 ka - ~366-390 ka)

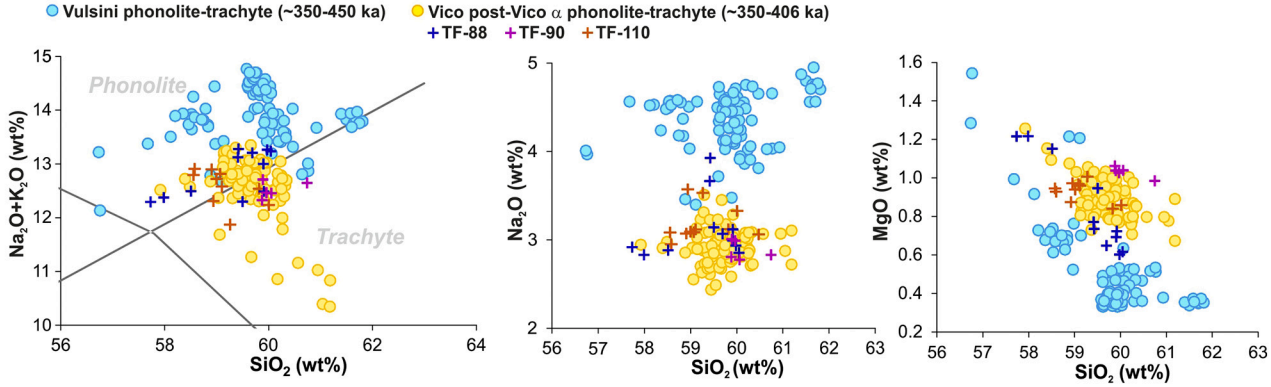

d) Vulsini unknown (~406-405 ka - ~366-390 ka)

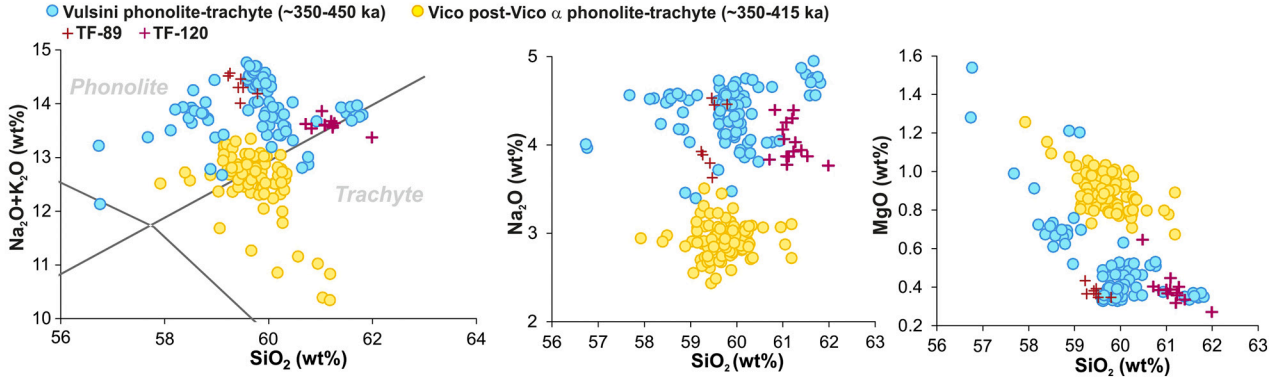

(caption on next page)

Fig. 13. TAS diagram after Le Maitre et al. (2002) and representative bi-plots for the tephra TF-88, TF-89, TF-90, TF-107, TF110, TF-111, TF-120 and TF-124, compared with the proximal Vulsini unit TSP-3 from Tuscania-San Pietro section and Riano R-1 from the Riano succession (panel a), VCO 163 from Vico area, SA C4 and SA C5 from the Sant'Abbondio Fall succession (panel b) and with the proximal Vulsini (Casale delle Piane, Castel Broco, TSP-2 and TSP-3 from Tuscania-San Pietro section), and Post-Vico α Vico trachyte-phonolites (Vico β, Vico β_{top}, Vico γ) shown as blue and yellow circles in panels c) and d). Data source: WDS glass composition of tephra TF-88, TF-89, TF-90, TF-107, TF-110, TF-111, TF-120, Vulsini (TSP-2, TSP-3) and Riano R-1: this study; VCO 163 whole-rock geochemistry: Perini et al. (2004); SA C4 and SA C5 whole-rock geochemistry and $^{40}Ar/^{39}Ar$ age: Marra et al. (2014); $^{40}Ar/^{39}Ar$ age of R-1: Marra et al. (2018); WDS glass composition of Post-Vico α Vico phonolite-trachytes (Vico β, Vico β_{top}, Vico γ): Pereira et al. (2020). $^{40}Ar/^{39}Ar$ ages are recalculated relative to an age of 1.1891 Ma for the Alder Creek sanidine monitor standard (Niespolo et al., 2017), with the uncertainties expressed at 2σ.

volcanic sources (Fig. 7c-III).

TF-98 and TF-97 form, together with the rhyolitic tephra TF-99 (unambiguously from Vico; see section 5.2.2.), a stratigraphically strictly related cluster located between TF-85/Villa Senni and TF-116/Vico β. The age of this cluster is therefore bracketed between ~366 ka and ~406 ka. Among the potential Vico equivalents for TF-97 and TF-98, Perini et al. (2004) described the so-called Sant'Angelo tephra, which is stratigraphically constrained between Vico β (406.5 ± 2.4 ka; Pereira et al., 2020) and the Lava di Vico formation (~258 ka), thus chronologically consistent with TF-97 and TF-98, as well as with TF-99, the latter unambiguously attributable to Vico due to its rhyolitic composition (Fig. 12a). However, no glass chemical composition is available for the Sant'Angelo tephra in literature, but only a single whole-rock composition in Perini et al. (2004). Whilst whole rock compositions only allow very limited comparison with glass data, a relatively good geochemical match can be observed between the least evolved end-member of TF-97/98, and especially of TF-98, and the Sant'Angelo tephra whole-rock composition (Fig. 13b).

On the other hand, the whole rock composition of the Sant'Angelo tephra (Perini et al., 2004) is similar to that of the lowermost unit (i.e., SA-C5) of the Sant'Abbondio lapilli and ash succession of Marra et al. (2014; Fig. 13b), which however yields a quite high loss on ignition, likely reflecting significant alkali loss. Nevertheless, less mobile elements make a tentative correlation of the Sant'Angelo tephra with SA-C5 still tenable (Fig. 13b). The Sant'Abbondio succession, comprising at least six fallout horizons, occurs at the boundary of the Vico and Sabatini volcanic districts (Fig. 1b). The base and the top of this succession were $^{40}Ar/^{39}Ar$ dated at 390.4 ± 4.0 ka (lowermost unit SAAS C5) and 380.4 ± 40.0 ka (uppermost unit SAAS C4; wide error associated with biotite dating), and tentatively attributed to the Sabatini activity (Marra et al., 2014). However, considering its chemical affinity with the Sant'Angelo tephra, the Sant'Abbondio lapilli and ash succession can be more likely ascribed to the Vico activity and, possibly, to the Sant'Angelo unit. Thus, transitively, also the TF-99/98 should correlate with Sant'Abbondio units. Unfortunately, the Sant'Abbondio units yielded no fresh glass for direct comparison with the potential Fucino equivalents. Therefore, to get an estimation of the interstitial glass composition of Sant'Abbondio/Sant'Angelo unit, based on literature (Perini et al., 2004) and new petrographic observations and mineral composition of the Sant'Abbondio and Sant'Angelo juvenile clasts, we performed a mass balance calculation (SD-1). Notably, according to this calculation, the residual melt of juvenile clasts, having bulk composition, petrographic characters, porphyritic degree, and mineral assemblage featuring the Sant'Angelo/Sant'Abbondio tephra, would be fully consistent with the average glass composition of the TF-98 tephra (Fig. 13b; see also SD-1). Specifically, we found that the bulk composition of Sant'Angelo/Sant'Abbondio tephra is consistent with the average glass composition of TF-98 (49.3 wt%) + Lct (15.9 wt%) + Cpx (12.4 wt%) + bmca (6.5 wt%) + Plg (12.5 wt%) + Ox (3.4 wt%), which substantially matches the textural features and the mineral assemblage observed in Sant'Angelo/Sant'Abbondio SA-C5 tephra. In conclusion, despite the lack of glass compositional data for the proximal counterpart, the correlation of this Vico unit with TF-97-98, and particularly with TF-98, appears quite convincing. As a preliminary tentative attribution, we thus consider the tephra layers TF-97/98, and likely TF-99, as the distal expression of the Sant'Angelo/Sant'Abbondio succession, which may represent the final explosive activity of the Vico Period I (Perini et al., 2004).

TF-88, TF-89, TF-90, TF-96, TF-110, TF-120 and TF-124, though apparently similar in composition and indistinguishable in the CaO/FeO vs diagram (Fig. 7c-III), can be easily attributed either to Vico or Vulsini using the TAS and other simple bivariate diagrams, as shown in Figs. 13c-d. Indeed, the glass geochemistry of the post-Vico α phonolite-trachytes (i.e., the phonolite-trachytes component of Vico β, Vico β_{top} and Vico δ) is quite different from that of the Vulsini phonolite-trachytes spanning a similar time-interval (Figs. 13c-d). Specifically, while TF-88, TF-89 and TF-110 systematically plot within the compositional fields of the post-Vico α phonolite-trachytes (Fig. 13c), TF-90, TF-96, TF-120 and the phonolite component of TF-124 plot in the field of the Vulsini phonolites (Fig. 13d).

As for their potential proximal equivalents, TF-120 stratigraphically occurs between TF-117/Pozzolane Nere (~408 ka) and TF-125/Vico α (~415 ka), i.e., geochronologically roughly consistent with PF-0 (399.8 ± 18.0 ka; Turbeville, 1992), and thus might be considered as an alternative correlative for this Vulsini eruption, other than the above-poposed TF-111. Finally, based on the available geochronological constraints, no specific correlative deposits have been identified in the proximal records for the other Vico (TF-88, TF-89 and TF-110) and Vulsini (TF-90, TF-96, TF-124) distal tephra layers.

5.3. Age model

Based on the direct and indirect (i.e., derived from geochemical fingerprinting) $^{40}Ar/^{39}Ar$ dating of the MIS 11 tephra record, we have developed a Bayesian age-depth model. Only a sub-set of radioisotopic ages (from direct dating or reliable geochemical and/or stratigraphical correlations) with the necessary requisites of both accuracy and precision were selected for this purpose. Specifically, for the investigated interval we selected nine ages from an equivalent number of tephra layers, as shown in Fig. 14. The age-depth curve (Fig. 14) shows a remarkable slope change at ~410 ka, indicating that the sedimentation rate was distinctly lower in the first part of the MIS 11 period (~424-410 ka). While this change in sedimentation rate shows no correlation with primary tephra deposition or volcaniclastic input, which is negligible, it coincides with a shift in Ca, from a relatively long and more stable period with higher Ca to a period characterized by large and rapid, millennial-scale variations of Ca (Fig. 15). Ca was addressed to represent lake primary productivity (Giaccio et al., 2019; Mannella et al., 2019) and thus the marked change in sedimentation rate is likely related to changing environmental conditions, a topic which will be addressed elsewhere. Here, we can only underscore that this change cannot be interpreted as a distortion of the age-depth curve due to age model uncertainty, because it occurs in a stratigraphic interval that is firmly constrained by several radioisotopic ages (Fig. 15).

The age-depth model allows us to reliably assess the age and climatostratigraphic position of each individual tephra in the F4-F5 MIS 11 section, as shown in Fig. 15. Such an integrated paleoenvironmental-tephra record provides a stratigraphically ordered series of tephra within the framework of the sub-millennial scale paleoclimatic variability of the MIS 11 period, which represents one of the most important features of this kind of integrated record. Indeed, while the chronology is susceptible of improvements through time, the climatostratigraphic position of each tephra is firmly and definitively established here. For instance, the TF-126 tephra is a valuable marker for the onset of a higher productivity interval, likely driven by higher temperature and enhanced

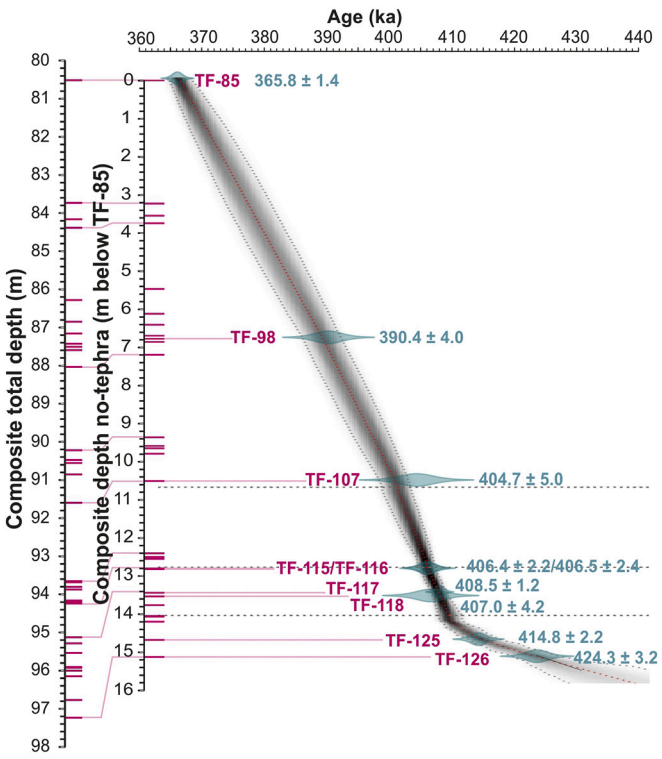

Fig. 14. Bayesian age-depth model for the investigated F4-F5 tephra record of the MIS 11 interval.

nutrients delivery, i.e., typical of interglacial conditions (i.e., MIS 11c; Fig. 15). This specific climatostratigraphic position is independent of the current geochronological (and source) uncertainties of TF-126 tephra and of any possible future improvement in accuracy and precision of the TF-126 dating itself.

5.4. The Fucino MIS 11 tephra record in the framework of central Mediterranean Middle Pleistocene tephrochronology and its relevance for the Quaternary sciences and volcanology

In the framework of the Mediterranean tephrostratigraphy, few relatively continuous sedimentary records span through the Middle Pleistocene (Fig. 1a). The on-land marine succession of Montalbano Jonico, southern Italy (Figs. 1a, 16), records the southern-Italy peri-Tyrrhenian and Vulture volcanic activity at the Early-Middle Pleistocene transition and provides the first evidence for an early onset of the volcanic activity in the Campania Area, at the beginning of the Middle Pleistocene (Petrosino et al., 2015). The radioisotopic geochronological data acquired from Montalbano Jonico also allowed a better constraint of the chronology of the MIS 19 paleoclimatic change (Nomade et al., 2019) and of the cosmogenic nuclide ^{10}Be increase during the Matuyama-Brunhes geomagnetic reversal (Simon et al., 2018).

The Sulmona Basin lacustrine succession, in central Italy (Figs. 1a, 16), represents another rich tephra archive encompassing the Early-Middle Pleistocene transition, which records an intense and frequent activity of the peri-Tyrrhenian volcanism (Giaccio et al., 2013b), poorly documented (or so-far unrecognized) in proximal settings (Marra et al., 2014; Sottili et al., 2019). The Sulmona succession also provided the basis for assembling a robust radiometric chronology for both local and extra-regional MIS 19 paleoclimatic records (Giaccio et al., 2015a; Regattieri et al., 2019) and for constraining the timing of the Matuyama-Brunhes geomagnetic reversal (e.g., Sagnotti et al., 2014). Furthermore, the Sulmona Basin tephra record spans discontinuously the MIS 15-MIS 10 period (e.g., Giaccio et al., 2013b; Giaccio et al., 2014; Regattieri et al., 2016), but a comprehensive tephra study for this interval is still pending. Specifically, among several tephra spanning the MIS 11 period (Fig. 16), currently only one has been geochemically characterized (Regattieri et al., 2016). Based on its trachyte-rhyolite composition, Regattieri et al. (2016) correlated it to Vico α, but according to the upgraded geochemical dataset obtained by Pereira et al. (2020) for the Vico Period I units, this tephra could be either attributed to Vico α or Vico β (Pereira et al., 2020).

The rich tephra record of the river-lagoon stacked aggradational successions of the Tiber River delta, in central Italy (Figs. 1a, 16), though discontinuous, radioisotopically constrained the timing of the sea-level rise during the last eleven deglaciations (e.g., Marra et al., 2016b; Luberti et al., 2017), including the MIS 11 period (Fig. 16). However, only few tephra layers have been so far geochemically fully characterized (e.g., Pereira et al., 2020), thus limiting the great potential of this succession for tephrochronological purposes.

The deep-sea core KC01B in the Ionian Sea (Fig. 1a) spans continuously the last 1.1 Ma (Lourens, 2004), but detailed tephrostratigraphic investigations are currently available only for the last 200 kyr (Insinga et al., 2014; Fig. 16). A recent detailed tephra and crypto-tephra study of the nearby core ODP Site 964 (Fig. 1) extended this tephrochronological record back to 625 ka (Fig. 16) and resulted in the first reliable synchronization of the marine and terrestrial records during specific intervals of MIS 13 and MIS 10 (Vakhrameeva et al., 2021).

The Mercure, Vallo di Diano and Acerno basins in southern Italy (Figs. 1a, 16), in addition to some known major eruptions from Latium volcanoes, revealed a conspicuous activity of the Roccamonfina Volcano during the MIS 15-MIS 12 period that is still fragmentarily known or currently not yet identified in the near-source volcanic area (Karner et al., 1999; Giaccio et al., 2014; Petrosino et al., 2014a, 2014b). Also located in southern Italy, the San Gregorio Magno lacustrine succession (Fig. 1a) provides a valuable tephra record of the poorly known Middle Pleistocene activity of the Campanian Volcanic Zone, although not extending beyond 250 ka (Petrosino et al., 2019; Fig. 16). Similarly, the Adriatic Sea core PRAD 1-2 (Fig. 1a), extends into the late Middle Pleistocene, reaching ~200 ka (Bourne et al., 2015; Fig. 16).

In the Eastern Mediterranean area, the marine cores KL49, KL51 and LC21 in the Aegean Sea, and the terrestrial (peatland) tephra record of the Tenaghi Philippon basin (Vakhrameeva et al., 2019) in Greece (Fig. 1a), were used in combination for reconstructing and indirectly dating the explosive activity of the Santorini Volcano during the last 360 kyr (Wulf et al., 2020; Fig. 16). The Tenaghi Philippon archive also documents a MIS 12-MIS 10 tephra record, which was dated climatostratigraphically using the high-resolution pollen profile, allowing a first age estimation of the tephra series of either known or unknown origin (Vakhrameeva et al., 2018; Fig. 16). Finally, the long and continuous tephra record from Lake Ohrid (Albania-North Macedonia; Fig. 1a), mostly from peri-Tyrrhenian potassic volcanic sources, provided important geochronological constraints for developing a robust age model for the outstanding 1.36 Myr-long palaeoclimatic succession, but also for currently unknown volcanic eruptions (Leicher et al., 2019; Wagner et al., 2019; Fig. 16).

In summary, of the above-mentioned Mediterranean Middle Pleistocene tephra records only four long and relatively continuous successions document in detail the MIS 11 period, i.e., the Sulmona Basin in central Italy, Lake Ohrid in Albania-North Macedonia, the Tenaghi Philippon peatland in Greece and the Ionian Sea core ODP Site 964 (Figs. 1a, 16). However, except for the incompletely explored Sulmona record, due to their remote location with respect to the peri-Tyrrhenian volcanoes, the remaining three MIS 11 records document none or only the largest explosive eruptions of the peri-Tyrrhenian potassic volcanoes, which are the only sources of the tephra found in Fucino Lake record. Specifically, among the Fucino MIS 11 tephra succession, only two tephra layers are found at Lake Ohrid, i.e., (i) Vico α/TF-125/OH-DP 1700.6 and (ii) Roccamonfina Monte Ofelio-Monte Capitolo/TF-96/OH-DP 1640 (Fig. 16), while a third layer, not identified at Fucino, was correlated to an undefined Roccamonfina eruption occurring at onset of

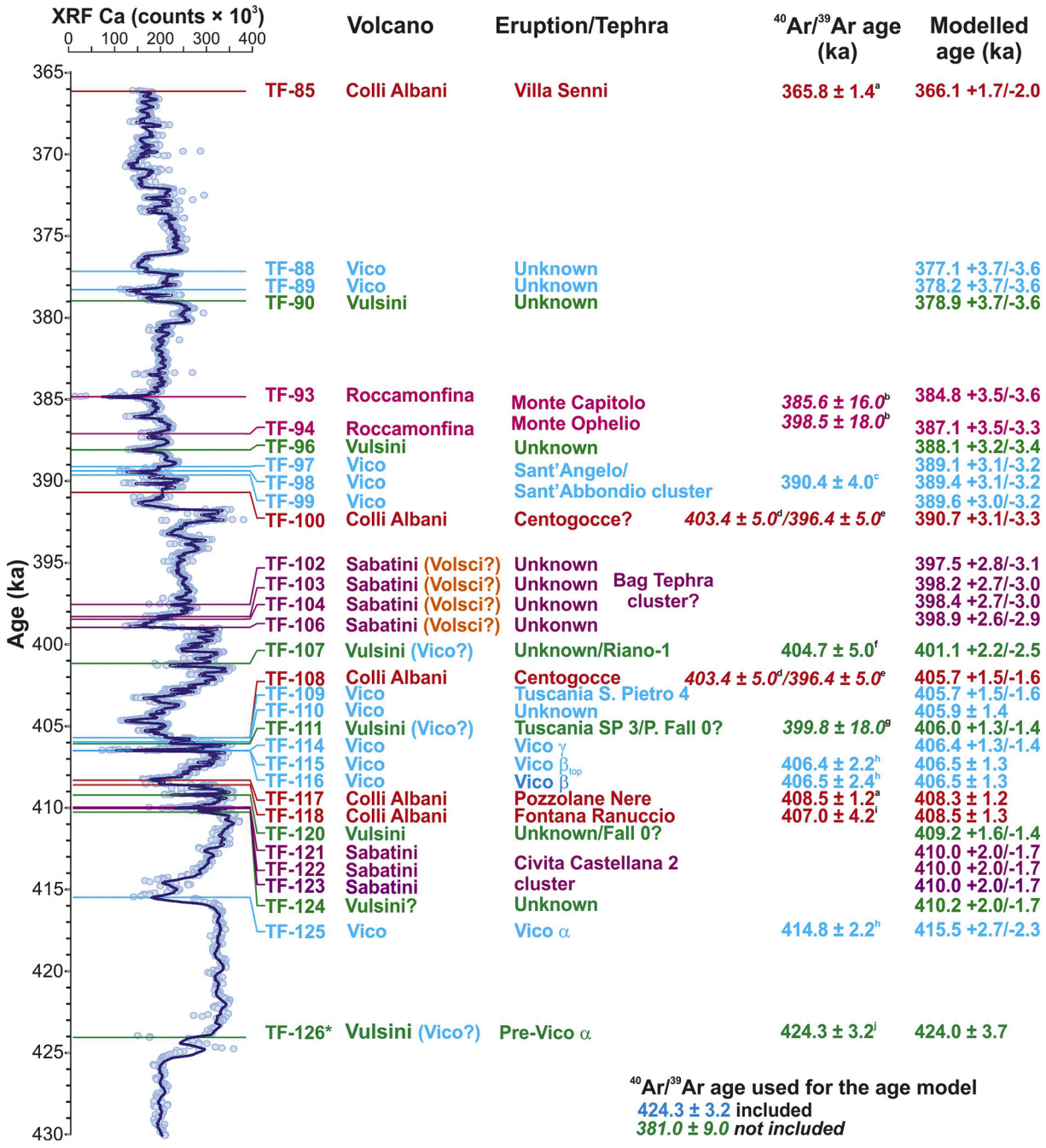

Fig. 15. Summary of the volcanic sources, individual correlation and chronology ($^{40}Ar/^{39}Ar$ and modelled ages) of the investigated Fucino F4-F5 tephra record. The MIS 11 temporal series of the calcium content in Fucino lacustrine sediments from F4-F5 core is also shown (XRF data from Giaccio et al., 2019). Ages not used for the age model are reported in italics. Data source: [a] this study; [b] Rouchon et al. (2008); [c] Perini et al. (2004); [d] Marra et al. (2014); [e] Marra et al. (2009); [f] Turbeville (1992); [g] Pereira et al. (2020); [h] Pereira et al. (2018); [i] Giaccio et al. (2019).

the MIS 11 period (Leicher et al., 2019). Due to their greater distance from the peri-Tyrrhenian potassic volcanic sources, the MIS 11 records of Tenaghi Philippon and ODP-964 sites document only few potentially unknown tephra from Neapolitan volcanoes, while the majority are related to the volcanic sources of Santorini, for Tenaghi Philippon, and Santorini, Aeolian Islands and South Aegean Volcanic Arc, for ODP-964 (Vakhrameeva et al., 2018, 2019, 2021). None of the MIS 11 tephra from Tenaghi Philippon or ODP-964 are found in the Fucino record.

In conclusion, the general tephrostratigraphic framework for MIS 11 is far from being satisfactorily developed for a reliable application to Quaternary sciences and volcanology. In this regard, the Fucino MIS 11 record arises as one of the fundamental reference geochemical and chronological datasets for the future development and application of the tephrochronology in the Mediterranean Region, especially for the areas closer to the highly productive tephra sources of peri-Tyrrhenian potassic volcanoes, i.e., which have the potential of capturing part of the activity recorded at Fucino and thus to benefit from its rich tephrochronological record.

5.5. *Implications for the peri-Tyrrhenian explosive volcanic history*

5.5.1. *Distal tephrostratigraphy for elucidating explosive eruption histories: Advantages and limitations*

Assessing the issue of the explosive volcanism history using distal

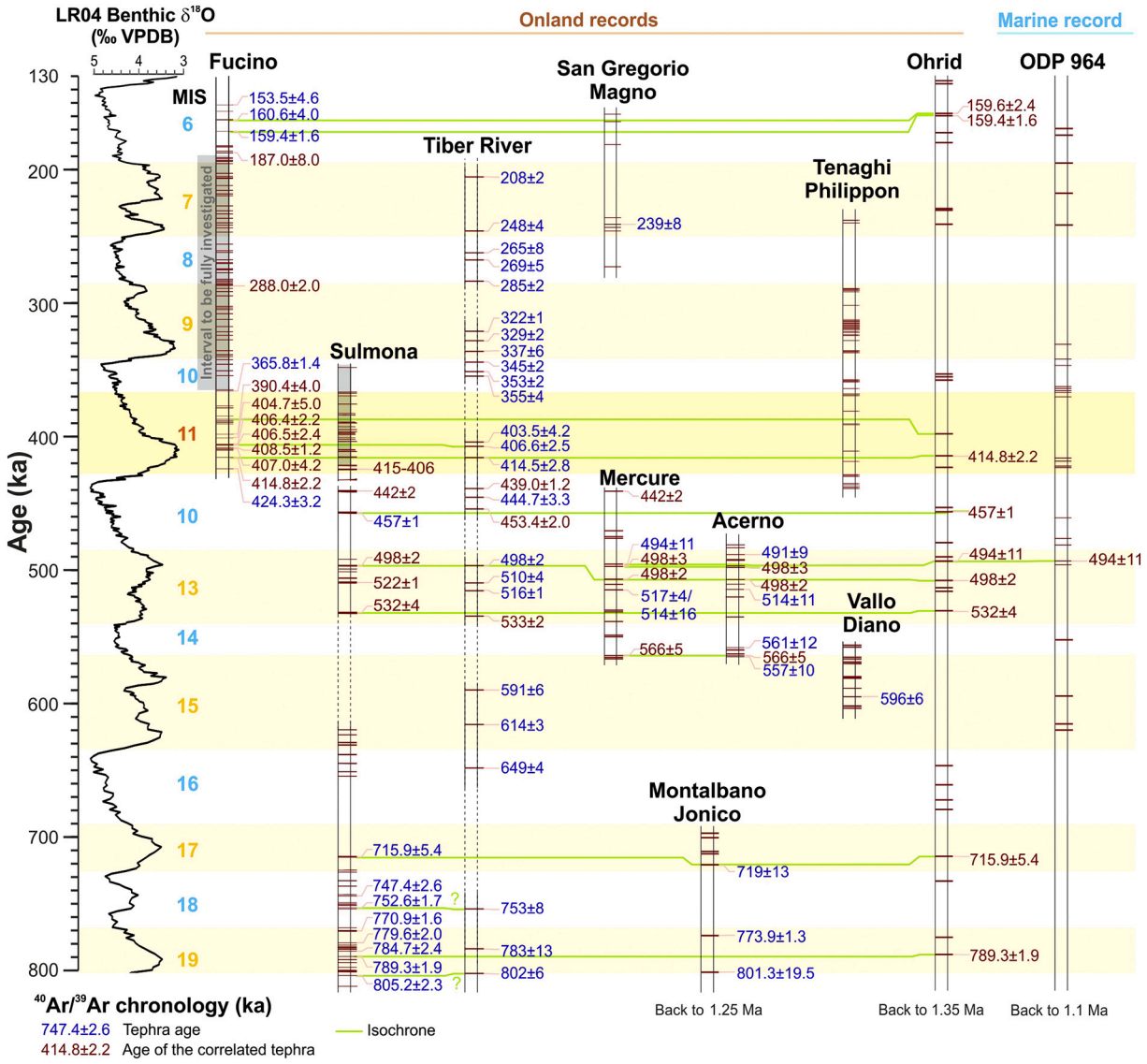

Fig. 16. The Fucino MIS 11 tephra record within the framework of the Mediterranen Middle Pleistocene tephrochronological records. Data source: Fucino: Giaccio et al. (2017, 2019), Mannella et al. (2019), This study; Sulmona: Giaccio et al. (2013a, 2013b, 2014, 2015a), Sagnotti et al. (2014), Regattieri et al. (2015, 2019); Tiber River: Florindo et al. (2007), Villa et al. (2016), Marra et al. (2016a, 2017, 2019, and references therein), Pereira et al. (2020); Mercure: Giaccio et al. (2014), Petrosino et al. (2014a); San Gregorio Magno: Munno and Petrosino (2007), Petrosino et al. (2019); Montalbano Jonico: Petrosino et al. (2015); Acerno; Petrosino et al. (2014b); Vallo di Diano: Karner et al. (1999); Tenaghi Philippon: Vakhrameeva et al. (2018, 2019), Wulf et al. (2020); Lake Ohrid: Leicher et al. (2016, 2019), Wagner et al. (2019); ODP 964: Vakhrameeva et al. (2021).

archives presents a series of advantages, but also limitations that need to be discussed. The general overview provided in previous sections shows that distal archives often document explosive activity that is hardly traceable to known eruptions or activity periods of a specific volcanic source. This highlights the great potential of distal tephrostratigraphy for the assessment of the explosive activity at regional scale (e.g., for the Mediterranean area, Munno and Petrosino, 2007; Paterne et al., 2008; Wulf et al., 2008, 2012; Giaccio et al., 2012a, 2012b, 2014; Leicher et al., 2019). However, several geographical, physical, and time-dependent factors can limit the approach of the distal tephrostratigraphy.

Specifically, the completeness of a distal archive with respect to a given volcano or cluster of volcanoes depends on the (i) relative distance from the volcanic sources, (ii) position with respect to the dominant winds, (iii) magnitude and intensity of the events, (iv) direction of the dispersal axis with respect to the volcano and distal archive location, (v) eruptive dynamics, (vi) variability of the atmospheric circulation pattern during glacial-interglacial and sub-orbital scale climate change (e.g., Bursik, 1998). In turn, the impact of all these factors in limiting the usefulness of the distal tephrostratigraphy depends on the number and geographical distribution of the distal archives documenting the same temporal interval and, more critical, the activity of the same volcanic system. Indeed, a dense network of distal archives distributed across a wide region surrounding a given volcano, sensibly enhances the possibility of capturing the whole activity of that volcanic system, reducing all the above-mentioned uncertainty and limitating factors, and allowing the construction of a composite record (e.g., Blockley et al., 2014; Lowe et al., 2015; Bronk Ramsey et al., 2015a, 2015b).

As stressed throughout the paper, at present only limited tephrostratigraphic records span the interval documented in detail in this study, and only one (i.e., Lake Ohrid) shares with Fucino some tephra from the peri-Tyrrhenian potassic volcanic sources (Fig. 16). Therefore, the framework of the explosive activity of these volcanic systems obtained using the distal records is likely to be far from complete because of the

poorly developed network of tephra records and correlations. Nevertheless, due to its privileged location, we demonstrate that the Fucino paleolake captured most of the known major eruptions and many other unknown explosive events of the peri-Tyrrhenian potassic volcanoes. Therefore, reconstructing the explosive history of the peri-Tyrrhenian potassic volcanoes during the MIS 11 period using the Fucino record alone is fully justified and supported by the data gathered, which illustrates that Fucino provides an extremely detailed eruptions record.

5.5.2. The proximal record

In order to compare the distal (Fucino) and proximal records of the peri-Tyrrhenian explosive volcanism of central Italy, we critically review the available geochronological data. The general framework of literature data for the peri-Tyrrhenian volcanic activity encompassing the MIS 11 period, or a slightly wider temporal interval, is provided in Table 6. Though partially and fragmentarily mentioned in previous sections, i.e., when the individual correlations where discussed, in the following section we provide a general overview summarizing the state of the art of the knowledge on the history of the peri-Tyrrhenian potassic explosive volcanism.

For the Vulsini Volcanic District, only one direct radioisotopic age determination is available for the studied interval, i.e., the already mentioned Pumice Fall 0 dated at 399.8 ± 18.0 ka (Turbeville, 1992; Table 6). Castel Broco and Casale delle Piane are two other prominent Vulsini eruption units potentially falling in the investigated interval, although lacking direct dating. Recently, Marra et al. (2020a) provided a tentative reconstruction of the eruptive history in this time span, based on xenocryst populations occurring in primary and reworked deposits of the eastern Vulsini (Bolsena-Orvieto and Vulsini Fields activities; Table 6), suggesting that the statistically most significant population age of 425.4 ± 1.6 ka may correspond to that of the Castel Broco eruption.

At Vico Volcano, multiple explosive eruptions of sub-Plinian to Plinian intensity occurred in the investigated interval, which roughly matches the Vico Period I stage (Perini et al., 2004), including Vico α, Vico β, Vico β_{top}, Vico γ, Vico δ and Sant'Angelo tephra (Cioni et al., 1987; Perini et al., 2004; Pereira et al., 2020) (Table 6). The chronology of the Vico Period I has recently been improved by Pereira et al. (2020) who reported new $^{40}Ar/^{39}Ar$ ages for 4 out of the 5 main eruption units recognised in proximal settings (Table 6). In addition, we provided an age constraint for the Sant'Angelo tephra (Perini et al., 2004), based on the proposed correlation to the Sant'Abbondio lapilli and ash succession (390.4 ± 4.0 ka; Marra et al., 2014).

In contrast, no relevant activity is documented at the Sabatini Volcanic District during the MIS 11 period. Indeed, the intense explosive activity of the Southern Sabatini stage took place between 500 ka ("Fall A" Plinian eruption) and 439 ka ("La Rosta" Plinian fall; Sottili et al., 2004; Marra et al., 2020b), while the subsequent Bracciano stage started at ~325 ka, thus suggesting a long phase of quiescence extending for more than ~100 kyr. However, the recent attribution of CC-2 pumice fall, which is bracketed between Vico α and Vico β, to the Sabatini activity (Pereira et al., 2020), would partially fill this seemingly long gap in activity. Moreover, as already mentioned in section 3.1., the Strombolian lithological features of the R-2 tephra occurring in the MIS 11 lacustrine succession cropping out near Riano (Fig. 1), laying below the Riano tephra R-1 dated at 404.7 ± 5.0 ka (Marra et al., 2018; Table 6), would also suggest the occurrence of a minor explosive activity at Sabatini during the MIS 11 period.

The 450-350 ka interval at the Colli Albani Volcanic District was characterized by the occurrence of three main eruption cycles, all belonging to the Tuscolano-Artemisio phase of activity: Pozzolane Rosse, Pozzolane Nere and Villa Senni eruption cycles (Freda et al., 1997, 2011; Giordano et al., 2006; Marra et al., 2009; Gaeta et al., 2016) (Table 6). Each cycle is characterized by large, caldera-forming eruptions, emplacing up to several tens of km^3 of pyroclastic-flow deposits (De Rita et al., 1988, 1995). The climactic phases were followed by several kyr-long post-caldera phases of activity, characterized by Strombolian and effusive eruptions revealed by numerous scoria cones and lava flows along peri-caldera ring faults, namely the Corcolle, Centogocce and Madonna degli Angeli successions (Giordano et al., 2006) (Table 6). The three eruption cycles were separated from each other by ~50 kyr-long quiescence intervals (Marra et al., 2009; Gaeta et al., 2016).

The Volsci Volcanic Field was characterized by diffuse, low-scale, magmatic (Strombolian and subordinate effusive) and phreatomagmatic activities from monogenetic scoria cones and tuff rings (e.g., Cardello et al., 2020; Marra et al., 2021). Several radioisotopic age determinations, encompassing the investigated interval, have been recently acquired (Boari et al., 2009; Nomade et al., 2011; Pereira et al., 2018; Marra et al., 2021) (Table 6). It appears that available $^{40}Ar/^{39}Ar$ ages are often grouped in statistically indistinguishable clusters (Table 6), which could be referred to either an individual eruptive event or multiple closely-spaced eruptions. In reconstructing the eruptive activity, this could lead to overestimate (i.e., multiple dating of the same eruption) or underestimate (i.e., grouping of statistically indistinguishable datings that refer to multiple events) the number, frequency, and recurrence of the events. Despite the quite distinctive compositional features of the Volsci products (Marra et al., 2021 and references therein), the lack of analyzable glass in the dated pyroclastic samples prevents their reliable application for tephrochronological purposes. Therefore, the current data available for the Volsci volcanic field prevent us from assessing the presence of tephra layers from this volcanic system in distal settings (including Fucino) and thus potentially improving its explosive history.

Finally, for the Roccamonfina Volcano, despite the large number of dated products, many of the samples ranging in age from 446 ± 4 ka to 353 ± 5 ka pertain to effusive or poorly defined products (Luhr and Giannetti, 1987; Radicati di Brozolo et al., 1988; Giannetti, 2001; Rouchon et al., 2008) (Table 6). Only the major Brown Leucitic Tuff eruption, and the minor Mt. Capitolo and Mt. Ofelio eruptions document explosive activity in the investigated timespan (Table 6). Moreover, several of these samples were dated by K/Ar method and yielded low precision age estimates, and therefore are scarcely reliable (Table 6). For instance, a previous date on the Brown Leucitic Tuff provided a quite imprecise age of 385 ± 23 ka (Luhr and Giannetti, 1987), and differs quite significantly from more recent age determinations obtained for this eruption (e.g., 358.2 ± 10.0 ka, Rouchon et al., 2008; 343.6 ± 6.0, Scaillet et al., 2008). Finally, a large uncertainty, and unreliability, is reflected by the scattered ages obtained by dating different material from the same sample (e.g., SP/R-30 and LP/R-247; Table 6).

5.5.3. Comparing the proximal and Fucino records of the peri-Tyrrhenian potassic volcanism

The above critical revision of the available literature data for the peri-Tyrrhenian explosive volcanism of central Italy allows a suitable comparison with Fucino MIS 11 tephra record. Overall, the history of the peri-Tyrrhenian explosive volcanism recorded at Fucino appears substantially richer and temporally better resolved with respect to the proximal settings (Fig. 17b). Notably, the Fucino record provides direct evidence for some Vulsini "ghost eruptions" (Marra et al., 2020a). Indeed, the age distribution of xenocrysts extracted from Vulsini pyroclastic units younger than MIS 11 (Marra et al., 2020a) defines three clusters at 425.4 ± 1.6 ka, 411.4 ± 2.4 ka and 400.5 ± 3.7 ka (Table 6; Fig. 17b) that do not correspond to any exposed products dated so far, which however are in good agreement with the $^{40}Ar/^{39}Ar$ and modelled ages of the Fucino tephra TF-126 (424.0 ± 3.7 ka), TF-120 (409.2 ± 1.6 ka) and TF-107 (401.1 ± 2.5 ka), ascribed to Vulsini (Figs. 15 and 17b). This provides further evidence for volcanic activity not yet identified in Vulsini proximal settings.

The Fucino record further refines our knowledge of the early explosive history of Vico Volcano (Pereira et al., 2020). Indeed, except for the missing Vico δ, Fucino documents the whole known activity of Vico Period I and highlights new eruptive events still unrecognised in

Table 6
Summary of the literature geochronological data for the peri-Tyrrhenian potassic volcanism of central Italy during the MIS 11, or a slightly wider interval. When possible, i.e., if all the required analytical data were published, $^{40}Ar/^{39}Ar$ ages are recalculated relative to an age of 1.1891 Ma for the Alder Creek sanidine or relative to an age of 28.294 Ma for the Fish Canyon sanidine monitor standards (Niespolo et al., 2017), with the uncertainty expressed at 2σ.

Volcanic source	Volcanic phase	Unit/sample	Type of activity/product	K/Ar and $^{40}Ar/^{39}Ar$ age (ka ±2σ)	References
Vulsini	Bolsena-Orvieto	Ponticello Pumices	Pumice fall	352.0±4.0	Nappi et al., 1995
				345.4±2.1	Marra et al., 2020a
	Vulsini	Fall 0	Pumice fall	399.8±18.0	Turbeville, 1992
	Fields	Castel Broco	Pumice fall-pyroclastic flow	n.d.	
		Piano della Selva	Pyroclastic flow	n.d.	
		Indirect evidence from xenocryst age populations	undefined	400.5±3.7	Marra et al., 2020a
				411.4±2.4	
				425.4±1.6	
				437.6±2.2	
Vico	Period I	SAAS-bottom	Pumice fall	390.4±4.0	Marra et al., 2014
		VICO δ	Pumice fall	399.7±3.0	Pereira et al., 2020
		VICO γ	Pumice fall	n.d.	
		VICO β_{top}	Pumice fall	406.4±2.0	
		VICO β	Pumice fall	406.5±2.4	
		VICO α	Pumice fall	414.8±2.2	
Sabatini	Southern Sabatini	CC-2	Pumice fall	n.d.	Pereira et al., 2020
		La Rosta	Pumice fall	439.1±1.0	Marra et al., 2020b
		FALL F	Pumice fall	448.5±7.0	Marra et al., 2014
Colli Albani	Villa Senni Eruption Cycle	Madonna degli Angeli succession	Lava dyke	354.5±6.0	Gaeta et al., 2006 and
			Lava flow	357.5± 9.0	references therein
			Lava flow	359.5±6.0	Marra et al., 2003
			Lava flow	359.5±8.0	
		Pantano Secco hydromagmatic center	Scoria fall	367.6±2.0	
		Madonna degli Angeli succession	Scoria fall	368.6±2.0	
			Lava flow	369.6±3.0	
		Tufo Lionato	Pyroclastic flow	368.6±4.0	
	Pozzolane Nere Eruption Cycle	Centogocce succession	Lava flow	396.0±5.0	
			Scoria fall	402.3±5.0	
		Pozzolane Nere	Pyroclastic flow	407±2.0	
	Pozzolane Rosse Eruption Cycle	Corcolle succession	Lava flow	439.5±5.0	
			Scoria	440.5±3.0	
		Pozzolane Rosse	Pyroclastic flow	455.5±2.0	
		Vallerano Lava	Lava flow	458.0±8.0	
Volsci volcanic field		Selva Piana	Lava	362.0±11.0	Boari et al., 2009
		Colle Avarone CA-CGT	Reworked volcanic horizon	360.8±6.5	Marra et al., 2021
		Isoletta III	Scoria fall	363.8±8.0	Pereira et al., 2018
		Isoletta II	Scoria fall	373.7±4.0	
		Valcatora	Lava dyke	379.0±8.0	Boari et al., 2009
		Lademagne II	Reworked volcanic horizon	387.7±5.0	Pereira et al., 2018
		Pofi-Colle La Grotta	Phreatomagmatic deposit	391.5±3.6	Marra et al., 2021
		Giuliano di Roma	Lava	394.6±6.0	Boari et al., 2009
		Pofi scoria cone	Scoria fall	393.0±3.5	Marra et al., 2021
		Cava Pompi	Scoria fall	392.7±3.0	Pereira et al., 2018
		Arnara scoria cone	Scoria fall	394.5±6.1	Marra et al., 2021
		Isoletta I	Scoria fall	401.7±3.0	Pereira et al., 2018
		Lademagne I	Scoria fall	404.0±5.0	
		Supino	Phreatomagmatic deposit	407.7±2.6	Marra et al., 2021
		La Tomacella, upper	Pyroclastic rock	410.0±10.0	Boari et al., 2009
		Tecchiena	Lava	416.1±11.0	Boari et al., 2009
		Celleta	Lava	417.1±6.0	
		La Tomacella, lower	Pyroclastic rock	425.2±13.0	
Roccamonfina	Rio Rava-Brown Leucitic Tuff stage	Brown Leucitic Tuff	Pyroclastic flow	343.6±6.0	Scaillet et al., 2008
				358.2±10.0	Rouchon et al., 2008
				385.0±23.0	Luhr and Giannetti, 1987
		Scipicciano 89X	Lava flow	361.7±10.0	Rouchon et al., 2008
		Fontana-radina RMF7	Lava flow	363.7±16.0	
		SP/R-30	Lava dome	360.0±42.0 (GM)	Giannetti, 2001
				382.0±3.0 (San)	
				390.0±30.0 (San)	
		SP/R-31	Effusive	370.8±3.0	
		La Frascara RMF4	Lava flow	373.9±18.0	Rouchon et al., 2008
		Galluccio RMF3	Lava flow	375.9±16.0	
		Monte Casi	Lava dome	370.0±9.0	Radicati di Brozolo et al., 1988

(*continued on next page*)

Table 6 (*continued*)

Volcanic source	Volcanic phase	Unit/sample	Type of activity/product	K/Ar and $^{40}Ar/^{39}Ar$ age (ka ±2σ)	References
		LP/R-247	Effusive	378.9±4.0 (San)	Giannetti, 2001
		430.0±6.0 (GM)		399.3±12.0	
		MLT/R-352	Lava flow	(San)	
		374.0±11.0			
		MLP/R-69	Lava dome	376.0±16.0	
		Monte Capitolo RMF6	Pyroclastic	396.2±16.0	Rouchon et al., 2008
		Masseria Robetti	Lava flow	397.0±18.0	Radicati di Brozolo et al., 1988
		MLT/R-290	Lava flow	408.4±9.0	Giannetti, 2001
		Monte Ofelio RMF12	Pyroclastic	409.4±18.0	Rouchon et al., 2008
		MLT/R-351	Lava flow	409.4±10.0	Giannetti, 2001
				415.5±18.0	
		LP/R-104	Lava dome	416.6±32.0	
		Masseria Robetti	Undefined	421.0±9.0	Radicati di Brozolo et al., 1988
LP/T-247	Lava dome	430.0±6.0	Giannetti, 2001		
Rio Rava RMF14	Lava flow	446.0±12.0	Rouchon et al., 2008		

GM, groundmass; San, sanidine.

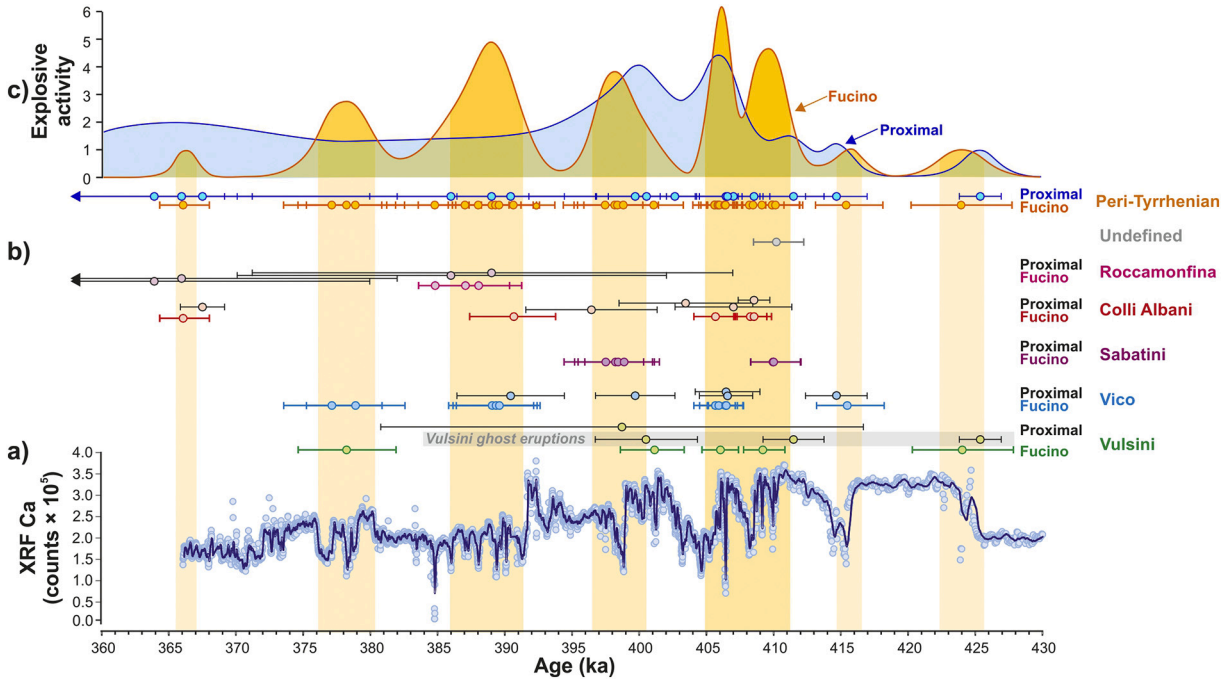

Fig. 17. Temporal distribution of the explosive activity of the peri-Tyrrhenian potassic volcanism of central Italy during the 430-360 ka interval, as inferred from the Fucino MIS 11 tephra record and chronological data from proximal volcanic areas. a) Temporal series of calcium content of the Fucino lacustrine sediments from F4-F5 core (XRF data from Giaccio et al., 2019). b) Comparison between the Fucino and proximal chronological databases from individual peri-Tyrrhenian volcanoes. c) Comparison between the probability density functions of the temporal distribution of the peri-Tyrrhenian explosive activity derived from available chronological data from Fucino and proximal volcanic areas. Source for the $^{40}Ar/^{39}Ar$ age of the proximal units: Vulsini: Turbeville (1992), Marra et al. (2020a); Vico: Marra et al. (2014), Pereira et al. (2020); Sabatini: no literature data; Colli Albani: Gaeta et al. (2016), Marra et al. (2016a); Roccamonfina: Rouchon et al. (2008).

proximal areas (i.e., TF-99 and TF-109). The age-depth model of Fucino indicates that the previously undated Vico γ eruption occurred around 406.4 ± 1.4 ka (Figs. 15 and 17b), i.e., immediately after the Vico β and Vico β_{top} eruption couplet, both with a modelled age of 406.4 ± 1.3 ka. Fucino provides evidence for three distinct tephra layers (i.e., TF-116, TF-115 and TF-114) within a very narrow stratigraphic interval of ~9 cm (Table 2; Fig. 5). They represent three distinct eruptive events of notable intensity occurred in a very short time span and may elude field observations in proximal exposures. Furthermore, while the uppermost fall deposit of the Sant'Abbondio succession, which is here tentatively ascribed to the Vico activity (Sant'Angelo tephra), yielded a poorly constrained age of 380 ± 40 ka (Marra et al., 2014), the Fucino record points out that this eruption cluster likely occurred in a short time span between ~389 ka and ~390 ka (Figs. 15 and 17b). Finally, the Fucino record allows us to refine the timing of the early Vico activity, indicating an age of ~377-379 ka for the emplacement of at least two additional, previously unknown, pyroclastic units (Figs. 15 and 17b).

Regarding the Sabatini volcanic district, the Fucino dataset improves the knowledge on the history and chronology of the activity, by providing a modelled age of 410.0 ± 2.0 ka for the CC-2 pumice fall (Pereira et al., 2020). Furthermore, Fucino records a cluster of four tephra (TF-102/TF-106) at ~397-400 ka, which may represent the equivalent of the Bag Tephra marker(s) of the Middle Pleistocene Hungarian loess, thus providing the first reliable age and climatostratigraphic position for this stratigraphic marker(s). If confirmed by future investigations, the recognition of this eruption cluster may shed new light on the Sabatini eruption frequency. Indeed, during the whole eruptive history (589 ± 4 ka to 70 ± 3 ka) of the district, the longest

dormancy of ~90 kyr has been so far documented in the time span 438 ± 1 to 329 ± 4 ka (Marra et al., 2020b). The Fucino dataset, showing a previously undetected eruption cluster at 398.9 + 2.6/2.9 ka - 397.5 + 2.8/-3.1 ka, allows us to estimate a maximum quiescence of 68.5 ± 4.1 kyr in the district (i.e., same as the time lapse since the last documented eruption), with implications for hazard assessment in the Roman area. However, at present we cannot exclude that this cluster of eruptions could have originated from the Volsci volcanic field (Fig. 15), which documents activity in a comparable timespan (Table 6).

With respect to the known stratigraphic and chronological framework of Colli Albani volcano (Marra et al., 2003, 2009, 2016b; Freda et al., 2006; Giaccio et al., 2009; Gaeta et al., 2011, 2016), the Fucino dataset integrates the chronology of the post-caldera phase that followed the major Pozzolane Nere eruption. Specifically, the last documented eruption of this phase (i.e., Centogocce succession; Fig. 15) occurs at 396.4 ± 5 ka in the Fucino record, which confirms the 30.6 ± 6.4 kyr-long dormancy preceding the onset of the Villa Senni eruption cycle (365.8 ± 1.4 ka), as previously suggested (Gaeta et al., 2016). Such dormancies have relevance in understanding the relationships between the geodynamic/tectonic and magmatic processes (Marra et al., 2004), stress-field and eruptive activity (Marra et al., 2009), as well as in assessing the volcanic hazard in the Roman area (Marra et al., 2016a, 2020b). In particular, the Colli Albani volcano is characterized by a quasi-periodic eruptive behaviour, with average recurrence times of 41 ± 2 kyr for the onset of the main eruptive cycles and average dormancies of 38 ± 2 kyr (Marra et al., 2016a). Notably, the last eruptive cycle started at 41 ± 2 ka and the last eruption occurred at 36 ± 1 ka, thus strongly evidencing a potentially still active (although quiescent) volcanic system.

Finally, the location of the Fucino paleolake NNW of Roccamonfina volcano is less favourable for intercepting the distal products of major (Plinian and Sub-plinian) eruption columns (usually dispersed toward the eastern quadrants at these latitudes), different from co-ignimbrite ash clouds and eruptive plumes from minor explosive events subject to lower altitude winds. Nevertheless, the MIS 11 Fucino dataset improves the chronology, both in term of accuracy and precision, of the post-Rio Rava/pre-Brown Leucitic Tuff stage of the Roccamonfina activity, through the identification of a possible distal equivalent of the Mt. Ofelio-Mt. Capitolo parasitic centers (Rouchon et al., 2008).

Overall, based on the updated chronological data for both proximal volcanic areas and Fucino succession, we obtained the probability density functions for the explosive activity of the peri-Tyrrhenian potassic volcanism during the MIS 11 period (Fig. 17c). By comparing these statistical expressions of the regional explosive volcanism, the proximal record would seem to show a single, monotonous increase of the eruptive frequency between ~410 ka and ~395 ka, followed by a quite homogenous activity during the following 395-365 ka interval. Instead, the better-resolved and richer record derived from Fucino shows a much more complex chronicle. Specifically, the temporal distribution of the peri-Tyrrhenian explosive volcanism is not homogenous and appears significantly clustered, with at least four (or possibly more) ~4-5 kyr-long periods of frequent activity separated by similarly long (5 kyr) periods of declining activity or quiescence. Although intriguing as a feature, here we do not speculate on the possible significance of such cyclicity (e.g., identifying a possible external forcing such as sea level change (Satow et al., 2021), astronomical factors and/or regional tectonics (Marra et al., 2004)), as the current analysed record of Fucino is still too short for performing a statistically significant analysis of the frequency distribution of the whole peri-Tyrrhenian potassic explosive activity. We remark that the shape and fluctuation of the reported curve of the temporal distribution (Fig. 17c) does not consider the magnitude and intensity of the events, whereas the actual rate of the erupted volume or mass of magma through time represents an even more important parameter than the mere recurrence interval or frequency of eruptive events. Therefore, further considerations on this key issue are postponed until the complete Fucino tephra record covering the last 430 kyr, or even a longer period, will be retrieved and fully investigated.

6. Summary and concluding remarks

Here, we have presented a comprehensive review of the state-of-the-art Mediterranean tephrochronology and explosive history of the peri-Tyrrhenian potassic volcanoes during the MIS 11 period. This was achieved in light of new lithostratigraphic, geochemical (major and trace glass composition and multi-phase $^{87}Sr/^{86}Sr$ composition) and geochronological ($^{40}Ar/^{39}Ar$ dating) characterization of 28 tephra layers from the Fucino F4-F5 succession, as well as of some, potentially equivalent, pyroclastic units collected in proximal areas of the peri-Tyrrhenian potassic volcanoes of central Italy. The integration of these new data with previous investigation from the F4-F5 core results in a record of 32 tephra layers spanning the 430-365 ka period, thus making Fucino the richest distal archive for this time interval over the entire Mediterranean region. The resulting dataset allowed us to detect the volcanic sources of most of the newly investigated tephra layers and, in many cases, to recognise the specific equivalent eruption or eruptive phase. A Bayesian age-depth model, based on nine, either directly or geochemically correlated, $^{40}Ar/^{39}Ar$ dated tephra layers yielded a continuously dated record for the Fucino MIS 11 tephra. A synopsis of all the investigated tephra, along with their volcanic sources, corresponding eruptions and related ages is shown in Fig. 15. By combining the updated stratigraphic, geochemical, and chronological datasets, we provide an overview of the MIS 11 tephrochronology for the central Mediterranean area (Fig. 16) and even beyond, as shown here by the discovering of a possible equivalent of the Hungarian Bag tephra.

Furthermore, regardless of the limitations of using a single location distal tephra archive to reconstruct past volcanism, the Fucino record clearly documents the eruptive history of the peri-Tyrrhenian explosive volcanoes of central Italy with unprecedented detail and at a higher chronological resolution with respect to available datasets from proximal areas. The improved knowledge of the activity histories of Vulsini, Vico, Sabatini, Colli Albani and Roccamonfina volcanoes, in many cases providing new evidence for previously unidentified eruptions and substantially improving the chronology of the known ones, sets the ground for refining the eruption timing and frequency, as well as the duration of intervening quiescence periods. This has key implications for hazard assessment, as well as for identifying a cyclic behaviour of explosive activity (Fig. 17) linked to still unkown external forcing(s).

Finally, from a wider methodological point of view, the results of this study strengthen and consolidate the relevance of the distal tephra archives as fundamental, integrative records for better reconstructing the behaviour of explosive volcanism, which is crucial for understanding the underlying dynamics and the assessment of the related hazards. This is particularly true in the perspective of future widening of the network of records throughout the regions surrounding Quaternary volcanic areas. Such network will be most valuable for extending the lattice of correlations and for tracing individual tephra layers, which in turn are crucial for both tephrochronological and volcanological purposes. In this perspective, the Fucino Basin, with its long and continuous sedimentary history and strategic position, arises as a cornerstone for the development and the application of this approach in the Mediterranean region for the Quaternary sciences and volcanology.

Declaration of Competing Interest

The authors declare that they have no known competing financial interests or personal relationships that could have appeared to influence the work reported in this paper.

Acknowledgments

This article is a contribution of project “FUcino Tephrochronology Unites Quaternary REcords (FUTURE)”, supported by the Italian

Ministry of Education, University and Research (MIUR, grant PRIN No. 20177TKBXZ_003; G. Zanchetta, coordinator). The Fucino project is co-funded by DFG (German Research Foundation) grant WA 2109/16. $^{40}Ar/^{39}Ar$ dating also received complementary contribution from the CNRS INSU-LEFE 2018-2020 action to S. Nomade. P.G. Albert is supported by a UKRI Future Leaders Fellowship (MR/S035478/1). INGV, OV laboratories have been also financially supported by the EPOS Research Infrastructure through the contribution of the Italian Ministry of University and Research (MUR). An earlier version of the manuscript benefited from useful comments from Roberto Sulpizio and an anonymous reviewer.

Appendix A. Supplementary data

Supplementary data to this article can be found online at https://doi.org/10.1016/j.earscirev.2021.103706.

References

Albert, P.G., Smith, V.C., Suzuki, T., Tomlinson, E.L., Nakagawa, T., McLean, D., Yamada, M., Staff, R.A., Schlolaut, G., Takemura, T., Nagahashi, Y., Kimura, J., Suigetsu 2006 Project Members, 2018. Constraints on the frequency and dispersal of explosive eruptions at Sambe and Daisen volcanoes (South-West Japan Arc) from the distal Lake Suigetsu record (SG06 core). Earth-Sci. Rev. 185, 1004–1028.

Albert, P.G., Giaccio, B., Isaia, R., Costa, A., Niespolo, E.M., Nomade, S., Pereira, A., Renne, P.R., Hinchliffe, A., Mark, D.F., Brown, R.J., Smith, V.C., 2019. Evidence for a large-magnitude eruption from Campi Flegrei Caldera (Italy) at 29 ka. Geology. https://doi.org/10.1130/G45805.1.

Amato, V., Aucelli, P.P.C., Cesarano, M., Jicha, B., Lebreton, V., Orain, R., Pappone, G., Petrosino, P., Russo Ermolli, E., 2014. Quaternary evolution of the largest intermontane basin of the Molise Apennine (Central Southern Italy). Rendiconti Lincei 25, 197–216.

Amato, V., Aucelli, P.P.C., Cesarano, M., Filocamo, F., Leone, N., Petrosino, P., Rosskopf, C.M., Valente, E., Casciello, E., Giralt, S., Jicha, B.R., 2018. Geomorphic response to late Quaternary tectonics in the axial portion of the Southern Apennines (Italy): A case study from the Calore River valley. Earth Surf. Process. Landf. 43, 2463–2480.

Belkin, H.E., Rolandi, G., Jackson, J.C., Cannatelli, C., Doherty, A.L., Petrosino, P., De Vivo, B., 2016. Mineralogy and geochemistry of the older (>40 ka) ignimbrites in the Campanian Plain, southern Italy. J. Volcanol. Geotherm. Res. 323, 1–18.

Bini, M., Zanchetta, G., Drysdale, R.N., Giaccio, B., Stocchi, P., Vacchi, M., Hellstrom, J. C., Couchoud, I., Monaco, L., Ratti, A., Martini, F., Sarti, L., 2020. An end to the Last Interglacial highstand before 120 ka: Relative sea-level evidence from Infreschi Cave (Southern Italy). Quat. Sci. Rev. 250, 106658.

Blaauw, M., Christen, J.A., 2011. Flexible paleoclimate age-depth models using an autoregressive gamma process. Bayesian Anal. 6 (3), 457–474.

Blockley, S.P.E., Bourne, A.J., Brauer, A., Davies, S.M., Hardiman, M., Harding, P.R., Lane, C.S., MacLeod, A., Matthews, I.P., Pyne-O'Donnel, S.D.F., Rasmussen, S.O., Wulf, S., Zanchetta, G., 2014. Tephrochronology and the extended intimate (integration of ice-core, marine and terrestrial records) event stratigraphy 8-128 ka 2bk. Quat. Sci. Rev. 106, 88–100.

Boari, E., Tommasini, S., Laurenzi, M.A., Conticelli, S., 2009. Transition from Ultrapotassic Kamafugitic to Sub-Alkaline Magmas: Sr, Nd, and Pb Isotope, Trace Element and ^{40}Ar-^{39}Ar Age Data from the Middle Latin Valley Volcanic Field, Roman Magmatic Province. Central Italy. J. Petrol. 50 (7), 1327–1357.

Boncio, P., Lavecchia, G., Pace, B., 2004. Defining a model of 3D seismogenic sources for seismic hazard assessment applications: The case of central Apennines (Italy). J. Seismol. 8 (3), 407–425. https://doi.org/10.1023/B:JOSE.0000038449.78801.05.

Bourne, A.J., Lowe, J.J., Trincardi, F., Asioli, A., Blockley, S.P.E., Wulf, S., Matthews, I. P., Piva, A., Vigliotti, L., 2010. Distal tephra record for the last ca 105,000 years from core PRAD 1-2 in the central Adriatic Sea: implications for the marine tephrostratigraphy. Quat. Sci. Rev. 29, 3079–3094.

Bourne, A.J., Albert, P.G., Matthews, I.P., Trincardi, F., Wulf, S., Asioli, A., Blockley, S.P. E., Keller, J., Lowe, J.J., 2015. Tephrochrunology of core PRAD 1-2 from the Adriatic Sea: insights into Italian explosive volcanism for the period 200-80 ka. Quat. Sci. Rev. 116, 28–43.

Bronk Ramsey, C., Albert, P.G., Blockley, S.P.E., Hardiman, M., Housley, R.A., Lane, C.S., Lee, S., Matthews, I.P., Smith, V.C., Lowe, J.J., 2015a. Improved age estimates for key Late Quaternary European tephra horizons in the RESET lattice. Quat. Sci. Rev. 118, 18–32.

Bronk Ramsey, C., Housley, R.A., Lane, C.S., Smith, V.C., Pollard, A.M., 2015b. The Reset tephra database and associated analytical tools. Quat. Sci. Rev. 118, 33–47.

Bursik, M., 1998. Tephra dispersal. In: Gilbert, J.S., Sparks, R.S.J. (eds). The physics of explosive volcanic eruptions. Geol. Soc. Lond. Spec. Publ. 145, 115–144.

Cardello, G.L., Consorti, L., Palladino, D.M., Carminati, E., Carlini, M., Doglioni, C., 2020. Tectonically controlled carbonate-seated maar-diatreme volcanoes: The case of the Volsci Volcanic Field, central Italy. J. Geodyn. 139, 101763.

Cavinato, G.P., Carusi, C., Dell'Asta, M., Miccadei, E., Piacentini, T., 2002. Sedimentary and tectonic evolution of Plio-Pleistocene alluvial and lacustrine deposits of Fucino Basin (central Italy). Sediment. Geol. 148, 29–59.

Centamore, E., Dramis, F., Di Manna, P., Fumanti, F., Milli, S., Rossi, D., Palombo, M.R., Palladino, D.M., Triglia, R., Zanon, V., Chiocchini, M., Didaskalou, P., Potetti, M., Nisio, S., 2010. Note illustrative del Foglio 402 Ceccano. In: Carta Geologica d'Italia 1:50000. Roma, Servizio Geologico d'Italia.

Cioni, R., Sbrana, A., Bertagnini, A., Buonasorte, G., Landi, P., Rossi, U., Salvati, L., 1987. Tephrostratigraphic correlations in the Vulsini, Vico and Sabatini volcanic succession. Periodico di Mineralogia 56, 137–155.

Cross, J.K., Tomlinson, E.L., Giordano, G., Smith, V.S., De Benedetti, A.A., Roberge, J., Manning, C.J., Wulf, S., Menzies, M.A., 2014. High level triggers for explosive mafic volcanism: Albano Maar, Italy. Lithos 190-191, 137–153.

D'Antonio, M., Mariconte, R., Arienzo, I., Mazzeo, F.C., Carandente, A., Perugini, D., Petrelli, M., Corselli, C., Orsi, G., Principato, M.S., Civetta, L., 2016. Combined Sr-Nd isotopic and geochemical fingerprinting as a tool for identifying tephra layers: Application to deep-sea cores from Eastern Mediterranean Sea. Chem. Geol. 443, 121–136.

D'Agostino, N., Jackson, J.A., Dramis, F., Funiciello, R., 2001. Interactions between mantle upwelling, drainage evolution and active normal faulting: an example from the central Apennines (Italy). Geophys. J. Int. 147 (2), 475–497.

de Fontaine, C.S., Kaufman, D.S., Anderson, R.S., Werner, A., Waythomass, C.F., Brown, T.A., 2007. Late Quaternary distal-fall deposits in lacustrine sediments, Kenai Peninsula, Alaska. Quat. Res. 68 (1), 64–78.

De Rita, D., Funiciello, R., Parotto, M., 1988. Carta geologica del complesso vulcanico dei Colli Albani (Vulcano Laziale). C.N.R.-Gruppo Nazionale Vulcanologia.

De Rita, D., Giordano, G., Rosa, C., Sheridan, M.F., 1995. Volcanic risk at the Alban Hills volcano and numerical simulations. In: Triglia, R. (Ed.), The Volcano of the Alban Hills. Tipografia SGS, Rome, pp. 267–283.

De Vivo, B., Rolandi, G., Gans, P.B., Calvert, A., Bohrson, W.A., Spera, F.J., Belkin, H.E., 2001. New constraints on the pyroclastic eruptive history of Campanian volcanic Plain (Italy). Mineral. Petrol. 73, 47–65.

Del Carlo, P., Smedile, A., Petrelli, M., Di Roberto, A., 2020. Evidence of an unknown explosive eruption of Mt. Etna volcano (Italy) during the Late Glacial. J. Volcanol. Geotherm. Res. 402, 106992.

Di Roberto, A., Smedile, A., Del Carlo, P., De Martini, P.M., Iorio, M., Petrelli, M., Pantosti, P., Pinzi, S., Todrani, A., 2018. Tephra and cryptotephra in a ~60,000-year old lacustrine sequence from the Fucino Basin: new insights into the major explosive events in Italy. Bull. Volcanol. 80, 20.

Doglioni, C., Harabaglia, P., Martinelli, G., Mongelli, F., Zito, G., 1996. A geodynamic model of the Southern Apennines accretionary prism. Terra Nova 8 (6), 540–547.

Donato, P., Albert, P.G., Crocitti, M., De Rosa, C., Menzies, M.A., 2016. Tephra layers along the southern Tyrrhenian coast of Italy: Links to the X-5 & X-6 using volcanic glass geochemistry. J. Volcanol. Geotherm. Res. 317, 30–41.

Dugmore, A.J., 1989. Icelandic volcanic ash in Scotland. Scottish Geographical Megazine 105 (3), 168–172. https://doi.org/10.1080/14702548908554430.

Dugmore, A.J., Newton, A.J., Smith, K.T., Mairs, K.A., 2013. Tephrochronology and the late Holocene volcanic and flood history of Eyjafjallajökull, Iceland. (2013). J. Quat. Sci. 28 (3), 237–247.

Florindo, F., Karner, D.B., Marra, F., Renne, P.R., Roberts, A.P., Weaver, R., 2007. Radioisotopic age constraints for Glacial Terminations IX and VII from aggradational sections of the Tiber River delta in Rome, Italy. Earth Planet. Sci. Lett. 256, 61–80. https://doi.org/10.1016/j.epsl.2007.01.014.

Freda, C., Gaeta, M., Palladino, D.M., Trigila, R., 1997. The Villa Senni eruption (Alban Hills, Central Italy): the role of H_2O and CO_2 on the magma chamber evolution and on the eruptive scenario. J. Volcanol. Geotherm. Res. 78 (1-2), 103–120.

Freda, C., Gaeta, M., Karner, D.B., Marra, F., Renne, P.R., Taddeucci, J., Scarlato, P., Christensen, J.N., Dallai, L., 2006. Eruptive history and petrologic evolution of the Albano multiple maar (Alban Hills, Central Italy). Bull. Volcanol. 68, 567–591.

Freda, C., Gaeta, M., Giaccio, B., Marra, F., Palladino, D.M., Scarlato, P., Sottili, G., 2011. CO_2-driven large mafic explosive eruptions: the Pozzolane Rosse case study from the Colli Albani Volcanic District (Italy). Bull. Volcanol. 73, 241–256.

Funiciello, R., De Rita, D., Sposato, A., Esposito, A., Fabbri, M., Marsili, P., Mazzini, I., Paccara, P., Trigari, A., Capelli, G., Faccenna, C., Fiorentino, A., Mazza, R., Rossetti, F., Sardella, R., Soligo, M., Tuccimei, P., Villa, I.M., 2012. Note Illustrative della Carta Geologica d'Italia alla scala 1:50.000, Foglio 354 "Tarquinia". Presidenza del Consiglio dei Ministri. Agenzia per la Protezione dell'Ambiente e per i servizi Tecnici: Roma, Italy, Servizio Geologico d'Italia, scale 1:50,000 (in press).

Gaeta, M., Freda, C., Christensen, J.N., Dallai, L., Marra, F., Karner, D.B., Scarlato, P., 2006. Time-dependent geochemistry of clinopyroxene from the Alban Hills (Central Italy): clues to the source and evolution of ultrapotassic magmas. Lithos 86, 330–346.

Gaeta, M., Freda, C., Marra, F., Di Rocco, T., Gozzi, F., Arienzo, I., Giaccio, B., Scarlato, P., 2011. Petrology of the most recent ultrapotassic magmas from the Roman Province (Central Italy). Lithos 127, 298–308.

Gaeta, M., Freda, C., Marra, F., Arienzo, I., Gozzi, F., Jicha, B., Di Rocco, T., 2016. Paleozoic metasomatism at the origin of Mediterranean ultrapotassic magmas: Constraints from time-dependent geochemistry of Colli Albani volcanic products (Central Italy). Lithos 244, 151–164.

Galadini, F., Galli, P., 2000. Active tectonics in the Central Apennines (Italy) - Input Data for Seismic Hazard Assessment. Nat. Hazards 22, 225–270.

Gatta, M., Sinopoli, G., Giardini, M., Giaccio, B., Hajdas, I., Pandolfi, L., Bailey, G., Spikins, P., Rolfo, M.F., Sadori, L., 2016. Pollen from Late Pleistocene hyena (Crocuta Crocuta spelaea) coprolites: An interdisciplinary approach from two Italian sites. Rev. Palaeobot. Palynol. 233, 56–66.

Gehrels, M.J., Lowe, D.J., Hazell, Z.J., Newnham, R.M., 2006. A continuous 5300-yr Holocene cryptotephrostratigraphic record from northern New Zealand and impllications for tephrochronlogy and volcanic hazard assessment. The Holocene 16 (2), 173–187.

Giaccio, B., Marra, F., Hajdas, I., Karner, D.B., Renne, P.R., Sposato, A., 2009. $^{40}Ar/^{39}Ar$ and ^{14}C geochronology of the Albano maar deposits: Implications for defining the age and eruptive style of the most recent explosive activity at Colli Albani Volcanic District, Central Italy. J. Volcanol. Geotherm. Res. 185, 203–213.
Giaccio, B., Nomade, S., Wulf, S., Isaia, R., Sottili, G., Cavuoto, G., Galli, P., Messina, P., Sposato, A., Sulpizio, R., Zanchetta, G., 2012a. The late MIS 5 Mediterranean tephra markers: a reappraisal from peninsular Italy terrestrial records. Quat. Sci. Rev. 56, 31–45.
Giaccio, B., Galli, P., Messina, P., Peronace, E., Scardia, G., Sottili, G., Sposato, A., Chiarini, E., Jicha, B., Silvestri, S., 2012b. Fault and basin depocentre migration over the last 2Ma in the L'Aquila 2009 earthquake region, central Italian Apennines. Quat. Sci. Rev. 56, 69–88.
Giaccio, B., Arienzo, I., Sottili, G., Castorina, F., Gaeta, M., Nomade, S., Galli, P., Messina, P., 2013a. Isotopic (Sr-Nd) and major element fingerprinting of distal tephras: An application to the Middle-Late Pleistocene markers from the Colli Albani volcano, central Italy. Quat. Sci. Rev. 67, 190–206.
Giaccio, B., Castorina, F., Nomade, S., Scardia, G., Voltaggio, M., Sagnotti, L., 2013b. Revised Chronology of the Sulmona Lacustrine Succession, Central Italy. J. Quat. Sci. 28, 545–551.
Giaccio, B., Galli, P., Peronace, E., Arienzo, I., Nomade, S., Cavinato, G.P., Mancini, M., Messina, P., Sottili, G., 2014. A 560-440 ka tephra record from the Mercure Basin, Southern Italy: volcanological and tephrostratigraphic implications. J. Quat. Sci. 29, 232–248.
Giaccio, B., Regattieri, E., Zanchetta, G., Nomade, S., Renne, P.R., Sprain, C.J., Drysdale, R.N., Tzedakis, P.C., Messina, P., Scardia, G., Sposato, A., Bassinot, F., 2015a. Duration and dynamics of the best orbital analogue to the present interglacial. Geology 43, 603–606.
Giaccio, B., Regattieri, E., Zanchetta, G., Wagner, B., Galli, P., Mannella, G., Niespolo, E., Peronace, E., Renne, P.R., Nomade, S., Cavinato, G.P., Messina, P., Sposato, A., Boschi, C., Florindo, F., Marra, F., Sadori, L., 2015b. A key continental archive for the last 2 Ma of climatic history of the central Mediterranean region: A pilot drilling in the Fucino Basin, central Italy. Sci. Drill. 20, 13–19.
Giaccio, B., Niespolo, E.M., Pereira, A., Nomade, S., Renne, P.R., Albert, P.G., Arienzo, I., Regattieri, E., Wagner, B., Zanchetta, G., Gaeta, M., Galli, P., Mannella, G., Peronace, E., Sottili, G., Florindo, F., Leicher, N., Marra, F., Tomlinson, E.L., 2017. First integrated tephrochronological record for the last ~190 kyr from the Fucino Quaternary lacustrine succession, central Italy. Quat. Sci. Rev. 158, 211–234.
Giaccio, B., Leicher, N., Mannella, G., Monaco, L., Regattieri, E., Wagner, B., Zanchetta, G., Gaeta, M., Marra, F., Nomade, S., Palladino, D.M., Pereira, A., Scheidt, S., Sottili, G., Wonik, T., Wulf, S., Zeeden, C., Ariztegui, D., Cavinato, G.P., Dean, R.J., Florindo, F., Leng, M.J., Macrì, P., Niespolo, E., Renne, P.R., Rolf, C., Sadori, L., Thomas, C., Tzedakis, P.C., 2019. Extending the tephra and paleoenvironmental record of the Central Mediterranean back to 430 ka: A new core from Fucino Basin, central Italy. Quat. Sci. Rev. 225, 106003.
Giannetti, B., 1996a. The geology of the Yellow Trachytic Tuff, Roccamonfina Volcano. J. Volcanol. Geotherm. Res. 71 (1), 53–72.
Giannetti, B., 1996b. Volcanology of trachytic and associated basaltic pyroclastic deposits at Roccamonfina volcano, Roman Region. Italy. J. Volcanology Geothermal Res. 71 (2-4), 229–248.
Giannetti, B., 2001. Origin of the calderas and evolution of Roccamonfina volcano (Roman Region, Italy). J. Volcanol. Geotherm. Res. 106, 301–319.
Giannetti, B., De Casa, G., 2000. Stratigraphy, chronology, and sedimentology of ignimbrites from the white trachytic tuff, Roccamonfina Volcano. Italy. J. Volcanology Geothermal Res. 96 (3-4), 243–295.
Giordano, G., De Benedetti, A.A., Diana, A., Diano, G., Gaudioso, F., Marasco, F., Miceli, M., Mollo, S., Cas, R.A.F., Funiciello, R., 2006. The Colli Albani mafic caldera (Roma, Italy): Stratigraphy, structure and petrology. J. Volcanol. Geotherm. Res. 155, 49–80.
Goldstein, S.L., Denis, P., Oelkers, E.H., Rudnick, R.L., Walter, L.M., 2003. Standards for publication of isotope ratio and chemical data in chemical geology. Chem. Geol. 202, 1–4.
Horváth, E., Bradák, B., 2014. Sárga föld, lősz, lösz: Short historical overview of loess research and litostratigraphy in Hungary. Quat. Int. 319, 1–10.
Hum, L., 2005. Középső pleisztocén tufithorizontok megjelenése dunaszekcsői és Mórágy környéki löszszelvényekben. Malakológiai Tájékoztató 23, 131–148 (in Hungarian).
Insinga, D.D., Tamburrino, S., Lirer, F., Vezzoli, L., Barra, M., De Lange, G.J., Tiepolo, M., Vallefuoco, M., Mazzola, S., Sprovieri, M., 2014. Tephrochronology of the astronomically-tuned KC01B deep-sea core, Ionian Sea: insights into the explosive activity of the Central Mediterranean area during the last 200 ka. Quat. Sci. Rev. 85, 63–84.
Jochum, K.P., Stoll, B., Herwig, K., Willbold, M., Hofmann, A.W., Amini, M., Aarbug, S., Abouchami, W., Hellebrand, E., Mocek, B., Raczek, I., Stracke, A., Alard, O., Bouman, C., Becker, S., Dücking, M., Brätz, H., Klemd, R., de Bruin, D., Canil, D., Cornell, D., de Hoog, C.-S., Dalpé, C., Danyushevsky, L., Eisenhauer, A., Gao, Y., Snow, J.E., Groschopf, N., Günther, D., Latkoczy, C., Guillong, M., Hauri, E.K., Höfer, H.E., Lahaye, Y., Horz, K., Jacob, D.E., Kasemann, S.A., Kent, A.J.R., Ludwig, T., Zack, T., Mason, P.R.D., Meixner, A., Rosner, M., Kisawa, K., Nash, P.B., Pfänder, J., Premo, W.R., Sun, W.D., Tiepolo, M., Vannucci, R., Vennemann, T., Wayne, D., Woodhead, J.D., 2006. MPI-DING reference glasses for in situ microanalysis: New reference values for element concentrations and isotope ratios. Geochem. Geophys. Geosyst. 7, 2.
Karner, D.B., Renne, P.R., 1998. $^{40}Ar/^{39}Ar$ geochronology of Roman volcanic province tephra in the Tiber River valley: Age calibration of middle Pleistocene sea-level changes. Geol. Soc. Am. Bull. 110 (6), 740–747.
Karner, D.B., Juvinge, E., Brancaccio, L., Cinque, A., Russo Ermolli, E., Santangelo, L., Bernasconi, S., Lirer, L., 1999. A potential early middle Pleistocene tephrostratotype for the Mediterranean basin: the Vallo Di Diano, Campania, Italy. Glob. Planet. Chang. 21, 1–15.
Keller, J., Ryan, W.B.F., Ninkovich, D., Altherr, R., 1978. Explosive volcanic activity in the Mediterranean over the last 200,000 yr as recorded in deep-sea sediments. Geol. Soc. Am. Bull. 89, 591–604.
Kousis, I., Koutsodendris, A., Peyron, O., Leicher, N., Francke, A., Wagner, B., Giaccio, B., Knipping, M., Pross, J., 2018. Centennial-scale vegetation dynamics and climate variability in SE Europe during Marine Isotope Stage 11 based on a pollen record from Lake Ohrid. Quat. Sci. Rev. 190, 20–38.
Kuehn, S.C., Froese, D.G., Shane, P.A.R., Intercomparison Participants, I.N.T.A.V., 2011. The INTAV intercomparison of electron-beam microanalysis of glass by tephrochronology laboratories: Results and recommendations. Quat. Int. 246, 19–47.
Lane, C.S., Brauer, A., Blockley, S.P.E., Dulski, P., 2013. Volcanic ash reveals time-transgressive abrupt climate change during the Younger Dryas. Geology 41 (12), 1251–1254.
Larsen, G., Róbertsdóttir, B.G., Oladottir, B.A., Eiríksson, J., 2020. A shift in eruption mode of Hekla volcano, Iceland, 3000 years ago: two-coloured Hekla tephra series, characteriscs, dispersal and age. J. Quat. Sci. 35 (1-2), 143–154. Special Issue.
Le Maitre, R.W., Streckeisen, A., Zanettin, B., Le Bas, M.J., Bonin, B., Bateman, P., Bellieni, G., Dudek, A., Efremova, S., Keller, J., Lameyre, J., Sabine, P.A., Schmid, R., SØrensen, H., Woolley, A.R., 2002. Igneous Rocks: A Classification and Glossary of Terms. Reccomendation of the International Union of Geological Sciences Subcommission on the Systematics of Igneous Rocks, 2nd edition. Cambridge University Press, Cambridge. 236 pages.
Lee, J.Y., Marti, K., Severinghaus, J.P., Kawamura, K., Yoo, H.S., Lee, J.B., Kim, J.S., 2006. A redetermination of the isotopic abundances of atmospheric Ar. Geochim. Cosmochim. Acta 70, 4507–4512.
Leicher, N., Zanchetta, G., Sulpizio, R., Giaccio, B., Wagner, B., Nomade, S., Francke, A., Del Carlo, P., 2016. First tephrostratigraphic results of the DEEP site record from Lake Ohrid (Macedonia and Alania). Biogeosciences 13, 2151–2178.
Leicher, N., Giaccio, B., Zanchetta, G., Wagner, B., Francke, A., Palladino, D.M., Sulpizio, R., Albert, P.G., Tomlinson, E.L., 2019. Central Mediterranean explosive volcanism and tephrochronology during the last 630 ka based on the sediment record from Lake Ohrid. Quat. Sci. Rev. 226, 106021.
Lisiecki, L.E., Raymo, M.E., 2005. A Pliocene-Pleistocene stack of 57 globally distributed benthic $\delta^{18}O$ records. Paleoceanography 20. https://doi.org/10.1029/2004PA001071.
Lourens, L.J., 2004. Revised tuning of Ocean Drilling Program Site 964 and KC01B (Mediterranean) and implicaions for the $d^{18}O$, tephra, calcareous nannofossil, and geomagnetic reversal chronologies of the past 1.1 Myr. Paleoceanography and Paleoclimatology 19. PA3010.
Lowe, D.J., 2011. Tephrochronology and its application: A review. Quater. Geochonol. 6, 107–153.
Lowe, D.J., Bronk Ramsey, C., Housley, R.A., Lane, C.S., Tomlinson, E.L., RESET Team, RESET Associates, 2015. The RESET project: constructing a European tephra lattice refined synchronisation of environmental and archaeological events during the last c. 100 ka. Quat. Sci. Rev. 118, 1–17.
Luberti, G.M., Marra, F., Florindo, F., 2017. A review of the stratigraphy of Rome (Italy) according to geochronologically and paleomagnetically constrained aggradational successions, glacio-eustatic forcing and volcano-tectonic processes. Quat. Int. 438 (Part B), 40–67.
Luhr, J.F., Giannetti, B., 1987. The Brown Leucitic Tuff of Roccamonfina Volcano (Roman Region, Italy). Contrib. Mineral. Petrol. 95, 420–436.
Lustrino, M., Duggen, S., Rosenberg, C.L., 2011. The Central-Western Mediterranean: Anomalous igneous activity in an anomalous collisional tectonic setting. Earth Sci. Rev. 104 (1-3), 1–40.
Mannella, G., Giaccio, B., Zanchetta, G., Regattieri, E., Niespolo, E.M., Pereira, A., Renne, P.R., Nomade, S., Leicher, N., Perchiazzi, N., Wagner, B., 2019. Paleoenvironmental and paleohydrological variability of mountain areas in the central Mediterranean region: A 190-ka-long chronicle from the independently dated Fucino paleolake record (central Italy). Quat. Sci. Rev. 210, 190–210.
Marra, F., Freda, C., Scarlato, P., Taddeucci, J., Karner, D.B., Renne, P.R., Gaeta, M., Palladino, D.M., Triglia, R., Cavaretta, G., 2003. Post-caldera activity in the Alban Hills volcanic district (Italy): $^{40}Ar/^{39}Ar$ geochronology and insights into magma evolution. Bull. Volcanol. 65, 227–247.
Marra, F., Taddeucci, J., Freda, C., Marzocchi, W., Scarlato, P., 2004. Recurrence of volcanic activity along the Roman Comagmatic Province (Tyrrhenian margin of Italy) and its tectonic significance. Tectonics 23, TC4013.
Marra, F., Karner, D.B., Freda, C., Gaeta, M., Renne, P., 2009. Large mafic eruptions at Alban Hills Volcanic District (Central Italy): chronostratigraphy, petrography and eruptive behavior. J. Volcanol. Geotherm. Res. 179, 217–232.
Marra, F., Sottili, G., Gaeta, M., Giaccio, B., Jicha, B., Masotta, M., Palladino, D.M., Deocampo, D.M., 2014. Major explosive activity in the Monti Sabatini Volcanic District (central Italy) over the 800-390 ka interval: geochronological-geochemical overview and tephrostratigraphic implications. Quat. Sci. Rev. 94, 74–101.
Marra, F., Gaeta, M., Giaccio, B., Jicha, B.R., Palladino, D.M., Polcari, M., Sottili, G., Taddeucci, J., Florindo, F., Stramondo, S., 2016a. Assessing the volcanic hazard for Rome: $^{40}Ar/^{39}Ar$ and In-SAR constraints on the most recent eruptive acivity and present-day uplift at Colli Albani Volcanic District. Geophys. Res. Lett. 43, 6898–6906.
Marra, F., Rohling, E.J., Florindo, F., Jicha, B., Nomade, S., Pereira, A., Renne, P.R., 2016b. Independent $^{40}Ar/^{39}Ar$ and ^{14}C age constraints on the last five glacial terminations from the aggradational successions of the Tiber River, Rome (Italy). Earth Planet. Sci. Lett. 449, 105–117.

Marra, F., Jicha, B., Florindo, F., 2017. $^{40}Ar/^{39}Ar$ dating of Glacial Termination VI: constraints to the duration of Marine Isotopic Stage 13. Sci. Rep. 7, 8908. https://doi.org/10.1038/s41598-017-08614-6.

Marra, F., Nomade, S., Pereira, A., Petronio, C., Salari, L., Sottili, G., Bahain, J.J., Boschian, G., Di Stefano, G., Falguères, C., Florindo, F., Gaeta, M., Giaccio, B., Masotta, M., 2018. A review of the geological sections and the faunal assemblages of Aurelian Mammal Age of Latium (Italy) in the light of a new chronostratigraphic framework. Quat. Sci. Rev. 181, 173–199.

Marra, F., Costantini, L., Di Buduo, G.M., Florindo, F., Jicha, B.R., Monaco, L., Palladino, D.M., Sottili, G., 2019. Combined glacio-eustatic forcing and volcano-tectonic uplift: geomorphological and geochronological constraints on the Tiber River terraces in the eastern Vulsini Volcanic District (central Italy). Glob. Planet. Chang. 182, 103009. https://doi.org/10.1016/j.gloplacha.2019.103009.

Marra, F., Jicha, B., Palladino, D.M., Gaeta, M., Costantini, L., Di Buduo, G.M., 2020a. $^{40}Ar^{39}Ar$ single crystal dates from pyroclastic deposits provide a detailed record of the 590-240 ka eruptive period at the Vulsini Volcanic District (central Italy). J. Volcanol. Geotherm. Res. 398, 106904.

Marra, F., Castellano, C., Cucci, L., Florindo, F., Gaeta, M., Jicha, B., Palladino, D.M., Sottili, G., Tertulliani, A., Tolomei, C., 2020b. Monti Sabatini and Colli Albani: the dormant twin volcanoes at the gates of Rome. Sci. Rep. 10, 8666. https://doi.org/10.1038/s41598-02-65394-2.

Marra, F., Cardello, G.L., Gaeta, M., Jicha, B.R., Montone, P., Niespolo, E.M., Nomade, S., Palladino, D.M., Pereira, A., De Luca, G., Florindo, F., Frepoli, A., Renne, P.R., Sottili, G., 2021. The Volsci Volcanic Field (central Italy): eruptive history, magma system and implications on continental subduction processes. Int. J. Earth Sci. https://doi.org/10.1007/s00531-021-01981-6.

Matthews, I.P., Trincardi, F., Lowe, J.J., Bourne, A.J., MacLeod, A., Abbott, P.M., Andersen, N., Asioli, A., Blockley, S.P.E., Lane, C.S., Oh, Y.A., Satow, C.S., Staff, R.A., Wulf, S., 2015. Developing a robust tephrochronological framework for Late Quaternary marine records in the Southern Adriatic Sea: new data from core station SA03-11. Quat. Sci. Rev. 118, 84–104.

Mcmanus, J., Oppo, D., Cullen, J., Healey, S., 2003. Marine isotope stage 11 (MIS 11): analog for Holocene and future Climate? Earth's climate and orbital eccentricity: the marine isotope stage 11 question, 137, pp. 69–85.

Morabito, S., Petrosino, P., Milia, A., Sprovieri, M., Tamburrino, S., 2014. A multidisciplinary approach for reconstructing the stratigraphic framework of the last 40 ka in a bathyal area of eastern Tyrrhenian Sea. Glob. Planet. Chang. 123 (Part A), 121–138.

Munno, R., Petrosino, P., 2007. The late Quaternary tephrostratigraphical record of the San Gregorio Magno basin (southern Italy). J. Quat. Sci. 22, 247–266.

Nappi, G., Renzulli, A., Santi, P., Gillot, Y.P., 1995. Geological evolution and geochronology of the Vulsini volcanic district (central Italy). Boll. Soc. Geol. Ital. 114, 599–613.

Narcisi, B., Vezzoli, L., 1999. Quaternary stratigraphy of distal tephra layers in the Mediterranean - an overview. Glob. Planet. Chang. 21, 31–50.

Newnham, R.M., Lowe, D.J., Alloway, B.V., 1999. Volcanic hazards in Auckland, New Zealand: a preliminary assessment of the threat posed by central North Island silicic volcanism based on the Quaternary tephrostratigraphical record. Geological Society, London, Special Pubblications 161, 27–45.

Niespolo, E.M., Rutte, D., Deino, A.L., Renne, P.R., 2017. Intercalibration and age of the Alder Creek Sanidine $^{40}Ar/^{39}Ar$ standard. Quat. Geochronol. 39, 205–213.

Nomade, S., Gauthier, A., Guillou, H., Pastre, J.-F., 2010. $^{40}Ar/^{39}Ar$ temporal framework for the Alleret maar lacustrine sequence (French Massif-Central): Volcanological and paleoclimatic implications. Quat. Geochronol. 5 (1), 20–27.

Nomade, S., Muttoni, G., Guillou, H., Robin, E., Scardia, G., 2011. First $^{40}Ar/^{39}Ar$ age of the Ceprano man (central Italy). Quat. Geochronol. 6, 453–457.

Nomade, S., Bassinot, F., Mariano, M., Simon, Q., Dewilde, F., Maiorano, P., Isguder, G., Blamart, D., Girone, A., Scao, V., Pereira, A., Toti, F., Bertini, A., Combourieu-Nebout, N., Peral, M., Bourlès, D.L., Petrosino, P., Gallicchio, S., Ciaranfi, N., 2019. High-resolution foraminifer stable isotope record of MIS 19 at Montalbano Jonico, southern Italy: A window into Mediterranean climatic variability during a low-eccentricity interglacial. Quat. Sci. Rev. 205, 106–125.

Palladino, D.M., Agosta, E., Freda, C., Spaziani, S., Trigila, R., 1994. Geo-petrographic and volcanological study of Southern Vulsini: the Valentano–Marta–La Rocca sector. Memorie Descrittive della Carta Geologica d'Italia 49, 255–276.

Palladino, D.M., Simei, S., Sottili, G., Trigila, R., 2010. Integrated approach for the reconstruction of stratigraphy and geology of Quaternary volcanic terrains: an application to the Vulsini Volcanoes (central Italy). In: Groppelli, G., Viereck, e L. (Eds.), Stratigraphy and Geology in Volcanic Areas. Geol. Soc. Am. Spec. Pap. 464, 66–84.

Patacca, E., Scandone, P., Di Luzio, E., Cavinato, G.P., Parotto, M., 2008. Structural architecture of the central Apennines: Interpretation of the CROP 11 seismic profile from the Adriatic coast to the orographic divide. Tectonics 27, TC3006. https://doi.org/10.1029/2005TC001917.

Paterne, M., Guichard, F., Labeyrie, J., Gillot, P.Y., Duplessy, J.C., 1986. Tyrrhenian Sea tephrochronology of the oxygen isotope record for the past 60,000 years. Mar. Geol. 72, 259–285.

Paterne, M., Guichard, F., Labeyrie, J., 1988. Explosive activity of the south Italian volcanoes during the past 80,000 years as determined by marine tephrochronology. J. Volcanol. Geotherm. Res. 34, 153–172.

Paterne, M., Guichard, F., Duplessy, J.C., Siani, G., Sulpizio, R., Labeyrie, J., 2008. A 90,000-200,000 yrs marine tephra record of Italian volcanic activity in the Central Mediterranean Sea. J. Volcanol. Geotherm. Res. 177, 187–196.

Peccerillo, A., 2017. Cenozoic Volcanism in the Tyrrhenian Sea Region. In: IAVCEI, Advances in Volcanology, 2 ed. Springer, p. 400.

Pereira, A., Nomade, S., Moncel, M.H., Voinchet, P., Bahain, J.J., Biddittu, I., Falgueres, C., Giaccio, B., Manzi, G., Parenti, F., Scardia, G., Scao, V., Sottili, G., Vietti, A., 2018. Integrated geochronology of Acheulian sites from the southern Latium (central Italy): insights on human-environment interaction and the technological innovations during the MIS 11-MIS 10 period. Quat. Sci. Rev. 187, 112–129.

Pereira, A., Monaco, L., Marra, F., Sébastien, N., Gaeta, M., Leicher, N., Palladino, D.M., Sottili, G., Guillou, H., Scao, V., Giaccio, B., 2020. Tephrochronology of the central Mediterranean MIS 11c interglacial (~425-395 ka): New constraints from the Vico volcano and the Tiber delta, central Italy. Quat. Sci. Rev. 243, 106–470.

Perini, G., Conticelli, S., 2002. Crystallization conditions of leucite-bearing magmas and their implications on the magmatological evolution of ultrapotassic magmas: the Vico Volcano, central Italy. Mineral. Petrol. 74, 253–276.

Perini, G., Conticelli, S., Francalanci, L., 1997. Inferences on the volcanic history of the Vico volcano, Roman Magmatic Province, central Italy: stratigraphic, petrographic and geochemical data. Mineral. Petrogr. Acta 40, 67–93.

Perini, G., Conticelli, S., Francalanci, L., Davidson, J.P., 2000. The relationship between potassic and calc-alkaline post-orogenic magmatism at Vico volcano, central Italy. J. Volcanol. Geotherm. Res. 95, 243–268.

Perini, G., Teplei III, F.-J., Davidson, J.P., Conticelli, S., 2003. The origin of K-feldspar megacrysts hosted in alkaline potassic rocks from central Italy: a track for low-pressure processes in mafic magmas. Lithos 66, 223–240.

Perini, G., Francalanci, L., Davidson, J.P., Conticelli, S., 2004. Evolution and Genesis of Magmas from Vico Volcano, Central Italy: Multiple Differentiation Pathways and Variable Parental Magmas. J. Petrol. 45 (1), 139–182.

Petrosino, P., Russo Ermolli, E., Donato, P., Jich, B., Robustelli, G., Sardella, R., 2014a. Using tephrochornology and palynology to date the MIS 13 lacustrine sediments of the Mercure basin (Southern Apennines - Italy). Ital. J. Geosci. 133, 169–186.

Petrosino, P., Jicha, B.R., Mazzeo, F.C., Russo Ermolli, E., 2014b. A high-resolution tephrochronological record of MIS 14-12 in the Southern Apennines (Acerno Basin, Italy). J. Volcanol. Geotherm. Res. 274, 34–50.

Petrosino, P., Jicha, B.R., Mazzeo, F.C., Ciaranfi, N., Girone, A., Maiorano, P., 2015. The Montalbano Jonico marine succession: An archive for distal tephra layers at the Early-Middle Pleistocene boundary in southern Italy. Quat. Int. 383, 89–103.

Petrosino, P., Morabito, S., Jicha, B.R., Milia, A., Sprovieri, M., Tamburrino, S., 2016. Multidisciplnary tephrochronological correlation of marker events in the eastern Tyrrhenian Sea between 48 and 105 ka. J. Volcanol. Geotherm. Res. 315, 79–99.

Petrosino, P., Arienzo, I., Mazzeo, F.C., Natale, J., Petrelli, M., Milia, A., Perugini, D., D'Antonio, M., 2019. The San Gregorio Magno lacusrine basin (Campania, southern Italy): improved characterization of the tephrostratigraphic markers based on trace elements and isotopic data. J. Quat. Sci. 34, 393–404.

Ponomareva, V.V., Portnyagin, M., Davies, S.M., 2015. Tephra without borders: far-reaching clues into past explosive eruptions. Front. Earth Sci. 3 (83) https://doi.org/10.3389/feart.2015.00083.

Pouclet, A., Horvat, E., Gabris, G., Juvignè, E., 1999. The Bag tephra, a widespread tephrochronological marker in Middle Europe: chemical and mineralogical investigations. Bull. Volcanol. 60, 265–272.

R Core Team, 2017. R: A Language and Environment for Statistical Computing.

Radicati di Brozolo, F., Di Girolamo, P., Turi, B., Oddone, M., 1988. ^{40}Ar-^{39}Ar and K-Ar dating of K-rich rocks from the Roccamonfina Volcano, Roman Comagmatic Region, Italy. Geochmica et Cosmochimica Acta 52, 1435–1441.

Regattieri, E., Giaccio, B., Zanchetta, G., Drysdale, R.N., Galli, P., Nomade, S., Peronace, E., Wulf, S., 2015. Hydrological variability over the Apennines during the Early Last Glacial precession minimum, as revelated by a stable isotope record from Sulmona basin, Central Italy. J. Quat. Sci. 30, 19–31.

Regattieri, E., Giaccio, B., Galli, P., Nomade, S., Peronace, E., Messina, P., Sposato, A., Boschi, C., Gemelli, M., 2016. A mmulti-proxy record of MIS 11-12 deglaciation and glacial MIS 12 instability from the Sulmona Basin (central Italy). Quternary Sci. Rev. 132, 129–145.

Regattieri, E., Giaccio, B., Mannella, G., Zanchetta, G., Nomade, S., Tognarelli, A., Perchiazzi, N., Vogel, H., Boschi, C., Drysdale, R.N., Wagner, B., Gemelli, M., Tzedakis, P., 2019. Frequency and dynamics of millennial-scale variability during marine isotope stage 19: insights from the Sulmona Basin (central Italy). Quat. Sci. Rev. 214, 28–43.

Renne, P.R., Balco, G., Ludwig, K.R., Mundil, R., Min, K., 2011. Response to the comment by WH Schwarz et al. on "Joint determination of 40 K decay constants and $^{40}Ar^*/^{40}K$ for the Fish Canyon sanidine standard, and improved accuracy for $^{40}Ar/^{39}Ar$ geochronology" by PR Renne et al. (2010). Geochim. Cosmochim. Acta 75, 5097–5100.

Renne, P.R., Sprain, C.J., Richards, M.A., Self, S., Vanderkluysen, L., Pande, K., 2015. State shift in Deccan volcanism at the Cretaceous Paleogene boundary, possibly induced by impact. Science 350, 76–78.

Rolandi, G., Bellucci, F., Heizler, M.T., Belkin, H.E., De Vivo, B., 2003. Tectonic controls on the genesis of ignimbrite from the Campanian Volcanic Zone, southern Italy. Mineral. Petrol. 79, 3–31.

Rouchon, V., Gillot, P.Y., Quidelleur, X., Chiesa, S., Floris, B., 2008. Temporal evolution of the Roccamonfina volcanic complex (Pleistocene), Central Italy. J. Volcanol. Geotherm. Res. 177, 500–514.

Russo Ermolli, E., Aucelli, P.P.C., Di Rollo, A., Mattei, M., Petrosino, P., Porreca, M., Rosskopf, C.M., 2010. An integrated stratigraphical approach to the Middle Pleistocene succession of the Sessano Basin (Molise, Italy). Quat. Int. 225, 114–127.

Sági, T., Kiss, B., Bradák, B., Harangi, S., 2008. Középső-pleisztocén löszben előforduló vulkáni képződmények Magyarországon: terepi és petrográfiai jellemzők (Middle Pleistocene volcanic sediments in loess in Hungary: field and petrographical characteristics). Földtani Közlöny 138, 297–310 (in Hungarian with English abstract).

Sagnotti, L., Scardia, G., Giaccio, B., Liddicoat, J.C., Nomade, S., Renne, P.R., Sprain, C. J., 2014. Extreamlly rapid directionl change during Matuyama-Brunhes geomagnetic polarity reversal. Geophys. J. Int. 199, 1110–1124.
Satow, C., Gudmundsson, A., Gertisser, R., Ramsey, C.B., Bazargan, M., Pyle, D., Wulf, S., Miles, A., Hardiman, M., 2021. A sea-level control on the eruptive activity of Santorini volcano. Greece, Nature Geoscience.
Sbrana, A., Marianelli, P., Pasquini, G., 2018. Volcanology of Ischia (Italy). J. Maps 14, 2.
Scaillet, S., Vita-Scaillet, G., Guillou, H., 2008. Oldest human footprints dated by Ar/Ar. Earth and Planestary Science Letters 275, 320–325.
Simon, Q., Bourlès, D.L., Thouveny, N., Horng, C.-S., Valet, J.-P., Bassinot, F., Choy, S., 2018. Cosmogenic signature of geomagnetic reversals and excursions from the Réunion event to the Matuyama-Brunhes transition (0.7-2.14 Ma interval). Earth Planet. Sci. Lett. 482, 510–524.
Smith, V.C., Isaia, R., Pearce, N.J.G., 2011. Tephrostratigrapy and glass compositions of post-15 kyr Campi Flegrei eruptions: implications for eruption history and chronostratigraphic markers. Quat. Sci. Rev. 30, 3638–3660.
Soligo, M., Tuccimei, P., 2010. Geochronology of Colli Albani volcano. In: Funicello, R., Giordano, G. (eds). The Colli Albani Volcano. Geological Society of London, Special IAVCEI Publication 3, 99–106.
Sottili, G., Palladino, D.M., Zanon, V., 2004. Plinian activity during the early eruptive history of the Sabatini volcanic district, central Italy. J. Volcanol. Geotherm. Res. 135, 361–379.
Sottili, G., Palladino, D.M., Marra, F., Jicha, B., Karner, D.B., Renne, P., 2010. Geochronology of the most recent activity in the Sabatini volcanic district, Roman Province, central Italy. J. Volcanol. Geotherm. Res. 196, 20–30.
Sottili, G., Arienzo, I., Castorina, F., Gaeta, M., Giaccio, B., Marra, F., Palladino, D.M., 2019. Time-dependent Sr and Nd isotope variations during the evolution of ultrapotassic Sabatini Volcanic District (Roman Province, Central Italy). Bull. Volcanol. 81, 67.
Tamburrino, S., Insinga, D.D., Sprovieri, M., Petrosino, P., Tiepolo, M., 2012. Major and trace element characterization of tephra layers offshore Pantelleria Island: insights into the last 200 ka of volcanic activity and contribution to the Med- iterranean tephrochronology. J. Quat. Sci. 27, 129–140.
Thirlwall, M.F., 1991. Long-term reproducibility of multicollector Sr and Nd isotope ratio analysis. Chem. Geol. 94, 85–104.
Thorarinsson, 1981a. Greetings from Iceland. Geografiska Annaler: Series A. Phys. Geogr. 63 (3-4), 109–118. https://doi.org/10.1080/04353676.1981.11880024.
Thorarinsson, 1981b. Tephra studies and tephrochronology: a historical review with special reference to Iceland. In: Self, S., Sparks, R.S.J. (Eds.), Tephra Studies. Reidel, Dordrecht, pp. 1–12.
Tomlinson, E.L., Thordarson, T., Muller, W., Thirlwall, M.T., Menzies, M.A., 2010. Microanalysis of tephra by LA-ICP-MS - strategies, advantages and limitations assessed using the Thorsmork ignimbrite (Southern Iceland). Chem. Geol. 279, 73–89.
Tomlinson, E.L., Arienzo, I., Civetta, L., Wulf, S., Smith, V.C., Hardiman, M., Lane, C.S., Carandente, A., Orsi, G., Rosi, M., Müller, W., Menzies, M.A., 2012. Geochemistry of the Phlegrean Fields (Italy) proximal sources for major Mediterranean tephras: Implications for the dispersal of Plinian and co-ignimbritic components of explosive eruptions. Geochmica et Cosmochimica Acta 93, 102–128.
Tomlinson, E.L., Albet, P.G., Wulf, S., Brown, R.J., Smith, V.C., Keller, J., Orsi, G., Bourne, A., Menzes, M.A., 2014. Age and geochemistry of tephra layers from Ischia, Italy: constraints from proximal-distal correlations with Lago Grande di Monticchio. J. Vollcanology and Geothermal Res.. 287, 22–39.
Tomlinson, E.L., Smith, V.C., Albert, P.G., Aydar, E., Civetta, L., Cioni, R., Cubukcu, E., Gertisser, R., Isaia, R., Menzies, M.A., Orsi, G., Rosi, M., Zanchetta, G., 2015. The major and trace element glass compositions of the productive Mediterranean volcanic sources: tools for correlating distal tephra layers in and around Europe. Quat. Sci. Rev. 118, 48–66.
Turbeville, B.N., 1992. $^{40}Ar/^{39}Ar$ ages and Stratigraphy of the Latera caldera, Italy. Bull. Volcanol. 55, 110–118.
Turbeville, B.N., 1993. Petrology and Petrogenesis of the Latera Caldera. Central Italy. J. Petrol. 34 (1), 77–123.
Tzedakis, P.C., 2010. The MIS 11–MIS 1 analogy, southern European vegetation, atmospheric methane and the" early anthropogenic hypothesis". Clim. Past 6 (2), 131–144.
Vakhrameeva, P., Koutsodendris, A., Wulf, S., Fletcher, W.J., Appelt, O., Knipping, M., Gertisser, R., Trieloff, M., Pross, J., 2018. The cryptotephra record of the Marine Isotope Stage 12 to 10 interval (460-335 ka) at Tenaghi Philippon, Greece: Exploring chronological markers for the Middle Pleistocene of the Mediterranean reion. Quat. Sci. Rev. 200, 313–333.
Vakhrameeva, P., Wulf, S., Koutsodendris, A., Tjallingii, R., Fletcher, W.J., Appet, O., Ludwig, T., Knipping, M., Trieloff, M., Pross, J., 2019. Eastern Mediterranean volcanism during. Marine isotope stages 9 to 7e (335-235 ka): Insights based on cryptotephra layers at Tenaghi Philippon, Greece. J. Volcanol. Geotherm. Res. 380, 31–47.
Vakhrameeva, P., Koutsodendris, A., Wulf, S., Portnyagin, M., Appelt, O., Ludwig, T., Trieloff, M., Pross, J., 2021. Land-sea correlations in the Eastern Mediterranean region over the past c. 800 kyr based on macro- and cryptotephras from ODP Site 964 (Ionian Basin). Quaternary Sci. Rev. 255, 106811.
Villa, P., Soriano, S., Grün, R., Marra, F., Nomade, S., Pereira, A., Boschian, G., Pollarolo, L., Fang, F., Bahain, J.J., 2016. The Acheulian and early Middle Paleolithic in Central Italy: Stability and Innovation. PLoS One 11, e0160516. https://doi.org/10.1371/journal.pone.0160516.
Wagner, B., Vogel, H., Francke, A., Friederich, T., Donders, T., Lacey, J.H., Leng, M.J., Regattieri, E., Sadori, L., Wilke, T., Zanchetta, G., Albrecht, C., Bertini, A., Combourieu-Nebout, N., Cvetkoska, A., Giaccio, B., Grazhdani, A., Hauffe, T., Holtvoeth, J., Joannin, S., Lagoos, M., Leicher, N., Levkov, Z., Lindhorst, K., Masi, A., Melles, M., Mercuri, A.M., Nomade, S., Nowaczyk, N., Panagiotopoulos, K., Peyron, O., Reed, J.M., Sagnotti, L., Sinopoli, G., Stellbrink, B., Sulpizio, R., Timmermann, A., Tofilovska, S., Torri, P., Wagner-Cremer, F., Wonik, T., Zhang, X., 2019. Mediterranean winter rainfall in phase with African monsoons during the past 1.36 million years. Nature 573, 256–260.
Washington, H.S., 1906. The Roman comagmatic region. Carnegie Inst. Wash. Publ. 57, 199 pp.
Wastergärd, S., 2002. Early to middle Holocenic silicic tephra horizons from Katlavolcanic system, Iceland: new results from the Faroe Islands. J. Quaternary Sci. 17 (8), 723–730.
Wulf, S., Kraml, M., Brauer, A., Keller, J., Negendank, J.F.W., 2004. Tephrochronology of the 100 ka lacustrine sediment record of Lago Grande di Monticchio (Southern Italy). Quat. Int. 122, 7–30.
Wulf, S., Kraml, M., Keller, J., 2008. Towards a detailed tephrostratigraphy in the Central Mediterranean: The last 20,000 yrs record of Lago Grande di Monticchio. J. Volcanol. Geotherm. Res. 177, 118–132.
Wulf, S., Keller, J., Paterne, M., Mingram, J., Lauterbach, S., Opitz, S., Sottili, G., Giaccio, B., Albert, P.G., Satow, C., Tomlinson, E.L., Viccaro, M., Brauer, A., 2012. The 100-133 ka record of Italian explosive volcanism and revised tephrochronology of Lago Grande di Monticchio. Quat. Sci. Rev. 58, 104–123.
Wulf, S., Keller, J., Satow, C., Gertisser, R., Kraml, M., Grant, K.M., Appelt, O., Vakhrameeva, P., Koutsodendris, A., Hardiman, M., Schulz, H., Pross, J., 2020. Advancing Santorini's tephrostratigraphy: New glass geochemical data and improved marine-terrestrial tephra correlations for the past ~360 kyrs. Earth Sci. Rev. 200, 102964.
Zanchetta, G., Giaccio, B., Bini, M., Sarti, L., 2018. Tephrostratigraphy of Grotta del Cavallo, Southern Italy: insights of the chronology of Middle to Upper Paleolithic transition in the Mediterranean. Quat. Sci. Rev. 182, 65–77.